NASA TECHNICAL NOTE

NASA TN D-2389

NASA TN D-2389

SUPERSONIC AERODYNAMIC CHARACTERISTICS OF A SERIES OF BODIES HAVING VARIATIONS IN FINENESS RATIO AND CROSS-SECTION ELLIPTICITY

by Bernard Spencer, Jr., W. Pelham Phillips, and Roger H. Fournier

Langley Research Center
Langley Station, Hampton, Va.

NATIONAL AERONAUTICS AND SPACE ADMINISTRATION • WASHINGTON, D. C. • AUGUST 1964

SUPERSONIC AERODYNAMIC CHARACTERISTICS OF A SERIES OF BODIES HAVING VARIATIONS IN FINENESS RATIO AND CROSS-SECTION ELLIPTICITY

By Bernard Spencer, Jr., W. Pelham Phillips, and Roger H. Fournier

Langley Research Center
Langley Station, Hampton, Va.

NATIONAL AERONAUTICS AND SPACE ADMINISTRATION

For sale by the Office of Technical Services, Department of Commerce, Washington, D.C. 20230 -- Price $2.00

SUPERSONIC AERODYNAMIC CHARACTERISTICS OF A SERIES OF BODIES HAVING VARIATIONS IN FINENESS RATIO AND CROSS-SECTION ELLIPTICITY

By Bernard Spencer, Jr., W. Pelham Phillips,
and Roger H. Fournier
Langley Research Center

SUMMARY

An investigation has been conducted in the Langley Unitary Plan wind tunnel to determine the effects of cross-sectional ellipticity and fineness ratio on the longitudinal and lateral aerodynamic characteristics of a series of 2/3-power low-wave-drag bodies at Mach numbers from 1.50 to 2.86. Reynolds number per foot was held constant at 2.75×10^6 for all Mach numbers. The angle-of-attack range was from approximately -5° to 29° at 0° and 5° of sideslip.

Increasing body major-to-minor axis ratio, with the major axis horizontal, resulted in large increases in the lift, drag, and pitching-moment coefficients and lift-drag ratios at positive angles of attack and at all test Mach numbers. The successive increases in major-to-minor axis ratio, with the major axis horizontal, resulted in gains in lift-curve slope for bodies of the same fineness ratio when the coefficients were based on the respective body projected planform areas; generally, only slight changes in the minimum-drag characteristics of the bodies were noted.

A rearward shift in the body center-of-pressure location is generally indicated when the horizontal-to-vertical axis ratio is increased from 0.50 to 2.00. Little or no effects of increasing Mach number on the center-of-pressure location of a given body were shown.

For the moment-reference-point location of the present investigation, each of the symmetrical bodies exhibited static directional instability at all test Mach numbers, and reductions in the level of directional instability were indicated for increases in major-to-minor axis ratio, with the major axis horizontal. These reductions in directional instability were generally accompanied by corresponding increases in the variation of positive effective dihedral with increasing angle of attack for the Mach number range of the present investigation.

INTRODUCTION

The National Aeronautics and Space Administration and others are presently conducting aerodynamic research from low subsonic to hypersonic speeds on low-fineness-ratio generalized lifting-body shapes with possible application as manned reentry configurations. (See refs. 1 to 7.) Research on low-fineness-ratio cones at supersonic speeds (ref. 5) and high-fineness-ratio low-wave-drag bodies at subsonic speeds (ref. 6) has indicated that notable gains in the aerodynamic performance may be realized from varying the body cross section from circular to elliptic (elongations in the horizontal plane). These improvements in performance realized from altering the configuration cross section may be reflected in improved maneuverability and range control throughout the range of Mach numbers to be encountered, and may considerably improve the landing capability of these basic body configurations. Significant gains in overall performance may also be expected from use of these lifting bodies with low-aspect-ratio wings of high sweep designed as hypersonic cruise or reentry configurations, since the body portion of this type of configuration will constitute a major portion of the lifting surface.

The present investigation was made to provide aerodynamic information at supersonic speeds on the effects of changing fineness ratio and cross-sectional ellipticity on the aerodynamic characteristics for a series of 2/3-power low-wave-drag lifting bodies. Variations in the horizontal-to-vertical axis ratio from 0.50 to 2.00 are included for effective body-fineness ratios of 3, 5, and 7. Tests were conducted in the low Mach number test section of the Langley Unitary Plan wind tunnel at Mach numbers of 1.50, 1.90, 2.36, and 2.86. The angle-of-attack range varied from approximately -5° to 29° at 0° and 5° of sideslip and at a Reynolds number per foot of 2.75×10^6.

SYMBOLS

Longitudinal data are presented about the stability axes, and lateral data are presented about the body axes. The coefficients are nondimensionalized with respect to the body base area (0.08727 sq ft), which was held constant for all configurations, and the base diameter of the circular-cross-sectional body, unless otherwise noted. The longitudinal location of the moment reference point was taken as 66.67 percent of the total length for each configuration. Vertical moment-reference-point locations for each body are indicated in figure 1.

A	aspect ratio, $\frac{(2a_{max})^2}{S_p}$, $\phi = 0^\circ$; $\frac{(2b_{max})^2}{S_p}$, $\phi = 90^\circ$
a	semimajor-axis length of elliptic cross section, ft
b	semiminor-axis length of elliptic cross section, ft

C_D drag coefficient, $\frac{\text{Drag}}{qS_b}$

$C_{D_{min}}$ minimum drag coefficient

C_L lift coefficient, $\frac{\text{Lift}}{qS_b}$

$C_{L_{(L/D)_{max}}}$ lift coefficient at maximum lift-drag ratio

C_{L_α} lift-curve slope ($\alpha = 0^\circ$), per degree

C_l rolling-moment coefficient, $\frac{\text{Rolling moment}}{qS_b d_b}$

$C_{l_\beta} = \left(\frac{\Delta C_l}{\Delta \beta}\right)_{\beta=0^\circ,5^\circ}$, per degree

C_m pitching-moment coefficient, $\frac{\text{Pitching moment}}{qS_b d_b}$

$C_{m_{(L/D)_{max}}}$ pitching-moment coefficient at maximum lift-drag ratio

C_{m_α} longitudinal stability parameter, per degree

C_N normal-force coefficient, $\frac{\text{Normal force}}{qS_b}$

C_n yawing-moment coefficient, $\frac{\text{Yawing moment}}{qS_b d_b}$

$C_{n_\beta} = \left(\frac{\Delta C_n}{\Delta \beta}\right)_{\beta=0^\circ,5^\circ}$, per degree

C_Y side-force coefficient, $\frac{\text{Side force}}{qS_b}$

$C_{Y_\beta} = \left(\frac{\Delta C_Y}{\Delta \beta}\right)_{\beta=0^\circ,5^\circ}$, per degree

d_b base diameter for circular-cross-section body, ft

FR body effective fineness ratio, $\frac{l}{2\sqrt{a_{max} b_{max}}}$

L/D lift-drag ratio

l total body length, ft

M Mach number

q	free-stream dynamic pressure, lb/sq ft
r	local radius, ft
$r_b = \frac{d_b}{2}$	
S_b	body base area $\pi\left(\frac{d_b}{2}\right)^2$ or πab, 0.08727 sq ft
S_{cross}	cross-sectional areas of body, sq ft
S_p	body projected planform area, sq ft
S_{wet}	wetted area of body (excluding base area), sq ft
x	longitudinal coordinate of body, ft
$\frac{x_{cp}}{l}$	longitudinal center-of-pressure location ($\alpha = 0^o$), $\frac{x_{cg}}{l} - \frac{C_{m_\alpha}}{C_{N_\alpha}}\left(\frac{d_b}{l}\right)$
α	angle of attack, deg
$\alpha_{(L/D)_{max}}$	angle of attack at maximum lift-drag ratio, deg
β	angle of sideslip, deg
ϕ	angle of roll about body-ordinate reference line, deg

Subscripts:

cg	center of gravity
max	maximum
min	minimum

MODELS

Three-view drawings of the body shapes used in the present investigation are shown in figure 1, along with pertinent geometric characteristics and configuration designations. The cross-section ellipticity is designated by the letters A, B, and C for a/b ratios of 1.0, 1.5, and 2.0, respectively. The numbers 3, 5, and 7 preceding configuration cross-section designations indicate the fineness ratio; whereas, the numbers 1, 2, and 4 used as subscripts on the cross-section designations have the following meaning:

1. Symmetrical body, $\phi = 0^\circ$

2. Negatively displaced body, $\phi = 0^\circ$

4. Symmetrical body, $\phi = 90^\circ$

For example, the designation $7C_1$ indicates the symmetrical $a/b = 2.00$ body with a fineness ratio of 7 at $\phi = 0^\circ$ whereas the designation $7C_4$ indicates the same body rotated through a roll angle $\phi = 90^\circ$.

Photographs of the circular bodies of revolution $3A_1$, $3A_2$, and $5A_1$ and of the elliptic bodies $5C_1$ and $7C_1$ are shown in figure 2. The body shapes of the investigation had effective fineness ratios of 3, 5, and 7. (Effective fineness ratio is defined as $\frac{l}{2\sqrt{a_{max}b_{max}}}$.) Cross-section radii of the bodies of revolution followed a 2/3-power contour $r = r_b(x/l)^{2/3}$, which represents a low-wave-drag body shape at hypersonic speeds. In varying the body cross sections from circular to elliptic, the body projected planforms were made to conform to the 2/3-power variation by holding the longitudinal cross-sectional area distributions ($\pi r^2 = \pi ab$) for a given fineness ratio constant, as shown in figure 3. All bodies of the investigation had a constant base area which has been used as the reference area.

The ratio of the horizontal-axis length to the vertical-axis length of 0.50 was obtained by rotation of the symmetrical $a/b = 2.00$ bodies through a roll angle of $\phi = 90^\circ$. Coordinates of the symmetrical bodies are given in table I, and pertinent geometric characteristics of each configuration tested are presented in table II.

The negatively displaced bodies were formed by displacing each cross section vertically so that the uppermost point of each section lay on the body reference line. (See fig. 1.)

TESTS, CORRECTIONS, AND ACCURACY

The investigation was conducted in the low Mach number test section of the Langley Unitary Plan wind tunnel at Mach numbers of 1.50, 1.90, 2.36, and 2.86 while maintaining a constant Reynolds number per foot of 2.75×10^6. The stagnation temperature was 150° F, and the dewpoint, measured at stagnation conditions, was held below -30° F to assure negligible condensation effects.

Forces and moments were measured by use of a sting-mounted six-component strain-gage balance. The range of angle of attack varied from -5° to a maximum of 29° at 0° and 5° of sideslip.

Transition was fixed on all bodies tested at a distance of 0.5 inch aft of the body apex by a circumferential band of carborundum grains having a nominal diameter of 0.0117 inch.

Corrections have been applied to the angle of attack to account for flow angularity and deflection of the balance and sting under load. Drag coefficients presented herein are for total drag of the configuration, including base drag. No attempt was made to correct the drag data for the induced effects of sting-support interference. Support-interference effects for elliptic cones and bodies of revolution at high subsonic to supersonic speeds are indicated in references 8 to 10. The maximum deviation of the local Mach number in the test medium is ±0.015. The estimated accuracies of the angle of attack and the coefficients, based on the balance calibration and repeatability of the data, are within the following limits, as based on the base area:

α, deg	±0.100
C_L	±0.040
C_D	±0.040
C_m	±0.040
C_l	±0.008
C_n	+0.040
C_Y	±0.040

PRESENTATION OF RESULTS

Typical schlieren photographs for several of the configurations tested are presented as figure 4. The basic longitudinal aerodynamic characteristics of the bodies tested are presented in figures 5 to 12, and the lateral-directional characteristics are presented in figures 13 to 16 as functions of angle of attack. Table III is included to aid in locating basic data figures for the various bodies tested. Summary plots of the longitudinal and lateral aerodynamic characteristics obtained from the basic data are presented as functions of Mach number and horizontal-to-vertical axis ratio in figures 17 and 18.

Longitudinal Aerodynamic Characteristics

The effects of increasing the ratio a/b on the longitudinal characteristics of the symmetrical bodies with fineness ratios of 3, 5, and 7 at Mach numbers from 1.50 to 2.86 are presented in figures 5 to 8. Large increases in C_L, C_M, and C_D for given positive angles of attack are realized from increasing the horizontal-to-vertical axis ratio from 0.50 to 2.00 ($a/b = 2.00$, $\phi = 90^\circ$ to $a/b = 2.00$, $\phi = 0^\circ$) at a Mach number of 1.50, for each fineness ratio (fig. 5(a)). These gains are primarily a result of the increases in planform area for a given fineness ratio. The increases in body lift-curve slope (fig. 17(a)), although primarily due to the increases in planform area, also result from increases in body aspect ratio, $a/b = 2.0$, $\phi = 90^\circ$ to $a/b = 2.0$, $\phi = 0^\circ$. This effect of increased lift-curve slope due to aspect ratio for a given fineness ratio is better illustrated in figure 17(e) where each value

of lift-curve slope is based on the individual body planform area and is presented as a function of Mach number.

The variation of minimum drag coefficient (fig. 17(a)) for the symmetrical bodies indicates an increasing trend in $C_{D_{min}}$ with increasing a/b ($\phi = 0^\circ$ or 90°) with the coefficients based on a constant reference area. However, noticeable increases in $C_{D_{min}}$ for increasing a/b ($\phi = 90^\circ$) and slight decreases in $C_{D_{min}}$ for increasing a/b ($\phi = 0^\circ$) are shown when the coefficient is based on the individual body planform (fig. 17(e)). These small changes in $C_{D_{min}}$ due to increasing a/b ($\phi = 0^\circ$) at a given Mach number and the fact that $(L/D)_{max}$ is constantly increasing with the increases in a/b ($\phi = 0^\circ$) indicate that drag due to lift is lower for the higher a/b ratio bodies ($\phi = 0^\circ$) as a result of the increases in lift-curve slope (figs. 17(a) and 17(b)). With regard to the variations of C_L, C_D, and C_m with increasing angle of attack, similar analysis may be made for the configurations discussed for Mach numbers of 1.90, 2.36, and 2.86; the nonlinear trends noted, however, in the C_L and C_m variations with α at the lower Mach numbers tend to disappear as Mach number is increased. Compare figures 8(a) and 8(c) with figures 5(a) and 5(c), respectively.

A rearward shift in body center-of-pressure location is generally indicated when the horizontal-to-vertical axis ratio is increased from 0.50 to 2.00 (figs. 17(a) to 17(d)). Similar results were found at low subsonic speeds on a 2/3-power body having a fineness ratio of 10 (ref. 6). It is interesting to note that there are little or no effects of increasing Mach number on the longitudinal center-of-pressure location for any of the fineness ratios.

Comparisons of the variations of C_L, C_D, C_m, and L/D for the negatively displaced bodies and the symmetrical bodies (a/b = 1.00 or 2.00, $\phi = 0^\circ$) are presented in figures 9 to 12. It is interesting to note that the variations of C_L and C_D with increasing angle of attack for the negatively displaced bodies are shifted by an increment in angle of attack approximately equal to the angle between a line connecting the body apex and the centroid of the body base and the angle-of-attack reference line. With regard to the pitching-moment characteristics, however, the angular shift in C_m due to body displacement is higher than that noted for the C_L and C_D curves; this indicates a slight effect of body displacement on the variation of C_m with α. These effects on C_m were also found when comparing circular and elliptical displaced and symmetrical bodies with a fineness ratio of 10 at subsonic speeds (ref. 6). The displacement in C_L and C_D, however, results in considerable reduction in the angle of attack for $(L/D)_{max}$ with only slight effects on $C_{L_{(L/D)_{max}}}$ or $C_{m_{(L/D)_{max}}}$. (See fig. 18.) The largest reductions in $\alpha_{(L/D)_{max}}$ occur for the lowest fineness-ratio body having a/b = 1.00 (fig. 18, configurations $3A_1$ and $3A_2$), since this body has the largest angular displacement of cross sections.

Lateral-Directional Characteristics

Comparisons of the lateral-directional characteristics of the symmetrical fineness-ratio-3 bodies with variations in a/b ratio from 1.00 to 2.00 ($\phi = 0^\circ$ and 90°) are presented in figure 13. Generally, an increase in directional stability results from changing $a/b = 2.00$, $\phi = 90^\circ$ to $a/b = 2.00$, $\phi = 0^\circ$, with accompanying increases in effective dihedral with increasing a/b ratio (fig. 13(a)). Similar results are indicated at all test Mach numbers, as shown in figures 13(b) to 13(d). However, directional instability was noted about the present moment reference point for all configurations with a fineness ratio of 3. The data for the $a/b = 2.00$, $\phi = 90^\circ$ configuration ($3C_4$) indicate static instability in roll throughout the test angle-of-attack range; however, positive effective dihedral was exhibited by body $3B_1$ or $3C_1$ ($a/b = 1.50$ or 2.00, $\phi = 0^\circ$) throughout the test angle-of-attack range at all Mach numbers.

Data obtained as a result of increasing fineness ratio from 3 to 7 generally indicate large reductions in directional stability for all a/b ratios, and considerable irregularity in the variation of C_{n_β} with increasing angle of attack is noted above approximately 8° for all Mach numbers (fig. 14). This irregularity suggests the possibility of dynamic stability problems similar to those experienced with high-fineness-ratio sharp-nosed bodies at subsonic speeds, as reported in reference 6. These irregularities were noted for the present configurations with the highest fineness ratio 7 at all test Mach numbers (figs. 14(b) to 14(d)).

With regard to the rolling-moment characteristics of the fineness-ratio-7 bodies, the resulting variations of C_{l_β} with increasing angle of attack are similar to the results obtained on the fineness-ratio-3 bodies, except for the large increases in the magnitude of the derivative C_{l_β} at all test Mach numbers.

The effects of body displacement on the lateral-directional characteristics of the configurations with fineness ratio 3 are presented in figure 15. Little or no effect on the variation of C_{n_β} or C_{l_β} with angle of attack is indicated for the range of test Mach numbers. Similar effects of displacement at angles of attack below 4° are exhibited for the bodies with a fineness ratio of 7 at all test Mach numbers. (See fig. 16.) Rather large variations in C_{n_β} result from body displacement at the higher angles of attack, however. It is interesting to note that displacing the body cross sections below a common reference line increased directional instability for the $a/b = 1.00$ body, whereas large reductions in directional instability were noted for the $a/b = 2.00$, $\phi = 0^\circ$ body ($7C_1$ and $7C_2$) at the high angles of attack.

SUMMARY OF RESULTS

An investigation has been conducted in the Langley Unitary Plan wind tunnel to determine the effects of cross-sectional ellipticity and fineness ratio on the longitudinal and lateral aerodynamic characteristics of a series of 2/3-power low-wave-drag bodies at Mach numbers from 1.50 to 2.86. Reynolds number per foot was held constant at 2.75×10^6 over the Mach number range of this investigation. The angle-of-attack range was from approximately -5° to 29° at 0° and 5° of sideslip. Results of the investigation may be summarized in the following observations:

1. Increasing body major-to-minor axis ratio, with the major axis horizontal, results in large increases in the lift, drag, and pitching-moment coefficients and lift-drag ratios at positive angles of attack and at all test Mach numbers. Successive increases in major-to-minor axis ratio, with the major axis horizontal, resulted in gains in lift-curve slope for bodies of the same fineness ratio when the coefficients were based on the respective body projected planform areas; generally, only slight changes in the minimum-drag characteristics of the bodies were noted.

2. A rearward shift in the body center-of-pressure location is generally indicated when the horizontal-to-vertical axis ratio is increased from 0.50 to 2.00. Little or no effects of increasing Mach number on the center-of-pressure location of a given body were shown.

3. For the moment-reference-point location of the present investigation, each of the symmetrical bodies exhibited static directional instability at all test Mach numbers, and reductions in the level of directional instability were indicated for increases in major-to-minor axis ratio, with the major axis horizontal. These reductions in directional instability were generally accompanied by corresponding increases in the variation of positive effective dihedral with increasing angle of attack for the Mach number range of the present investigation.

Langley Research Center,
National Aeronautics and Space Administration,
Langley Station, Hampton, Va., March 20, 1964.

REFERENCES

1. Rainey, Robert W., compiler: Summary of Aerodynamic Characteristics of Low-Lift-Drag-Ratio Reentry Vehicles From Subsonic to Hypersonic Speeds. NASA TM X-588, 1961.

2. Dennis, David H., and Edwards, George G.: The Aerodynamic Characteristics of Some Lifting Bodies. NASA TM X-376, 1960.

3. Armstrong, William O.: Hypersonic Aerodynamic Characteristics of Several Series of Lifting Bodies Applicable to Reentry Vehicle Design. NASA TM X-536, 1961.

4. Carleton, W. E., and Matthews, R. K.: The Aerodynamic Characteristics of Three Elliptical-Cone Lifting Bodies at Transonic Speeds. AEDC-TDR-63-53 (Contract No. AF 40(600)-1000), Arnold Eng. Dev. Center, Apr. 1963.

5. Jorgensen, Leland H.: Elliptic Cones Alone and With Wings at Supersonic Speeds. NACA Rep. 1376, 1958. (Supersedes NACA TN 4045.)

6. Spencer, Bernard, Jr., and Phillips, W. Pelham: Effects of Cross-Section Shape on the Low-Speed Aerodynamic Characteristics of a Low-Wave-Drag Hypersonic Body. NASA TN D-1963, 1963.

7. Fuller, Dennis E., Shaw, David S., and Wassum, Donald L.: Effect of Cross-Section Shape on the Aerodynamic Characteristics of Bodies at Mach Numbers From 2.50 to 4.63. NASA TN D-1620, 1963.

8. Stivers, Louis S., Jr., and Levy, Lionel L., Jr.: Effects of Sting-Support Diameter on the Base Pressures of an Elliptic Cone at Mach Numbers From 0.60 to 1.40. NASA TN D-354, 1961.

9. Fuller, Dennis E., and Langhans, Victor E.: Effect of Afterbody Geometry and Sting Diameter on the Aerodynamic Characteristics of Slender Bodies at Mach Numbers From 1.57 to 2.86. NASA TN D-2042, 1963.

10. Perkins, Edward W.: Experimental Investigation of the Effects of Support Interference on the Drag of Bodies of Revolution at a Mach Number of 1.5. NACA TN 2292, 1951. (Supersedes NACA RM A8B05.)

TABLE I.- DESIGN BODY ORDINATES FOR SYMMETRICAL BODIES

x, in.	a/b = 1.00	a/b = 1.50		a/b = 2.00	
	r, in.	a, in.	b, in.	a, in.	b, in.
		Fineness-ratio-3 body			
0	0	0	0	0	0
2	.606	.742	.495	.857	.428
4	.961	1.178	.785	1.360	.680
6	1.260	1.543	1.029	1.782	.891
8	1.526	1.869	1.246	2.158	1.079
10	1.771	2.169	1.446	2.505	1.252
12	2.000	2.449	1.633	2.828	1.414
		Fineness-ratio-5 body			
0	0	0	0	0	0
2	.431	.528	.352	.609	.305
4	.684	.838	.558	.967	.484
6	.896	1.098	.732	1.267	.634
8	1.086	1.300	.886	1.535	.768
10	1.260	1.543	1.029	1.782	.891
12	1.423	1.742	1.162	2.012	1.006
14	1.577	1.931	1.287	2.229	1.115
16	1.724	2.111	1.407	2.437	1.219
18	1.864	2.283	1.522	2.636	1.318
20	2.000	2.449	1.633	2.828	1.414
		Fineness-ratio-7 body			
0	0	0	0	0	0
2	.344	.422	.281	.488	.244
4	.547	.669	.446	.774	.387
6	.716	.877	.585	1.014	.507
8	.868	1.063	.708	1.228	.614
10	1.007	1.233	.822	1.424	.712
12	1.137	1.392	.928	1.608	.804
14	1.260	1.543	1.029	1.782	.891
16	1.377	1.687	1.125	1.948	.974
18	1.490	1.825	1.216	2.107	1.054
20	1.598	1.957	1.305	2.261	1.130
22	1.703	2.086	1.391	2.409	1.204
24	1.805	2.210	1.474	2.553	1.276
26	1.904	2.331	1.554	2.693	1.346
28	2.000	2.449	1.633	2.828	1.414

TABLE II.- BODY GEOMETRIC CHARACTERISTICS

$[S_b = 12.5626$ sq in.$]$

Body shape	A	Volume, cu in.	S_{wet}, sq in.	S_p, sq in.	$\frac{S_{wet}}{S_b}$	$\frac{S_p}{S_b}$
Fineness-ratio-3 body						
A_1	0.5556	64.6667	92.0880	28.7994	7.3303	2.2924
B_1	.6803		94.9104	35.2649	7.5550	2.8071
C_1	.7857		100.3968	40.7281	7.9917	3.2420
C_4	.3928		100.3968	20.3641	7.9917	1.6210
Fineness-ratio-5 body						
A_1	0.3334	107.9550	151.1424	47.9990	12.0311	3.8207
B_1	.4082		155.7936	58.7748	12.4013	4.6784
C_1	.4713		164.7792	67.8706	13.1166	5.4025
C_4	.2357		164.7792	33.9353	13.1166	2.7012
Fineness-ratio-7 body						
A_1	0.2381	151.0000	211.1616	67.1987	16.8087	5.3490
B_1	.2862		217.6416	83.8135	17.3245	6.6716
C_1	.3367		230.2128	95.0189	18.3252	7.5635
C_4	.1683		230.2128	47.5095	18.3252	3.7818

TABLE III.- INDEX FOR BASIC DATA FIGURES

Body shape	Fineness ratio	a/b	Displacement	ϕ, deg	Mach number	Figure
Longitudinal data						
A_1, B_1, C_1, and C_4	3, 5, and 7	1.00, 1.50, and 2.00	0	0 and 90	1.50	5
	3, 5, and 7	1.00, 1.50, and 2.00	0	0 and 90	1.90	6
	3, 5, and 7	1.00, 1.50, and 2.00	0	0 and 90	2.36	7
	3, 5, and 7	1.00, 1.50, and 2.00	0	0 and 90	2.86	8
A_1, A_2, C_1, and C_2	3 and 7	1.00 and 2.00	0 and negative	0	1.50	9
	3 and 7	1.00 and 2.00	0 and negative	0	1.90	10
	3 and 7	1.00 and 2.00	0 and negative	0	2.36	11
	3 and 7	1.00 and 2.00	0 and negative	0	2.86	12
Lateral data						
A_1, B_1, C_1, and C_4	3	1.00 and 2.00	0	0 and 90	1.50 to 2.86	13
	7	1.00 and 2.00	0	0 and 90	1.50 to 2.86	14
A_1, A_2, C_1, and C_2	3	1.00 and 2.00	0 and negative	0	1.50 to 2.86	15
	7	1.00 and 2.00	0 and negative	0	1.50 to 2.86	16

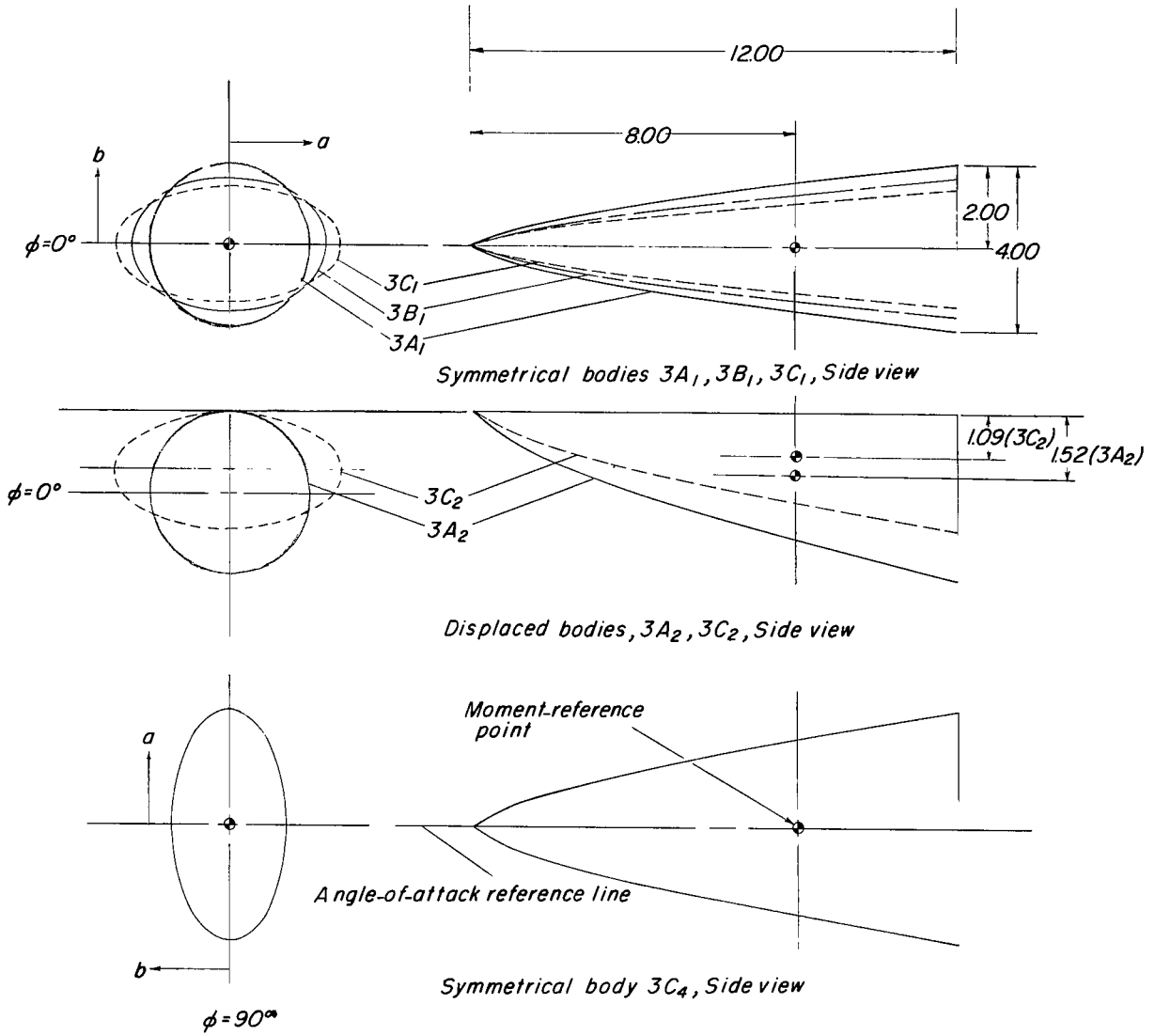

(a) Bodies with fineness ratio 3.

Figure 1.- Geometric characteristics of various bodies tested. All dimensions are in inches unless otherwise noted.

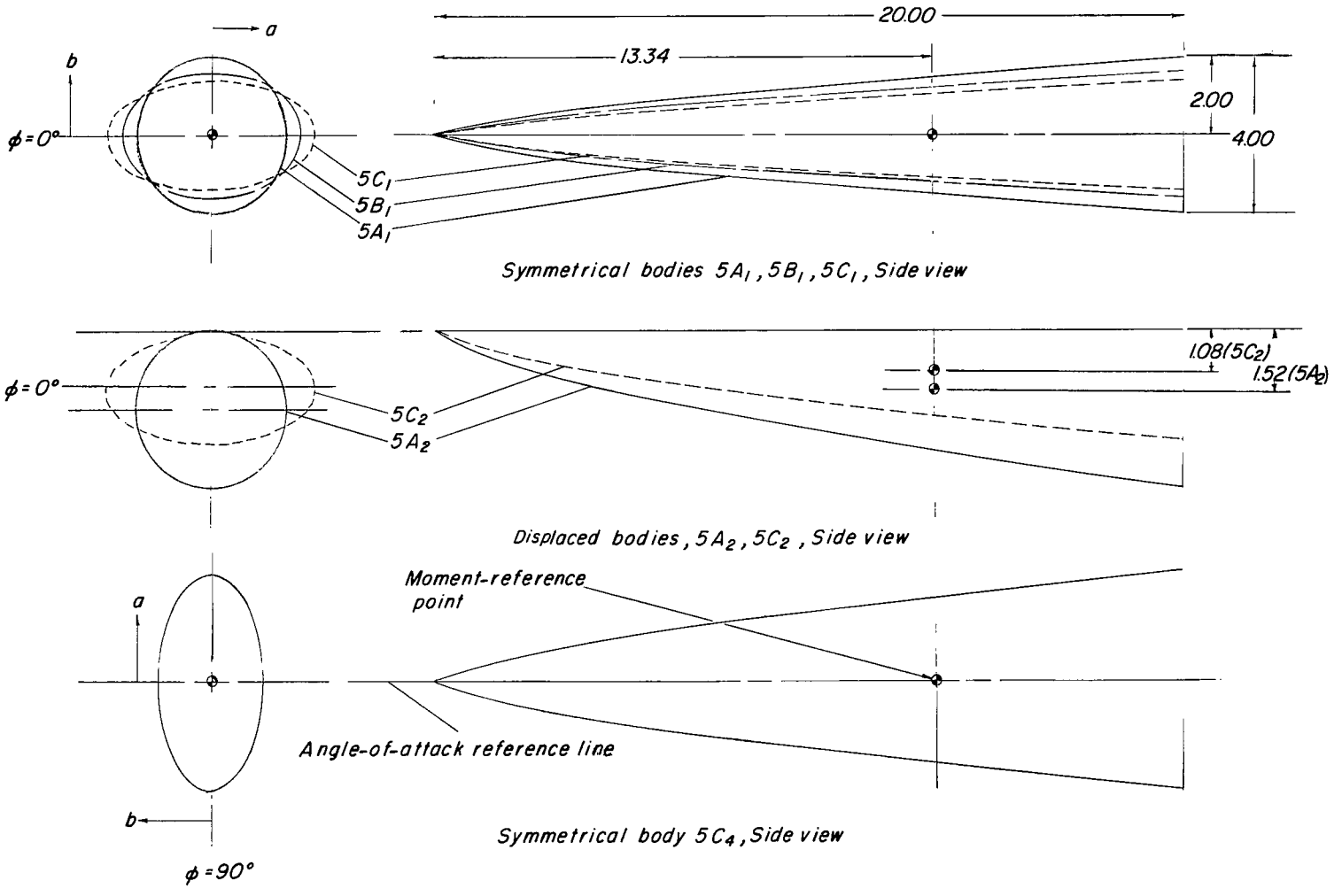

(b) Bodies with fineness ratio 5.

Figure 1.- Continued.

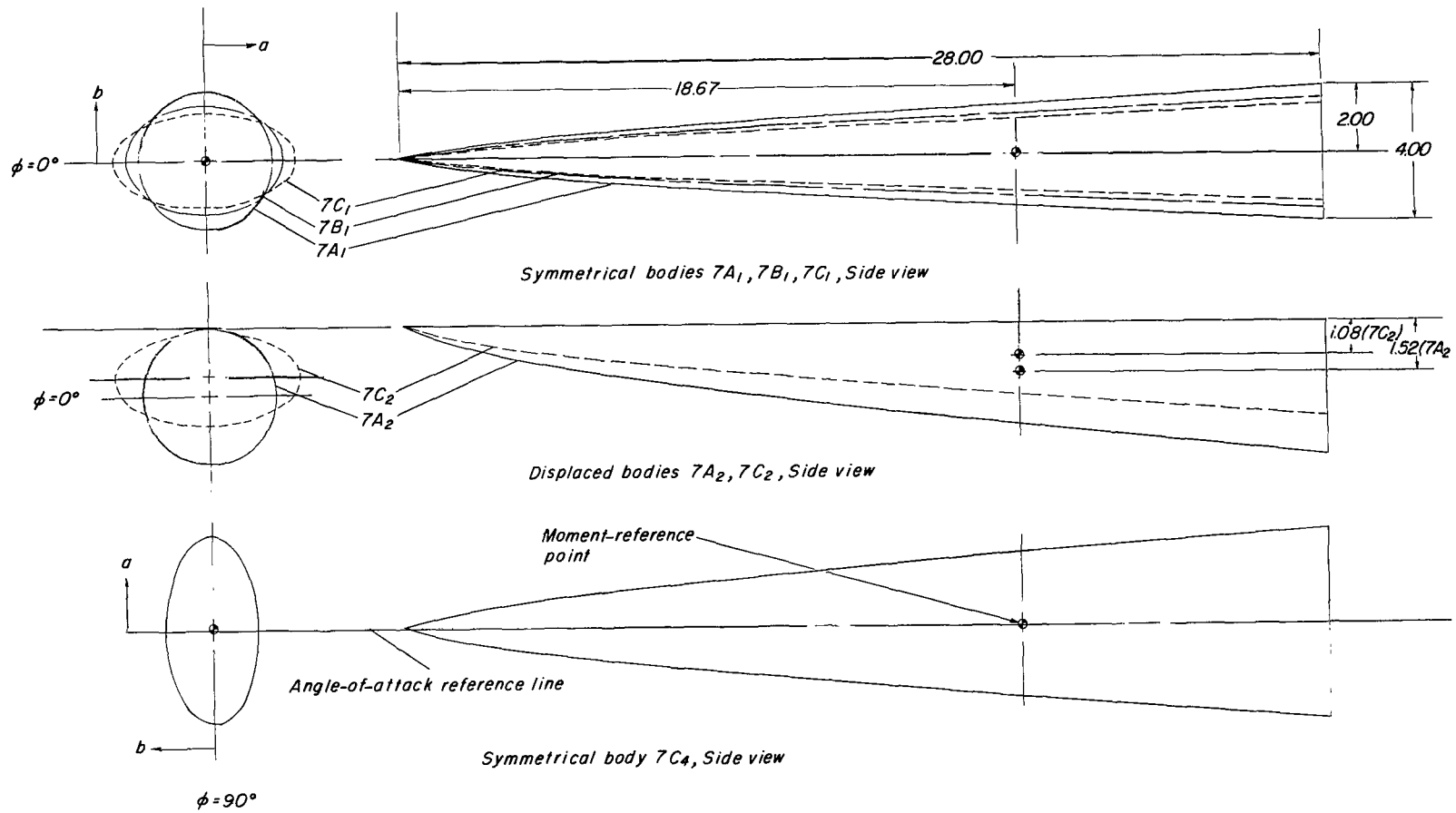

(c) Bodies with fineness ratio 7.

Figure 1.- Concluded.

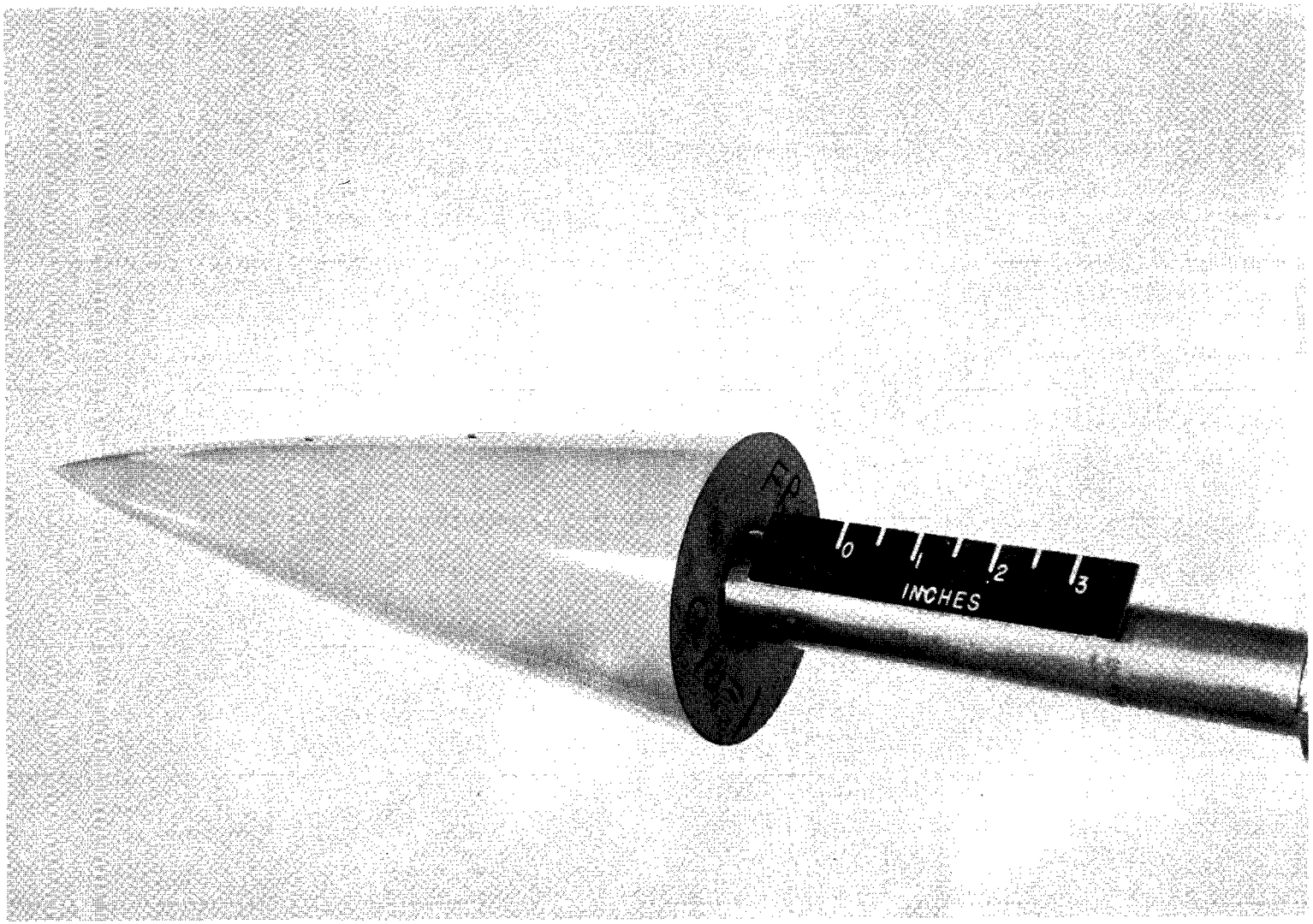

(a) Body $3A_1$. L-63-490

Figure 2.- Photographs of some of body configurations tested.

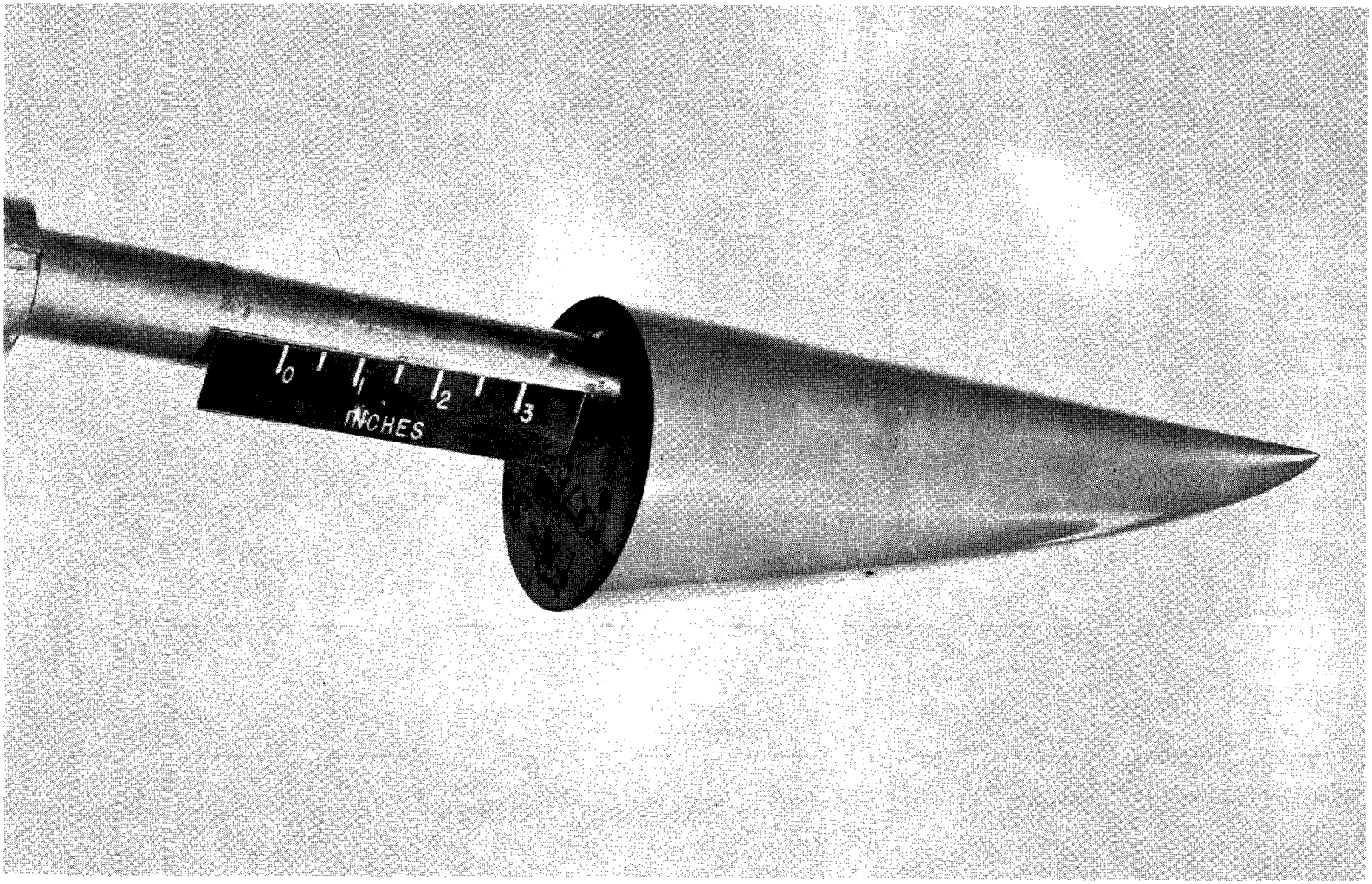

(b) Body $3A_2$.

L-64-3031

Figure 2.- Continued.

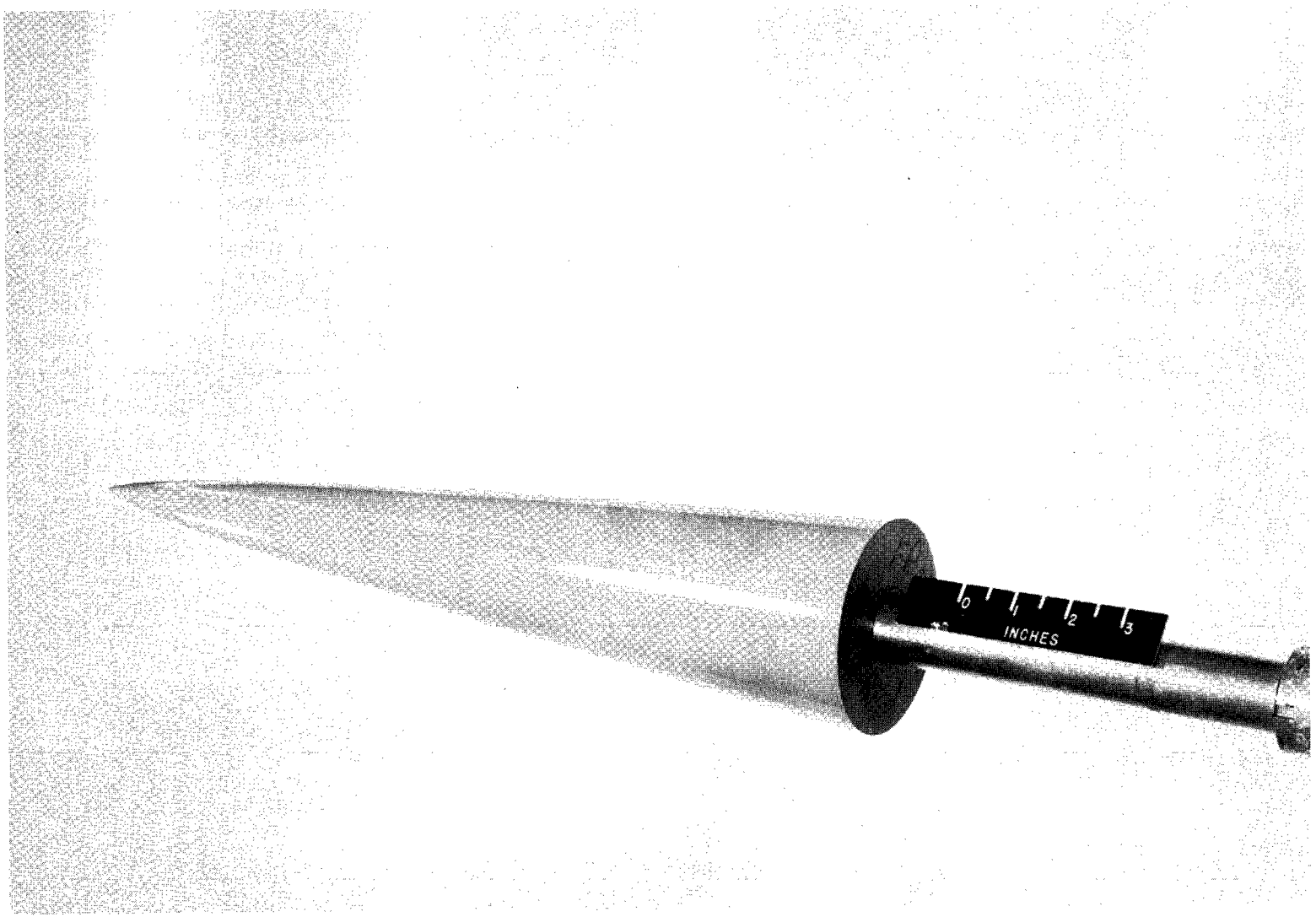

(c) Body $5A_1$. L-63-487

Figure 2.- Continued.

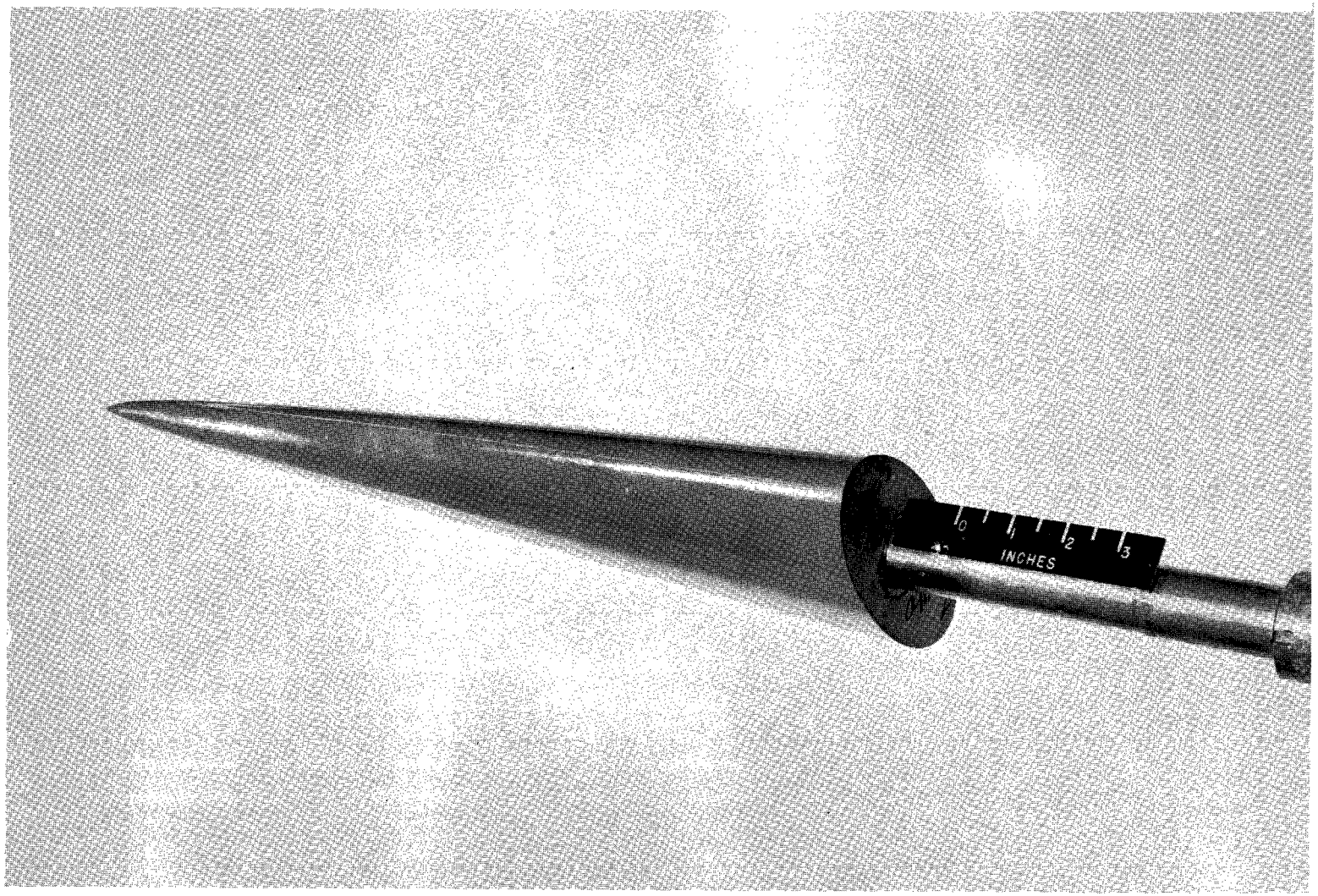

(d) Body $5C_1$. L-63-483

Figure 2.- Continued.

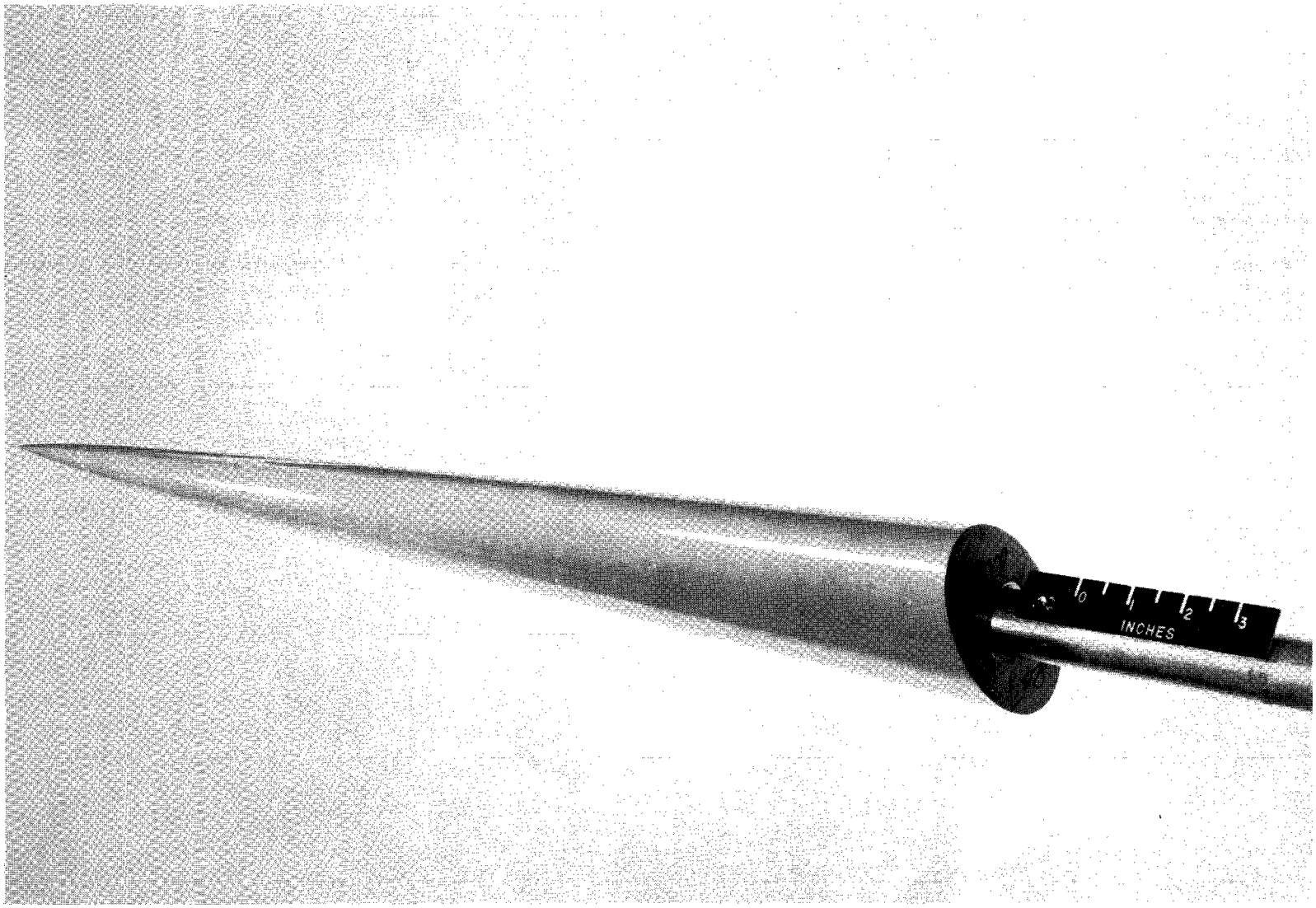

(e) Body $7C_1$.

L-63-486

Figure 2.- Concluded.

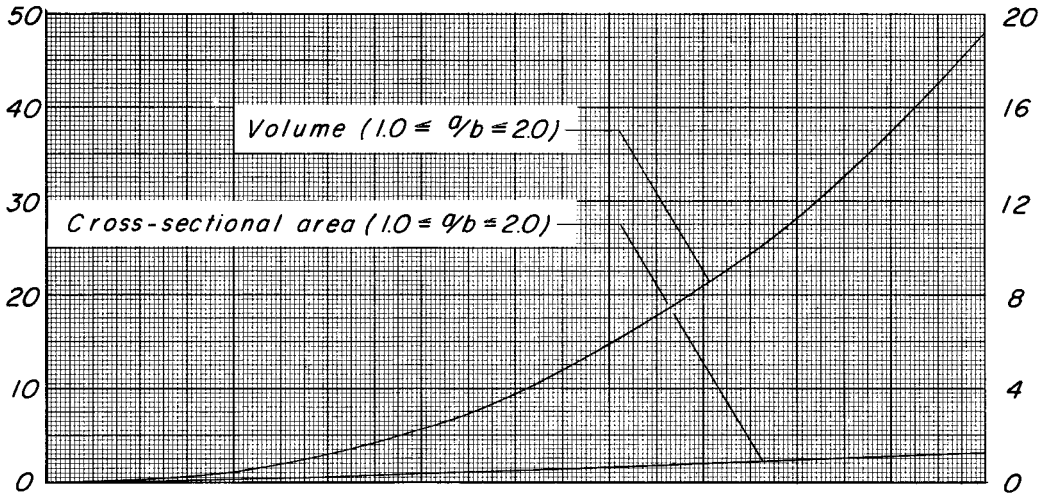

(a) FR = 7.

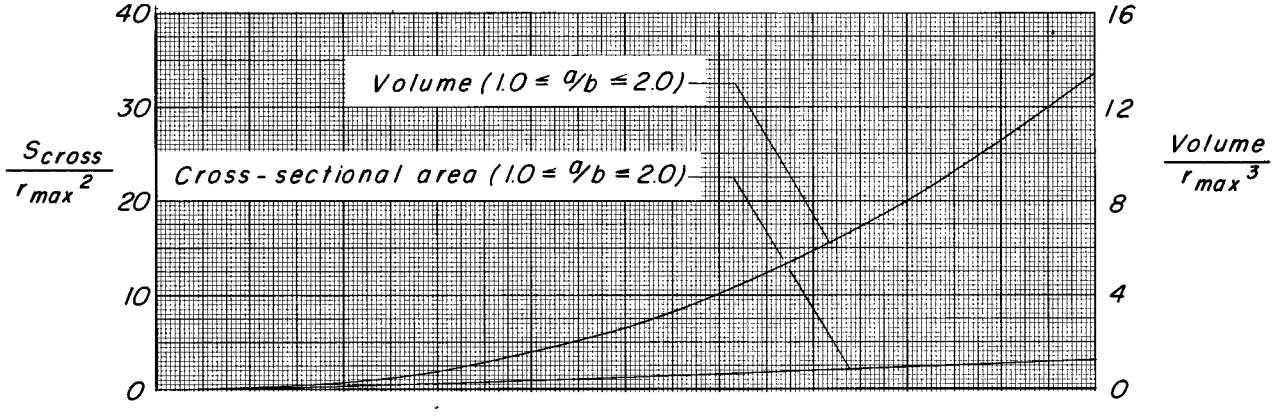

(b) FR = 5.

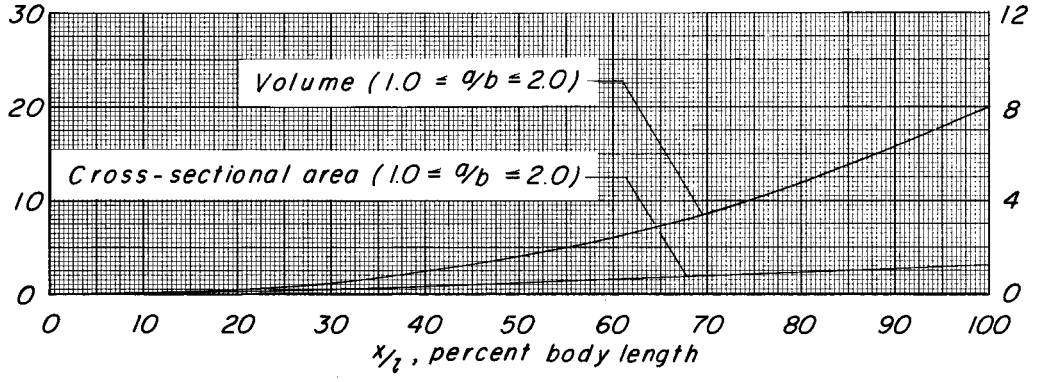

(c) FR = 3.

Figure 3.- Variation of cross-sectional area, volume, and wetted area distributions with body length.

$\alpha = 0.58°$

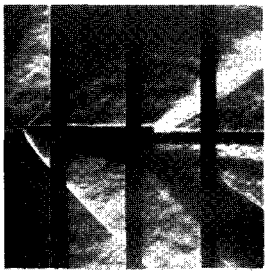

$\alpha = 0.97°$

$\alpha = 10.75°$

Symmetrical

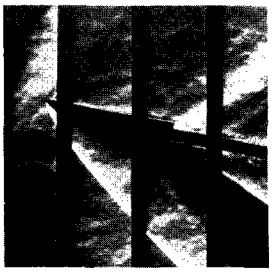

$\alpha = 10.86°$

Displaced

(a) M = 1.50; FR = 3; a/b = 1.0; $\phi = 0°$.

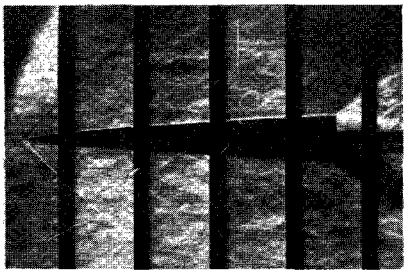

$\alpha = 0.56°$

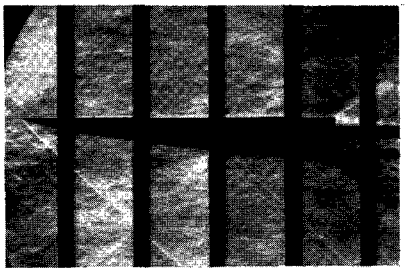

$\alpha = 0.65°$

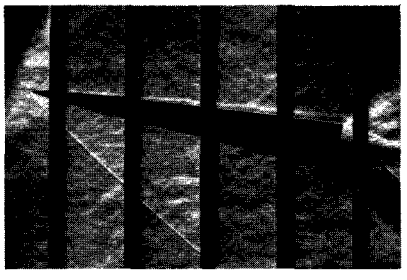

$\alpha = 10.80°$

Symmetrical

$\alpha = 10.89°$

Displaced

(b) M = 1.50; FR = 7; a/b = 1.0; $\phi = 0°$. L-64-3032

Figure 4.- Typical schlieren photographs.

$\alpha = 1.45°$

$\alpha = 1.49°$

$\alpha = 11.58°$

Symmetrical

$\alpha = 11.72°$

Displaced

(c) M = 2.36; FR = 3; a/b = 1.0; $\phi = 0°$.

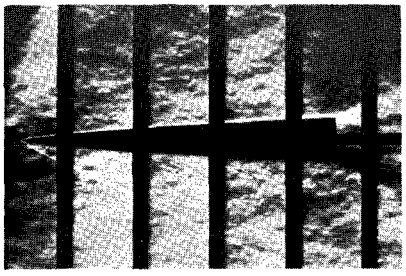

$\alpha = 0.00°$

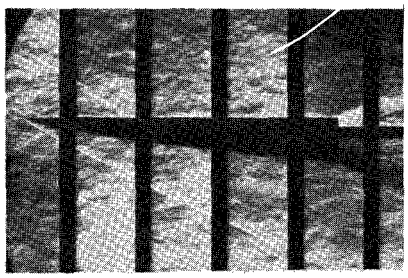

$\alpha = 1.62°$

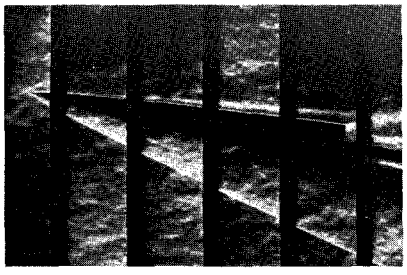

$\alpha = 10.00°$

Symmetrical

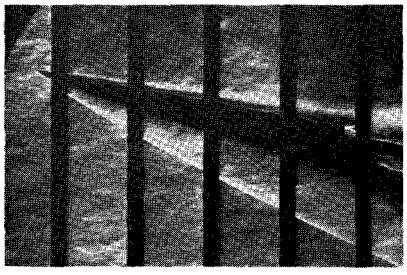

$\alpha = 12.00°$

Displaced

(d) M = 2.36; FR = 7; a/b = 1.0; $\phi = 0°$. L-64-3033

Figure 4.- Concluded.

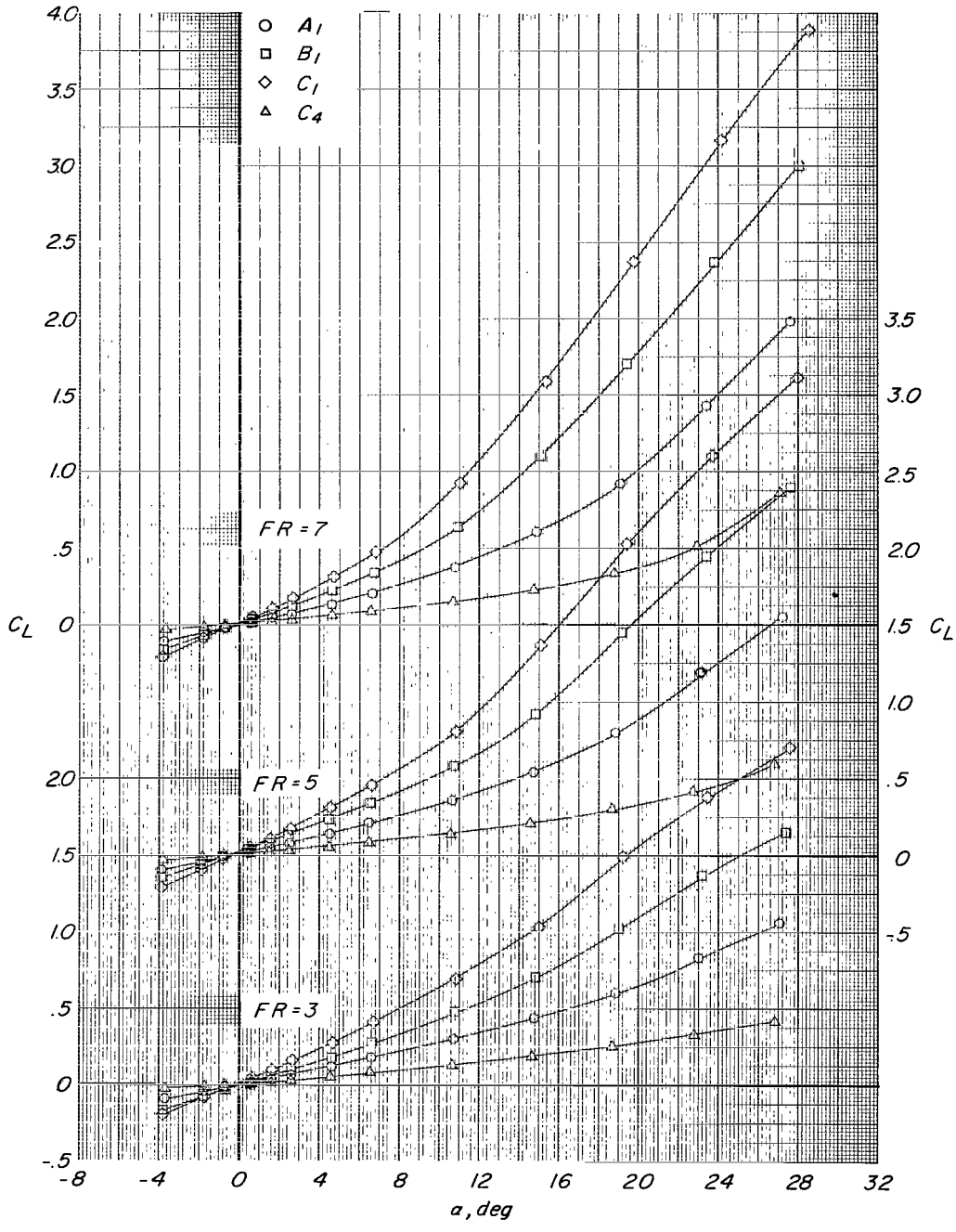

(a) Variation of C_L with α.

Figure 5.- Effects of increasing a/b ratio from 1.00 to 2.00 at $\phi = 0^\circ$ and 90° on longitudinal aerodynamic characteristics for symmetrical bodies with fineness ratios 3, 5, and 7 at Mach number 1.50.

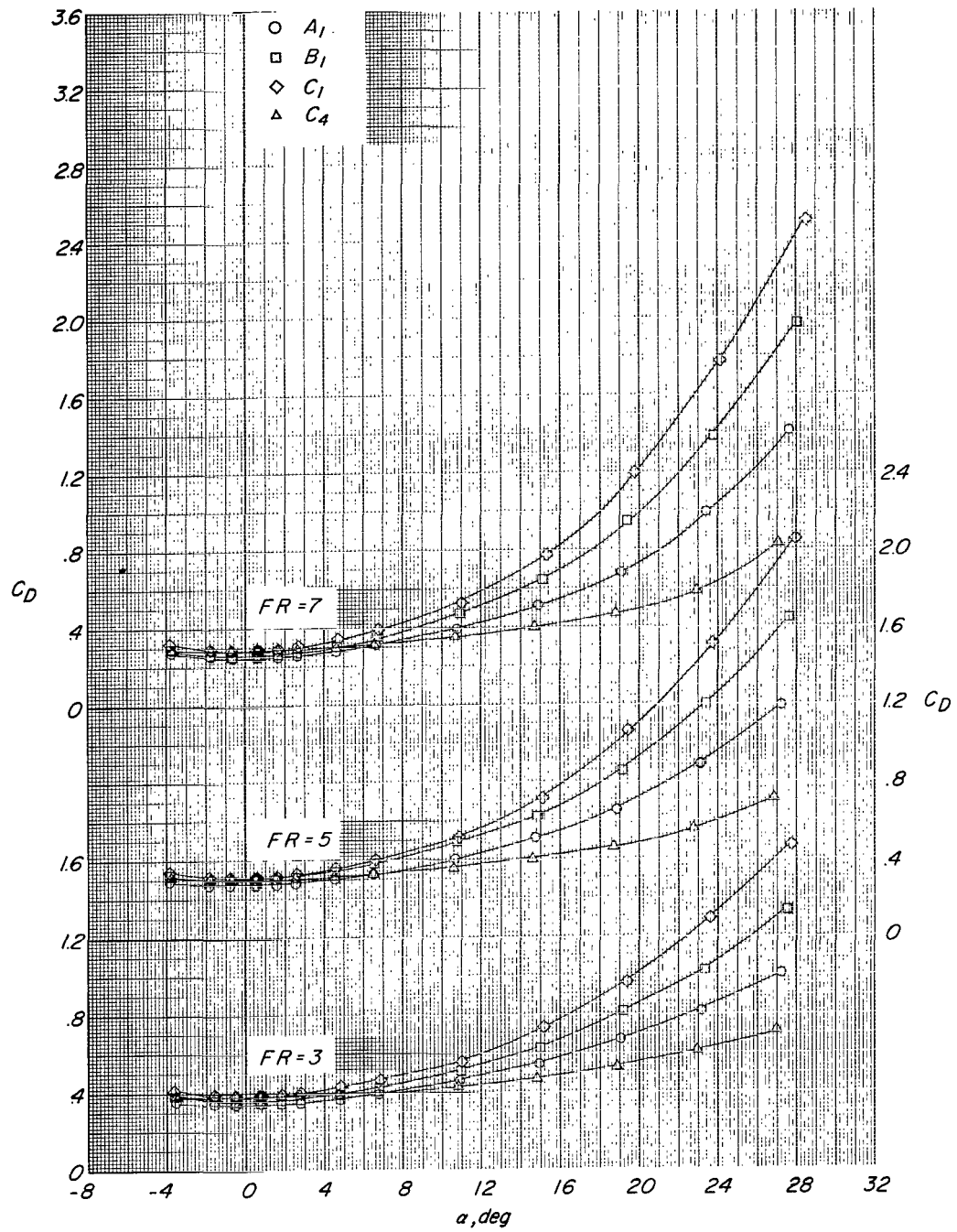

(b) Variation of C_D with α.

Figure 5.- Continued.

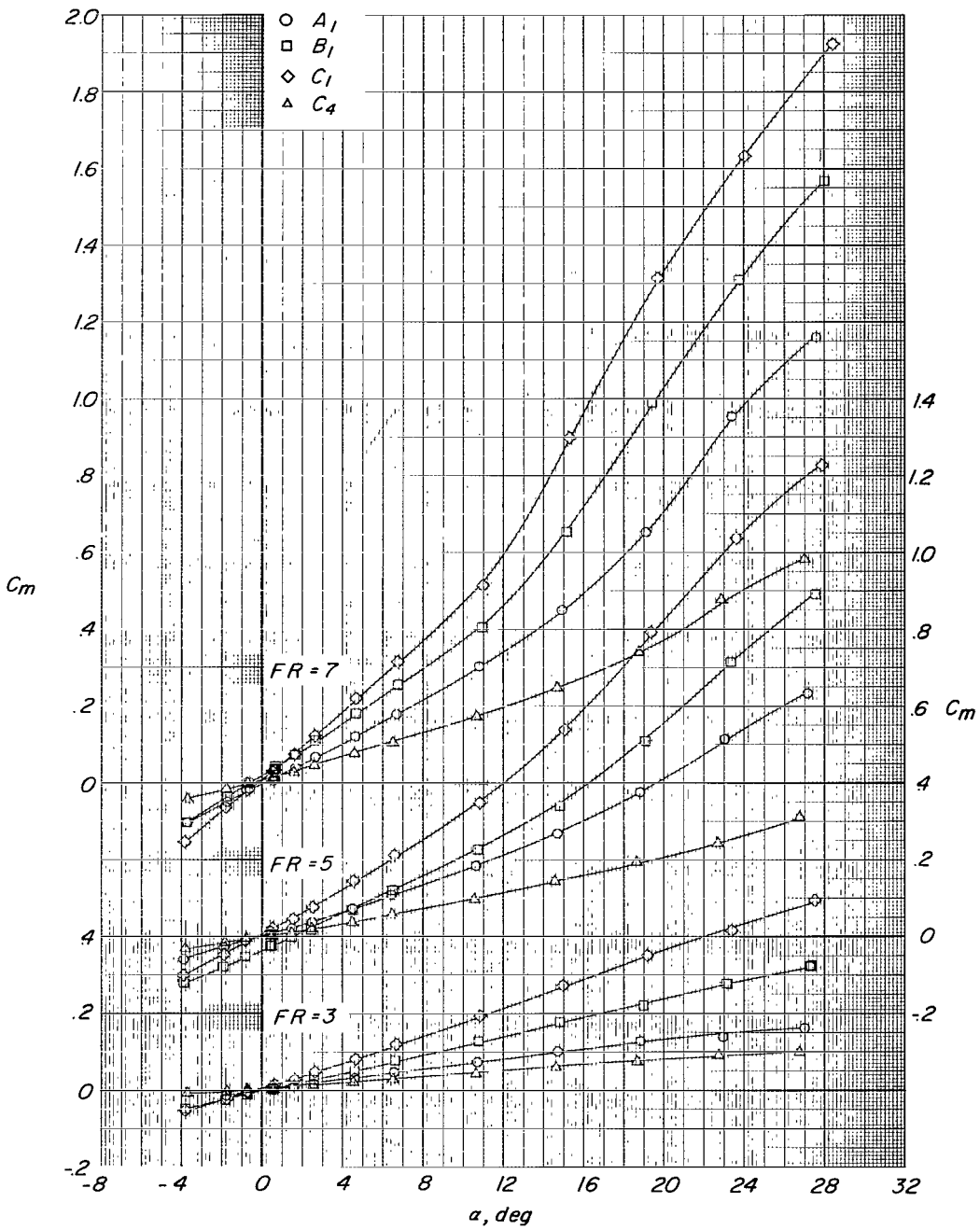

(c) Variation of C_m with α.

Figure 5.- Continued.

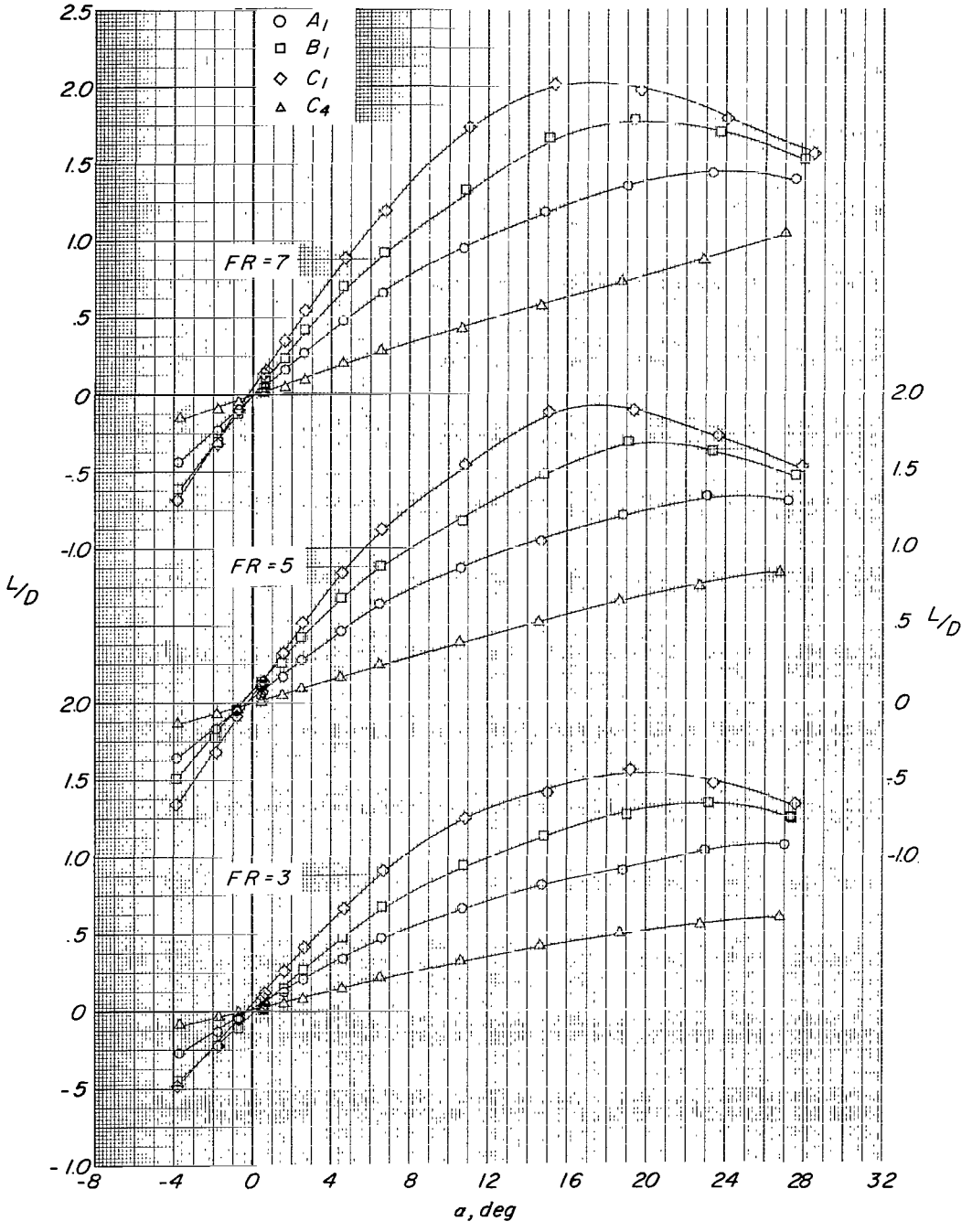

(d) Variation of L/D with α.

Figure 5.- Concluded.

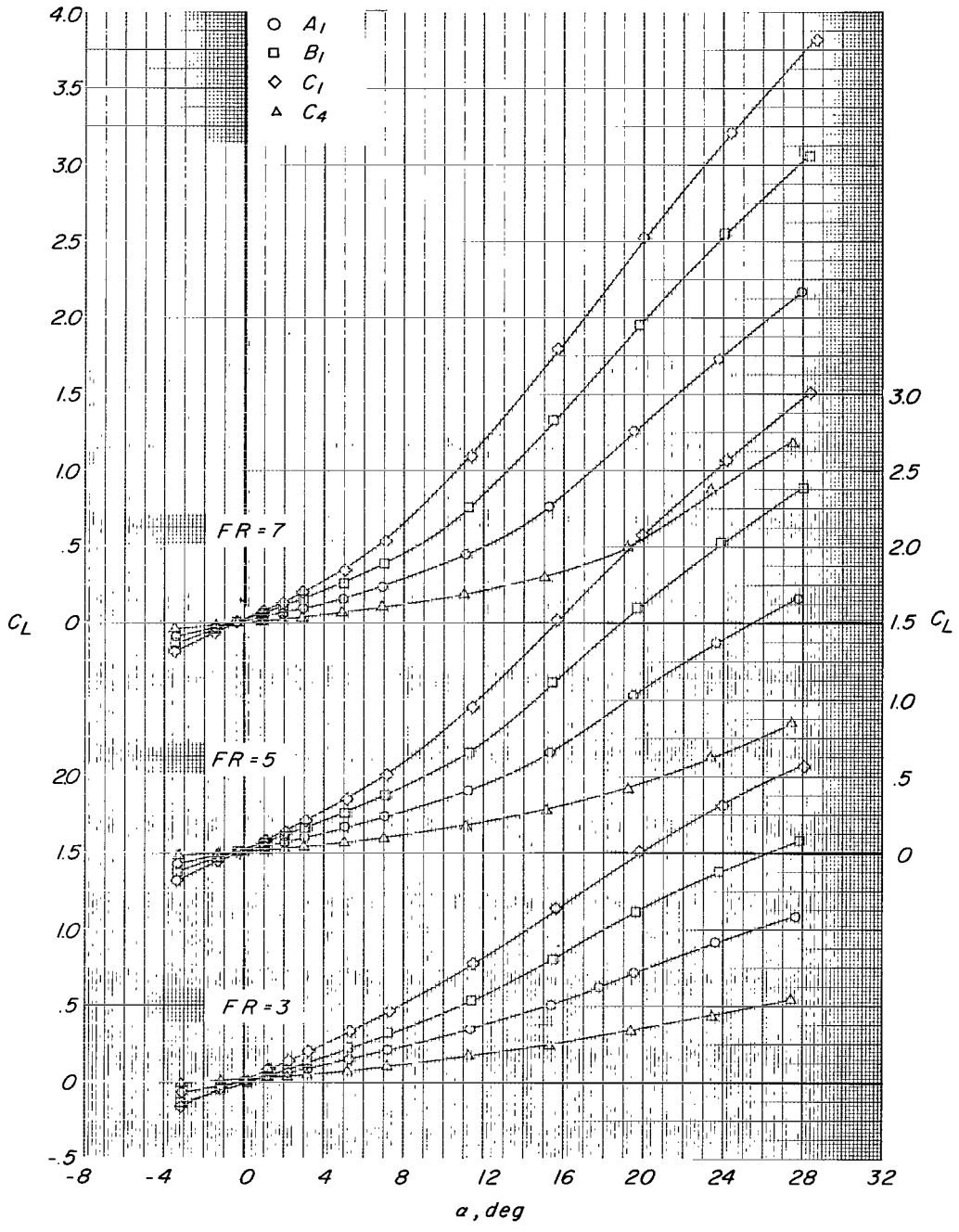

(a) Variation of C_L with α.

Figure 6.- Effects of increasing a/b ratio from 1.00 to 2.00 at $\phi = 0^\circ$ and 90° on longitudinal aerodynamic characteristics for symmetrical bodies with fineness ratios 3, 5, and 7 at Mach number 1.9.

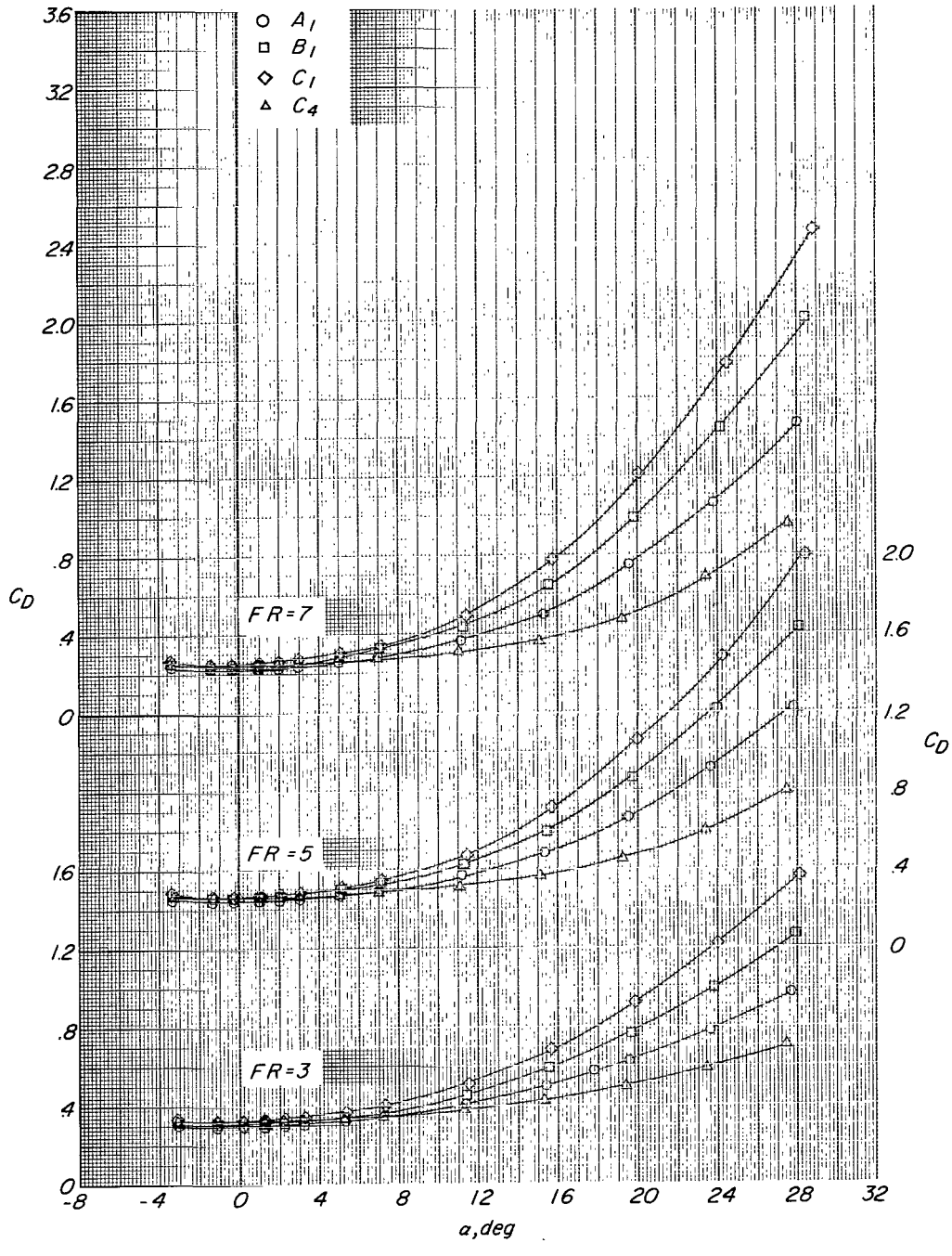

(b) Variation of C_D with α.

Figure 6.- Continued.

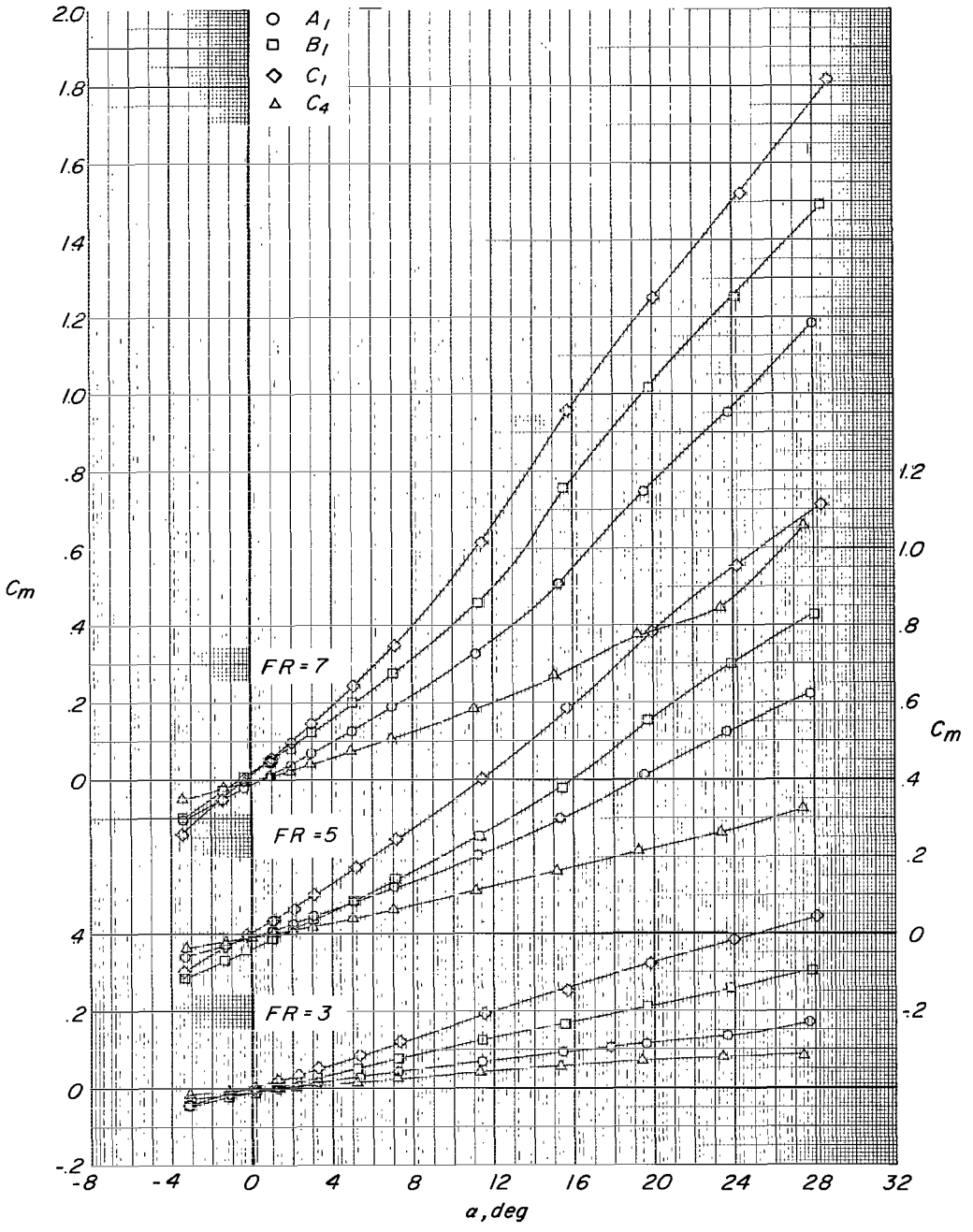

(c) Variation of C_m with α.

Figure 6.- Continued.

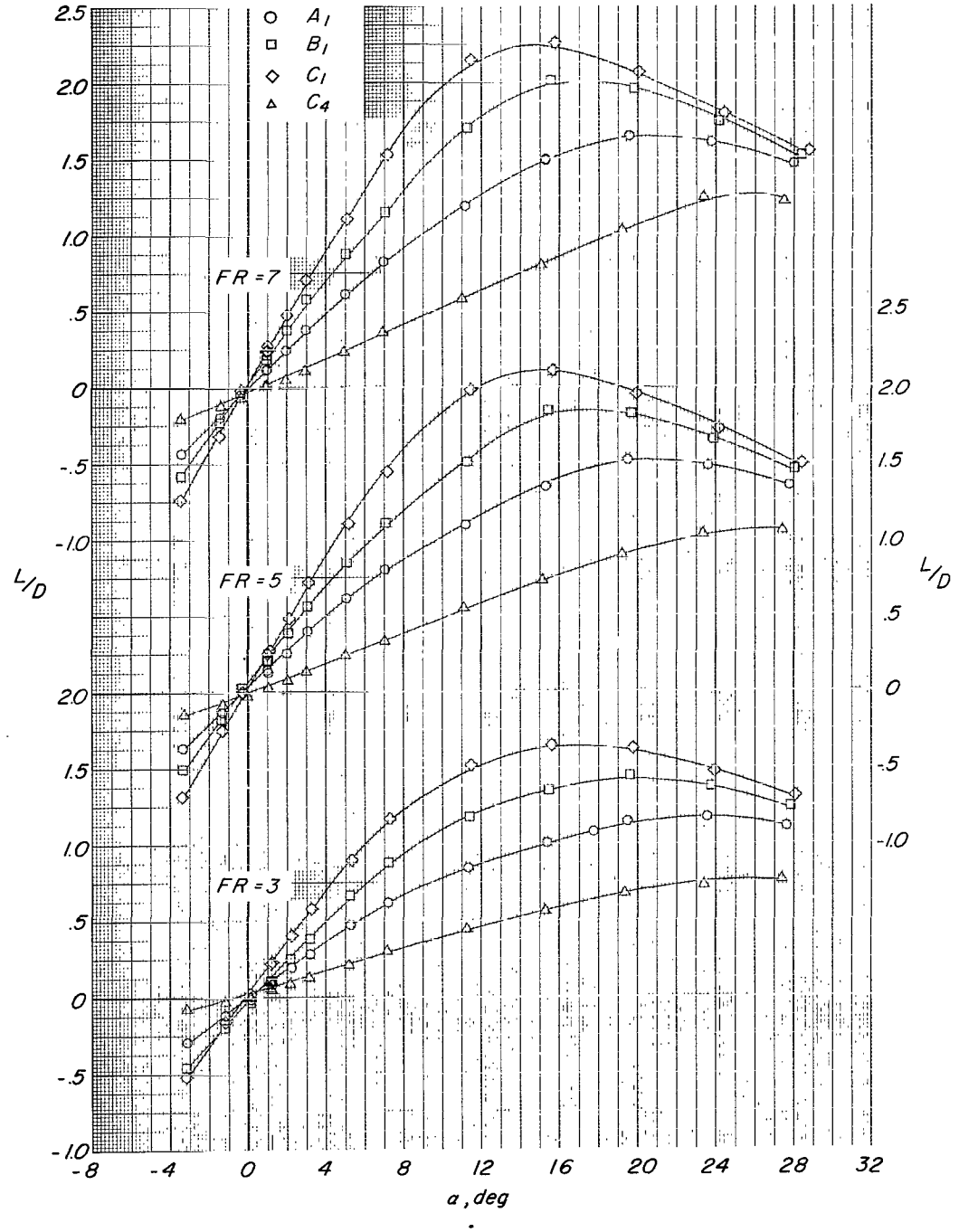

(d) Variation of L/D with α.

Figure 6.- Concluded.

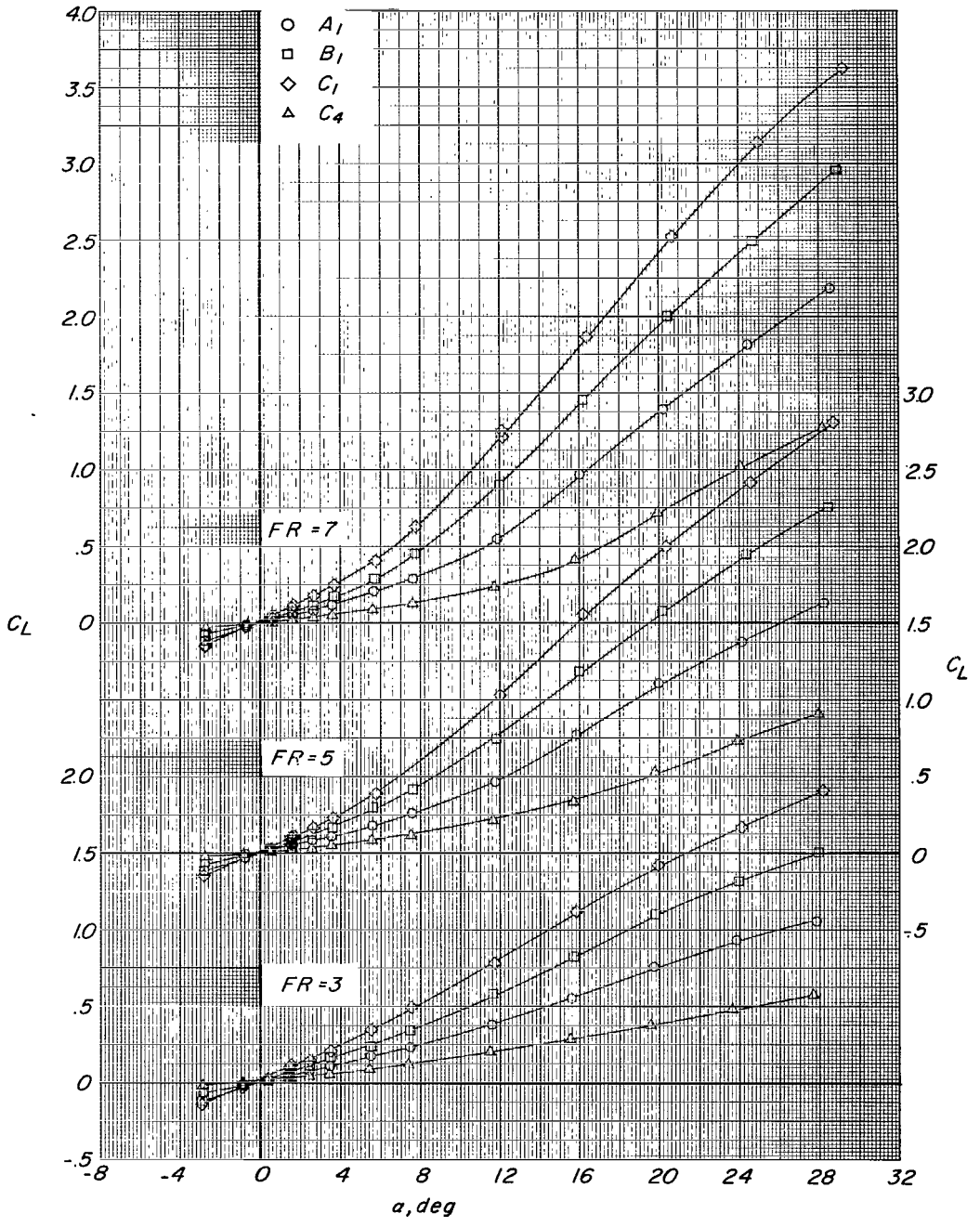

(a) Variation of C_L with α.

Figure 7.- Effects of increasing a/b ratio from 1.00 to 2.00 at $\phi = 0^\circ$ and 90° on longitudinal aerodynamic characteristics for symmetrical bodies with fineness ratios 3, 5, and 7 at Mach number 2.36.

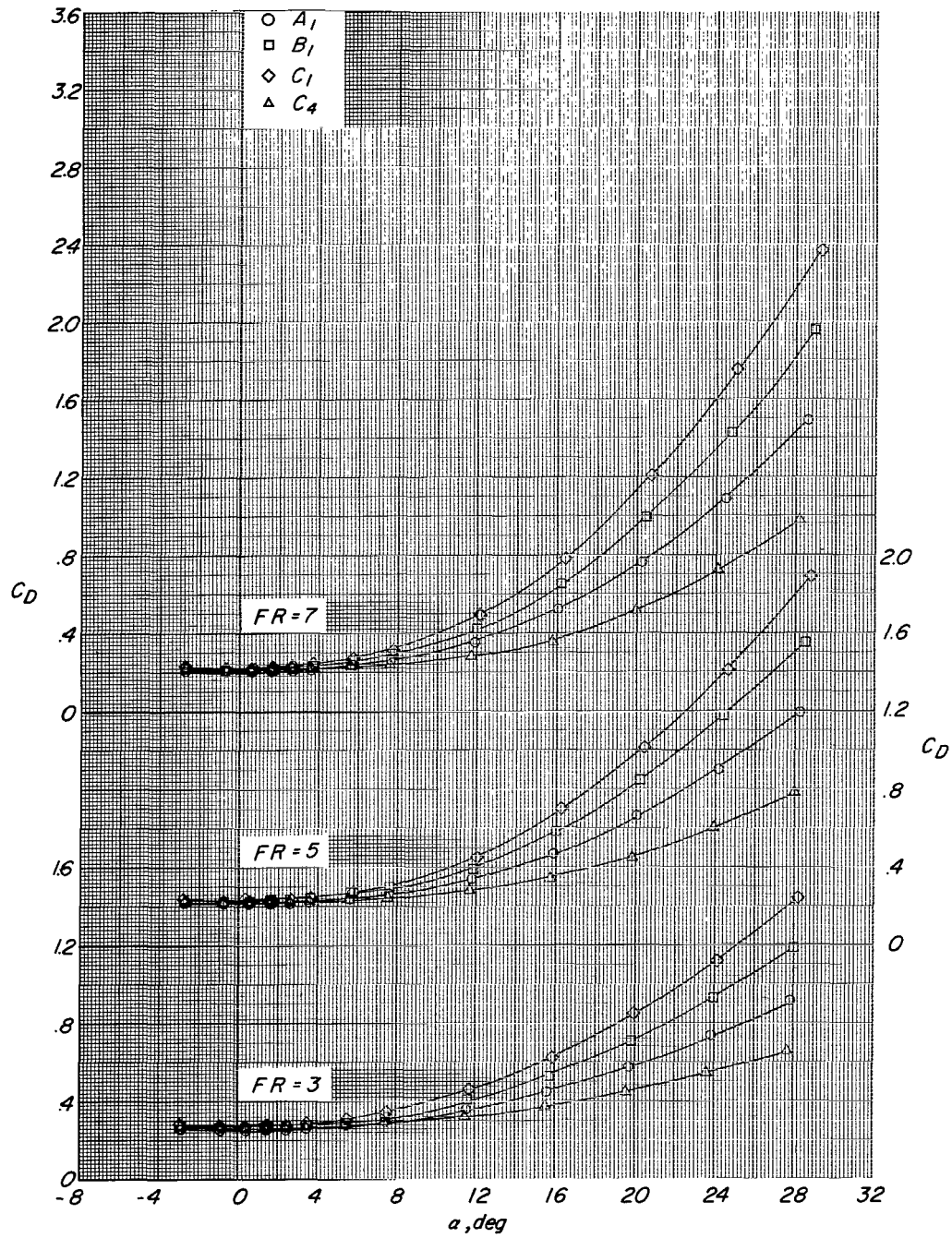

(b) Variation of C_D with α.

Figure 7.- Continued.

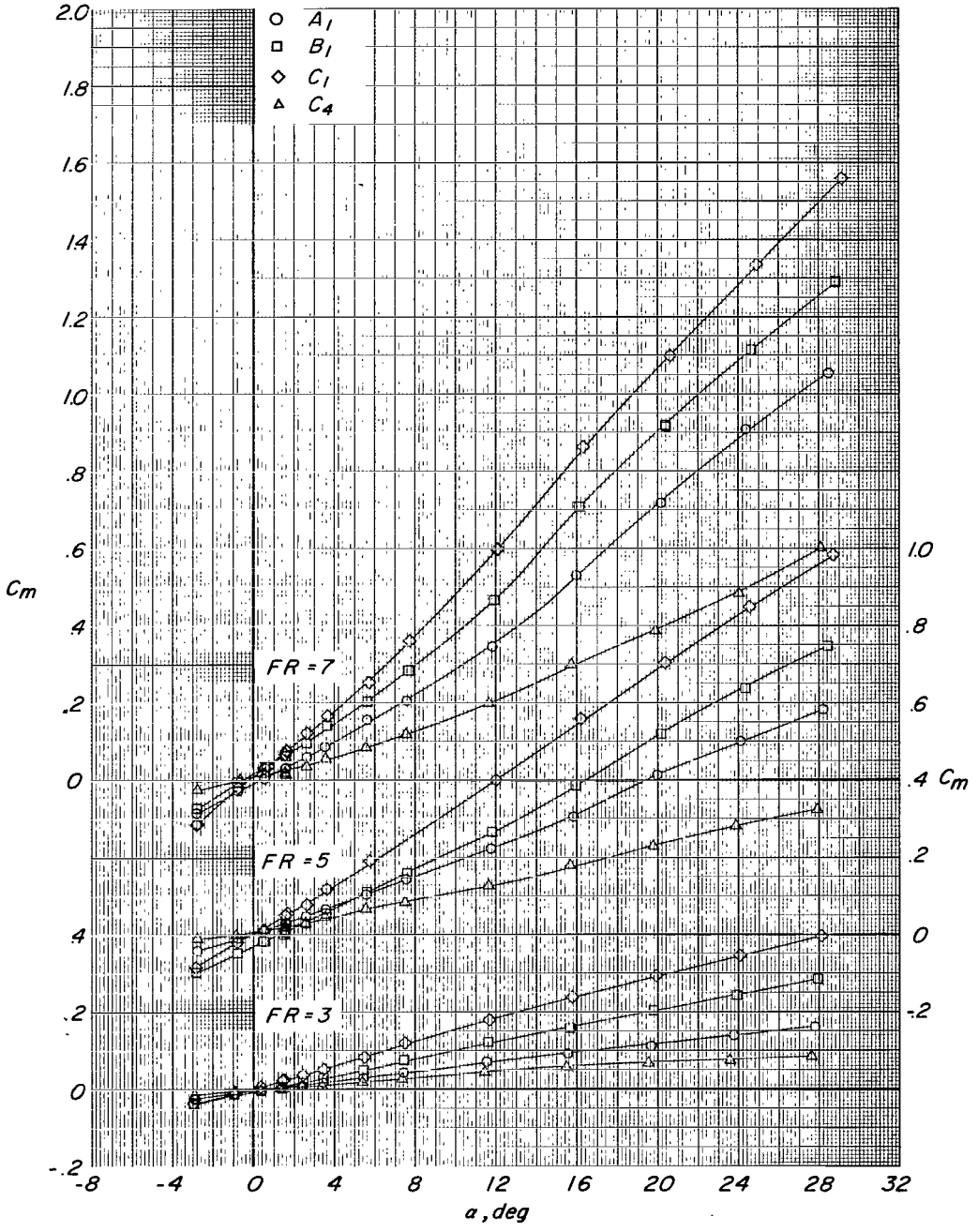

(c) Variation of C_m with α.

Figure 7.- Continued.

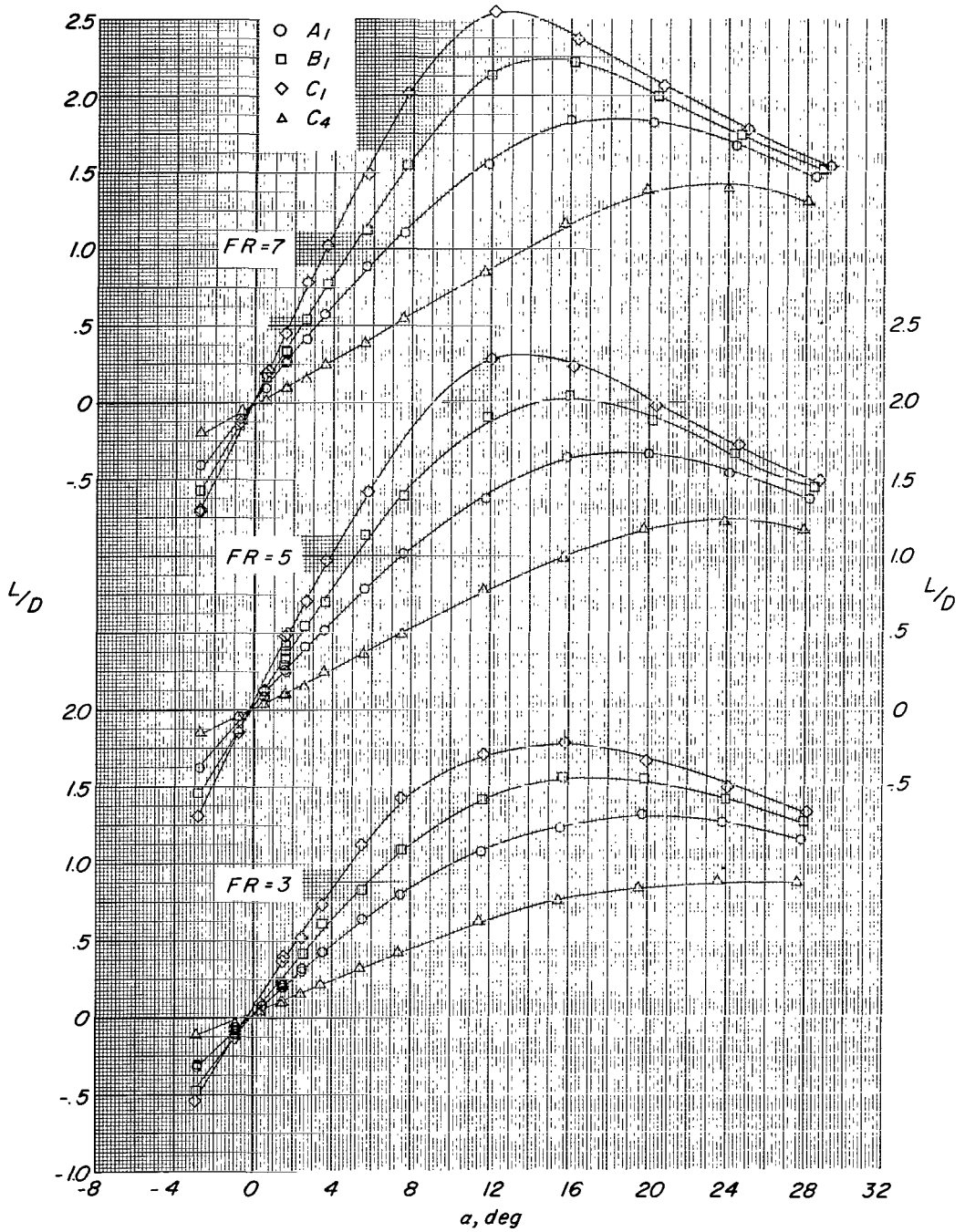

(d) Variation of L/D with α.

Figure 7.- Concluded.

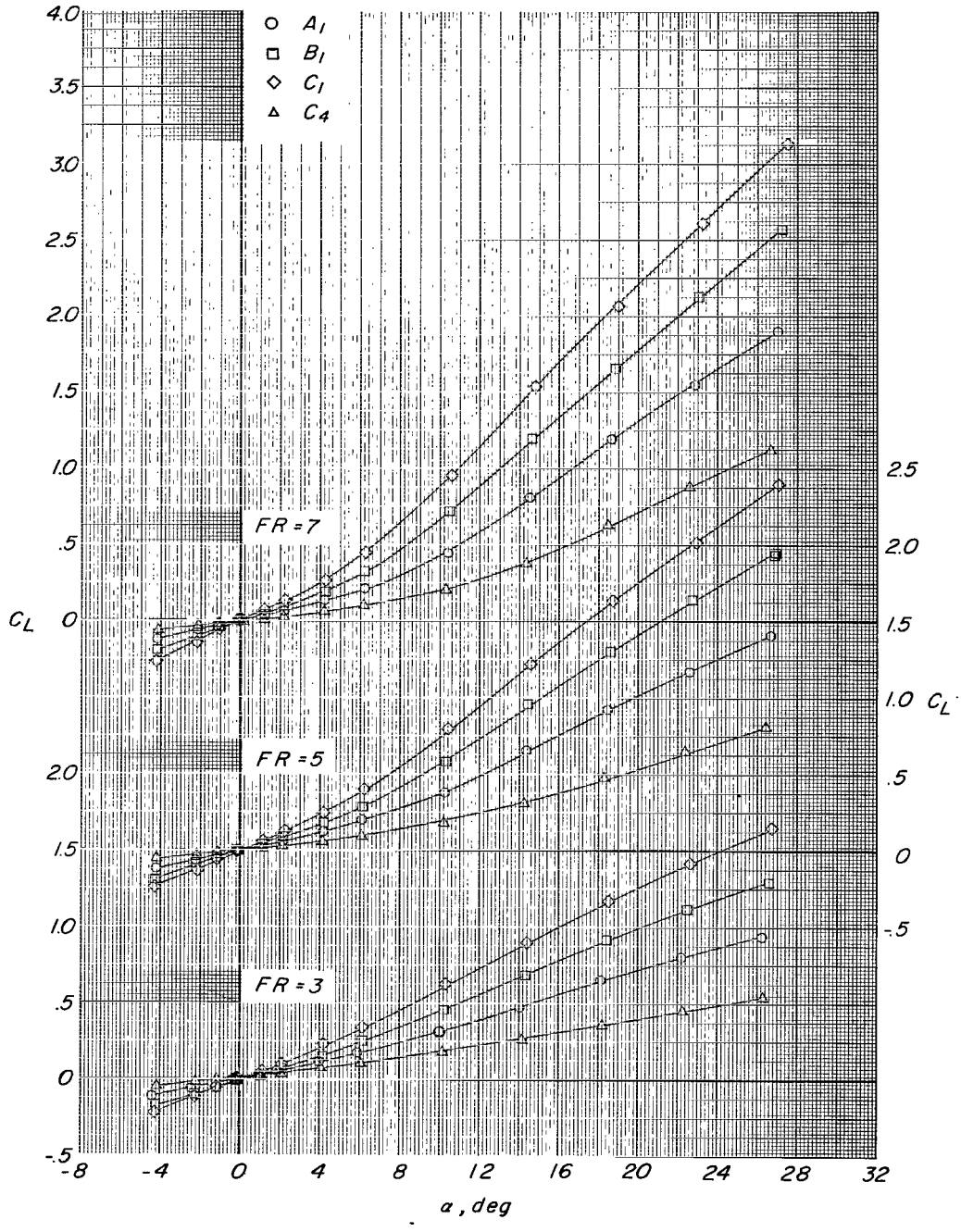

(a) Variation of C_L with α.

Figure 8.- Effects of increasing a/b ratio from 1.00 to 2.00 at $\phi = 0^\circ$ and 90° on longitudinal aerodynamic characteristics for symmetrical bodies with fineness ratios 3, 5, and 7 at Mach number 2.86.

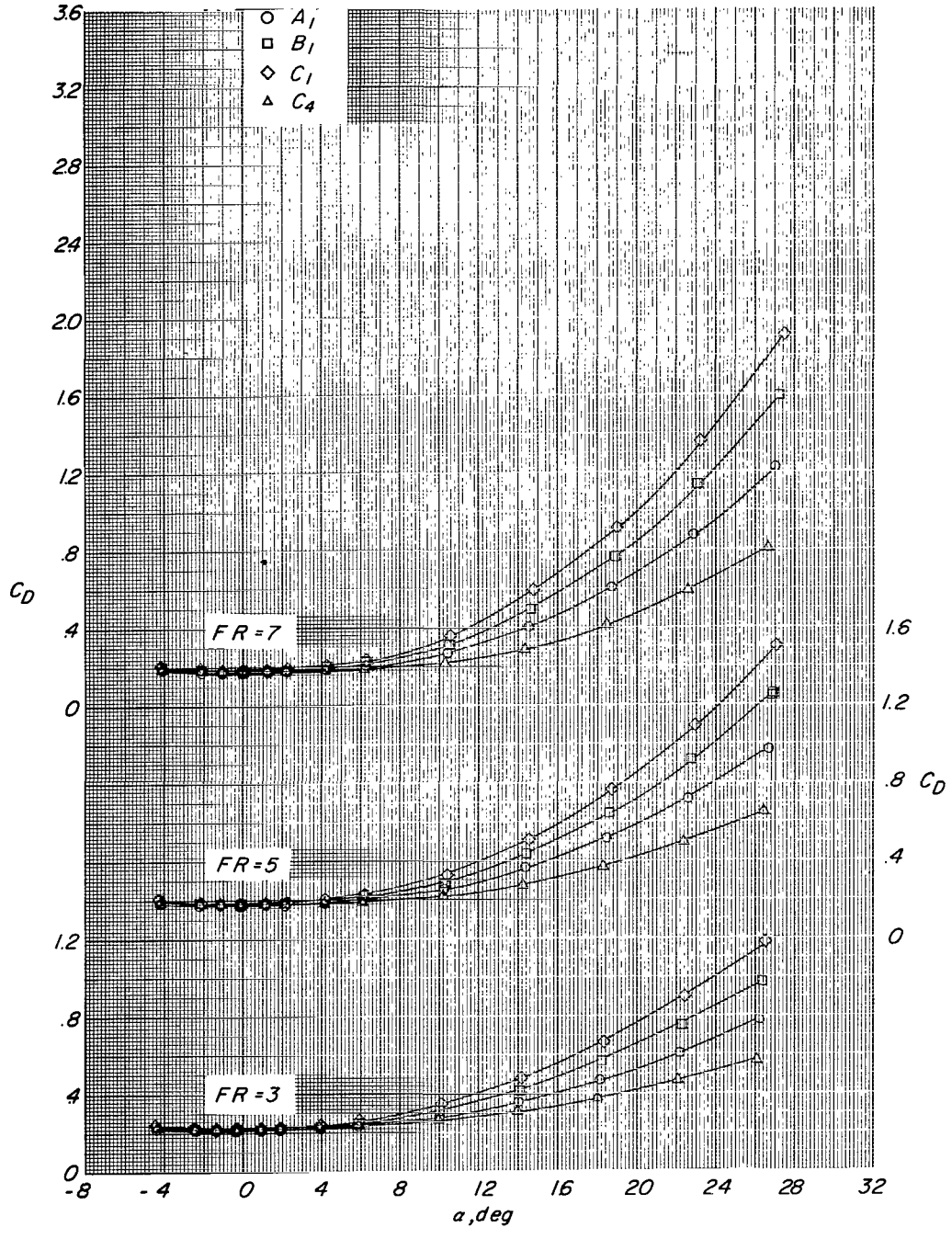

(b) Variation of C_D with α.

Figure 8.- Continued.

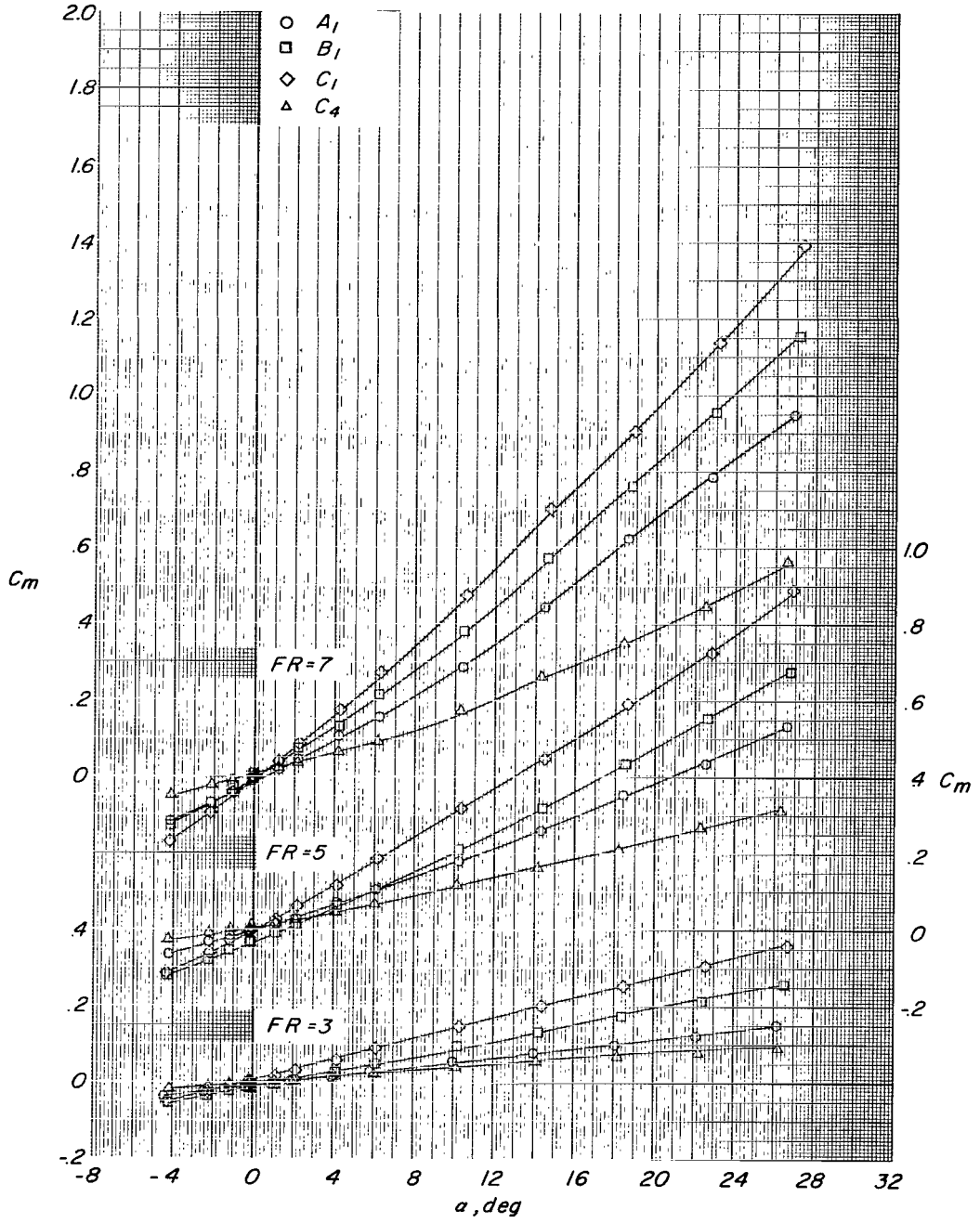

(c) Variation of C_m with α.

Figure 8.- Continued.

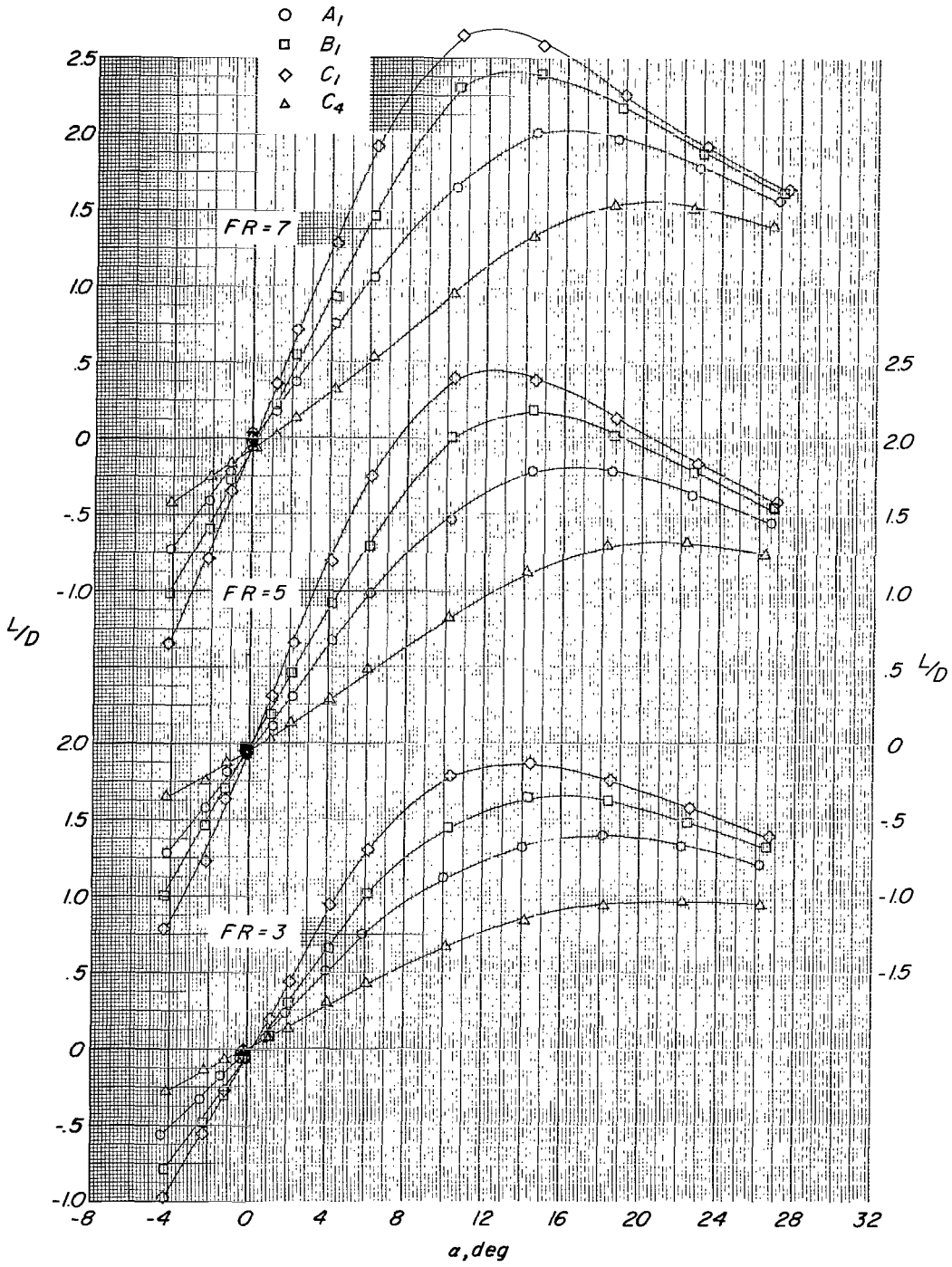

(d) Variation of L/D with α.

Figure 8.- Concluded.

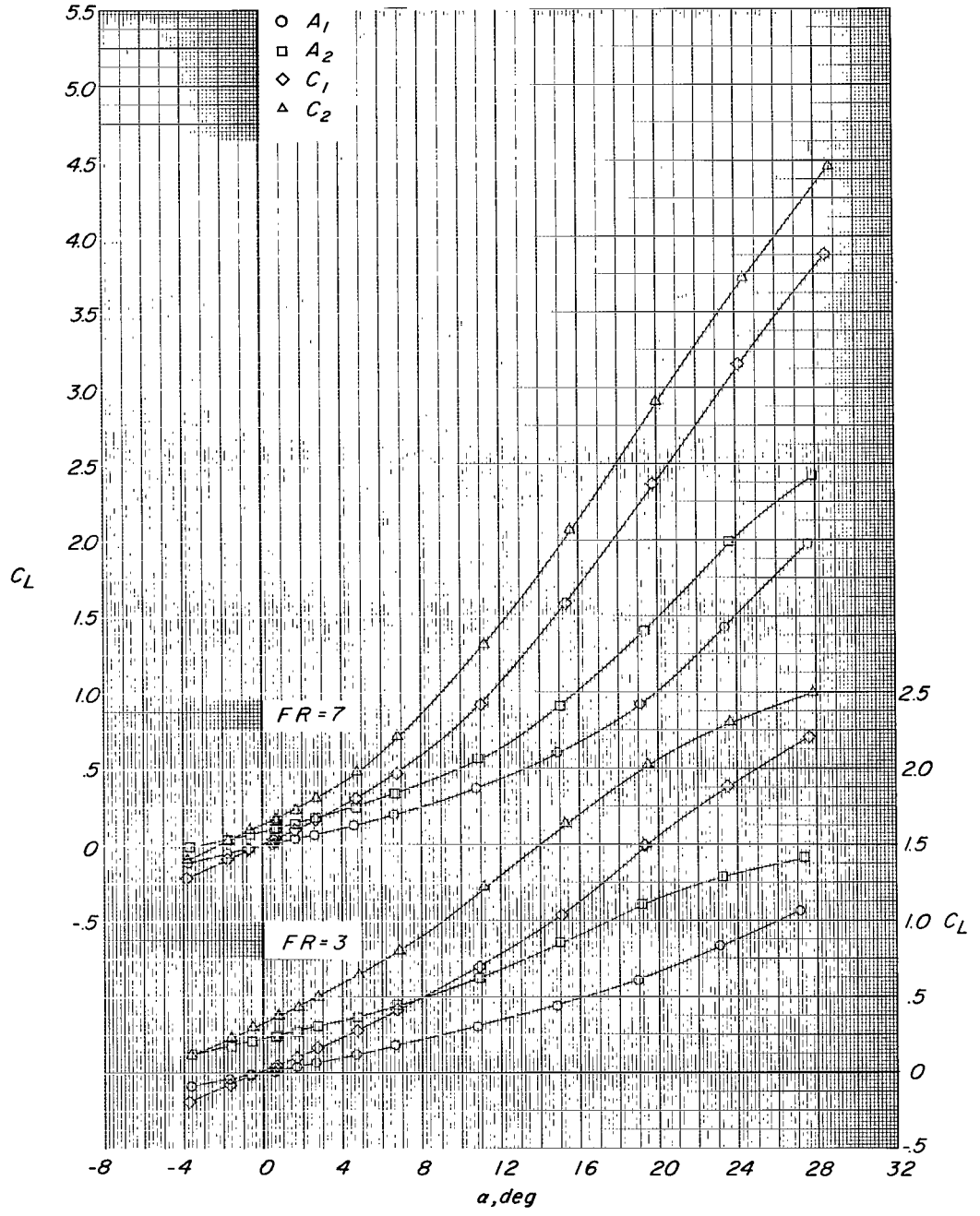

(a) Variation of C_L with α.

Figure 9.- Effect of body section displacement on longitudinal aerodynamic characteristics for bodies with fineness ratios 3 and 7, and a/b ratios 1.00 and 2.00 at $\phi = 0^\circ$ and Mach number 1.5.

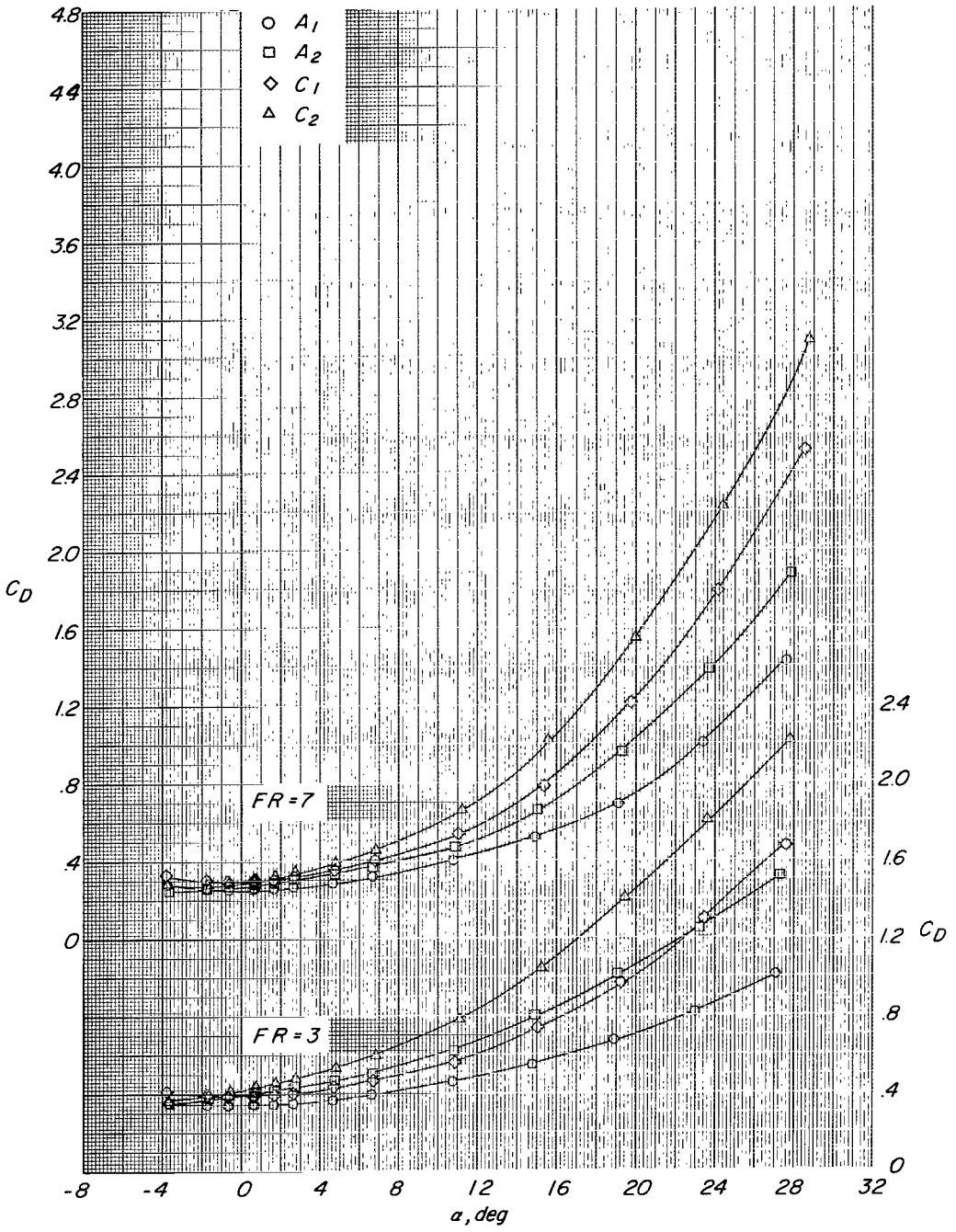

(b) Variation of C_D with α.

Figure 9.- Continued.

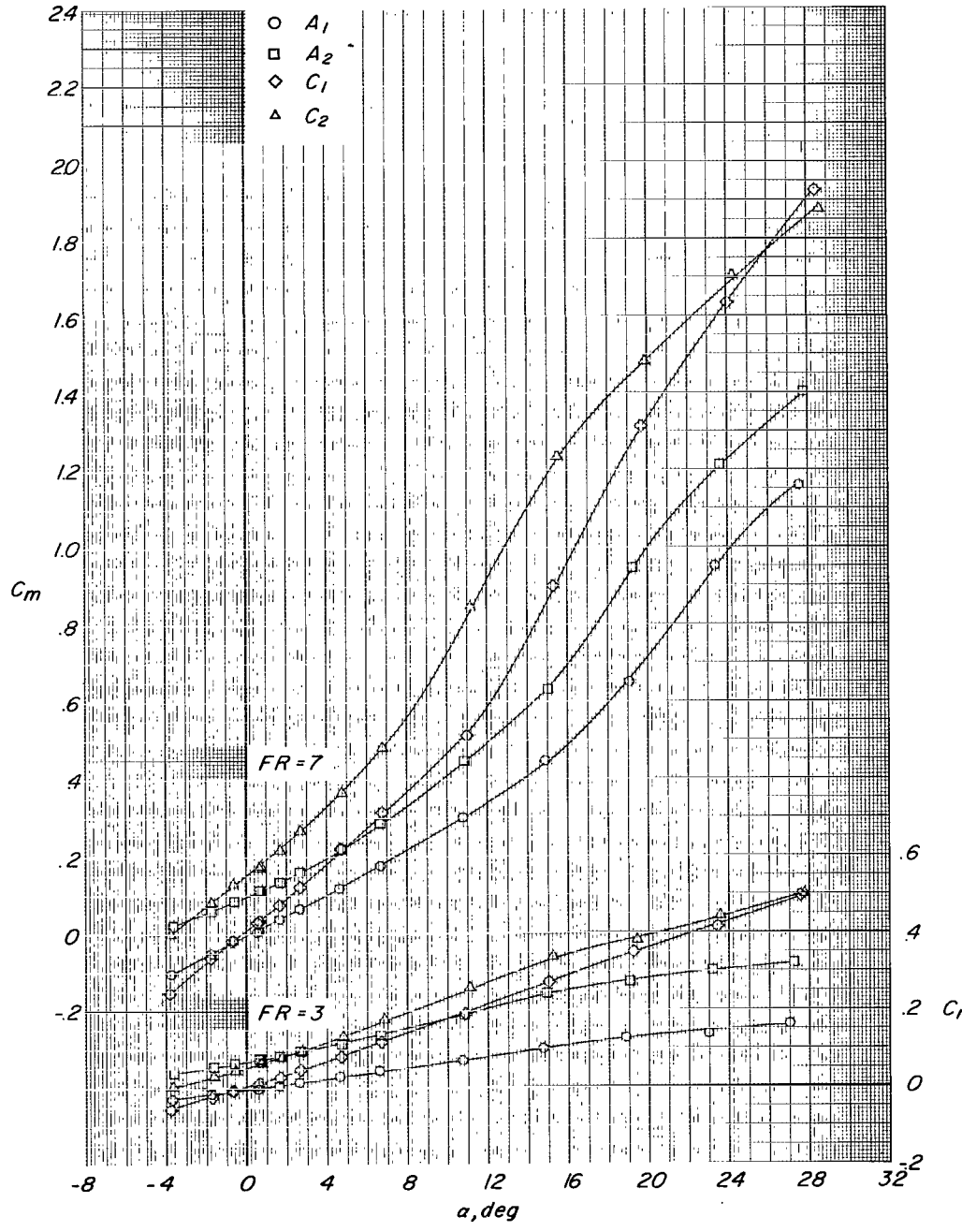

(c) Variation of C_m with α.

Figure 9.- Continued.

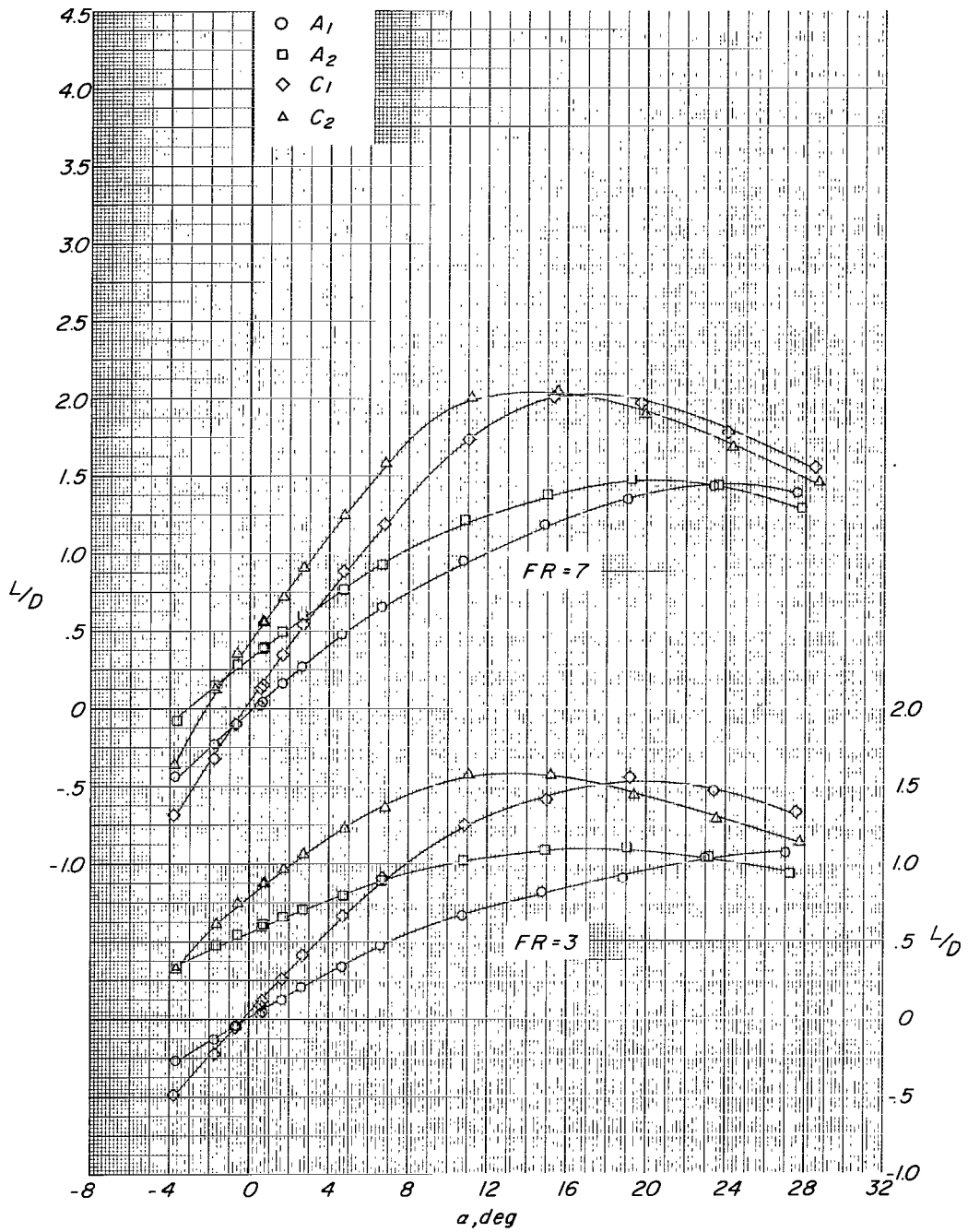

(d) Variation of L/D with α.

Figure 9.- Concluded.

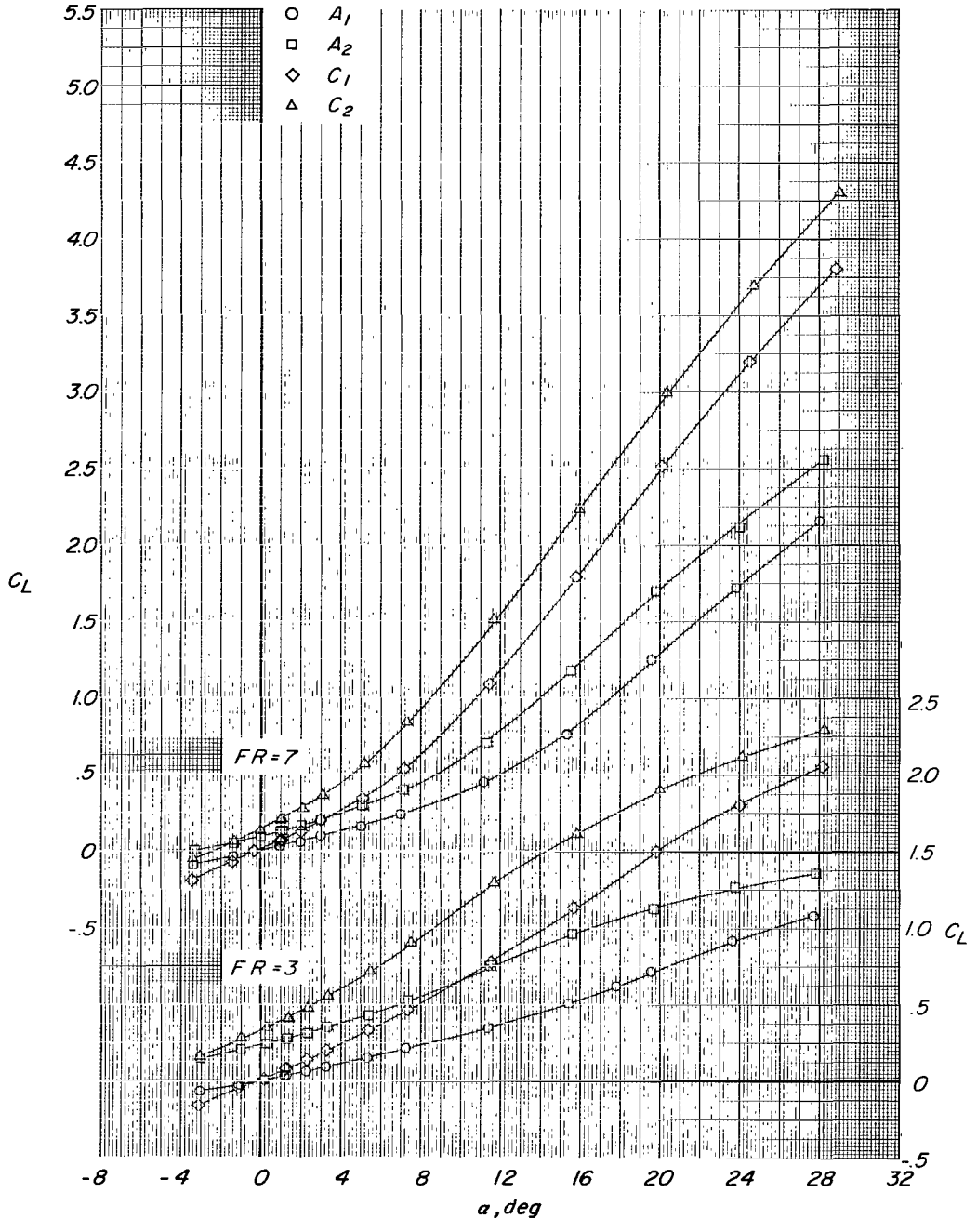

(a) Variation of C_L with α.

Figure 10.- Effect of body section displacement on longitudinal aerodynamic characteristics for bodies with fineness ratios 3 and 7, and a/b ratios 1.00 and 2.00 at $\phi = 0^\circ$ and Mach number 1.90.

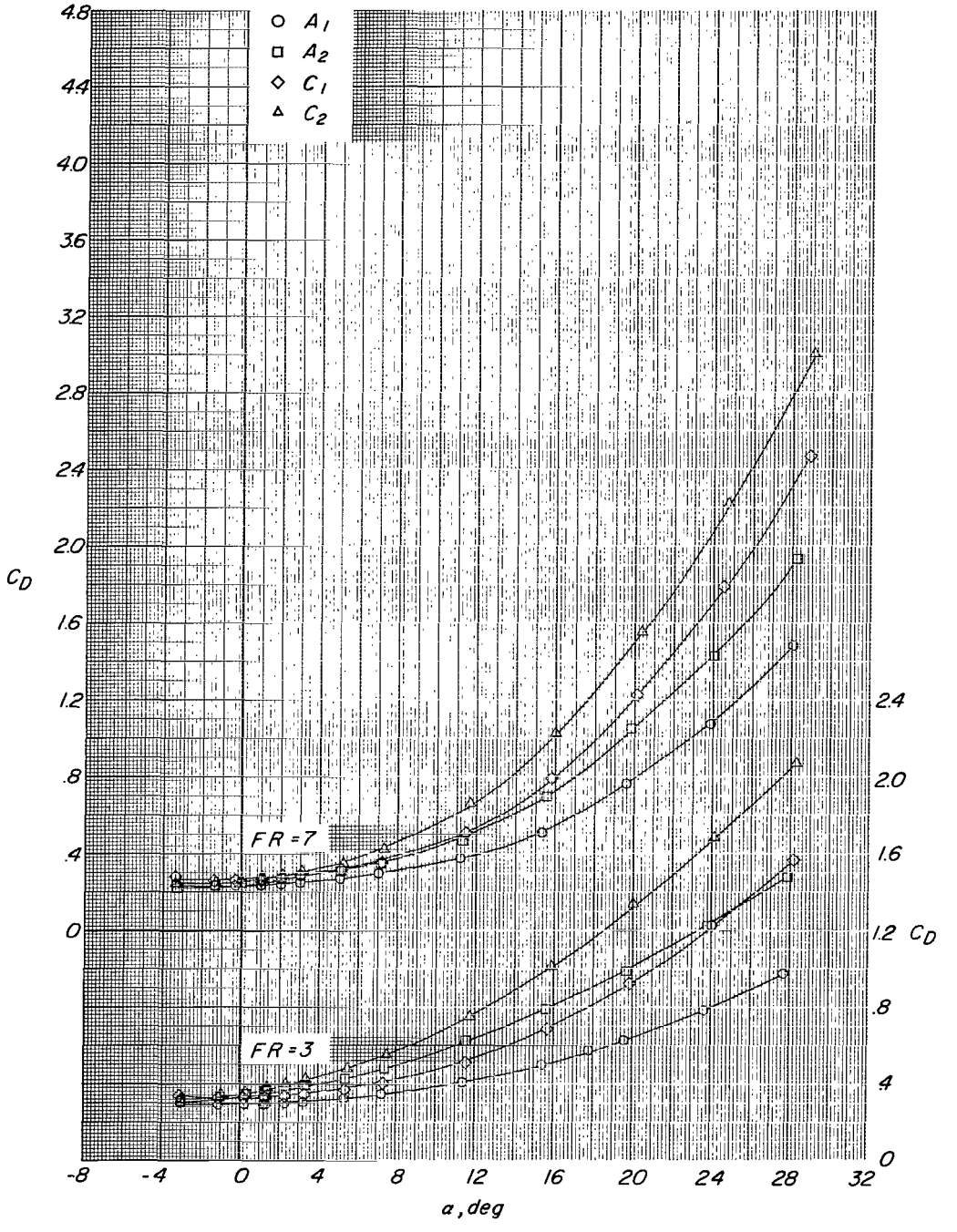

(b) Variation of C_D with α.

Figure 10.- Continued.

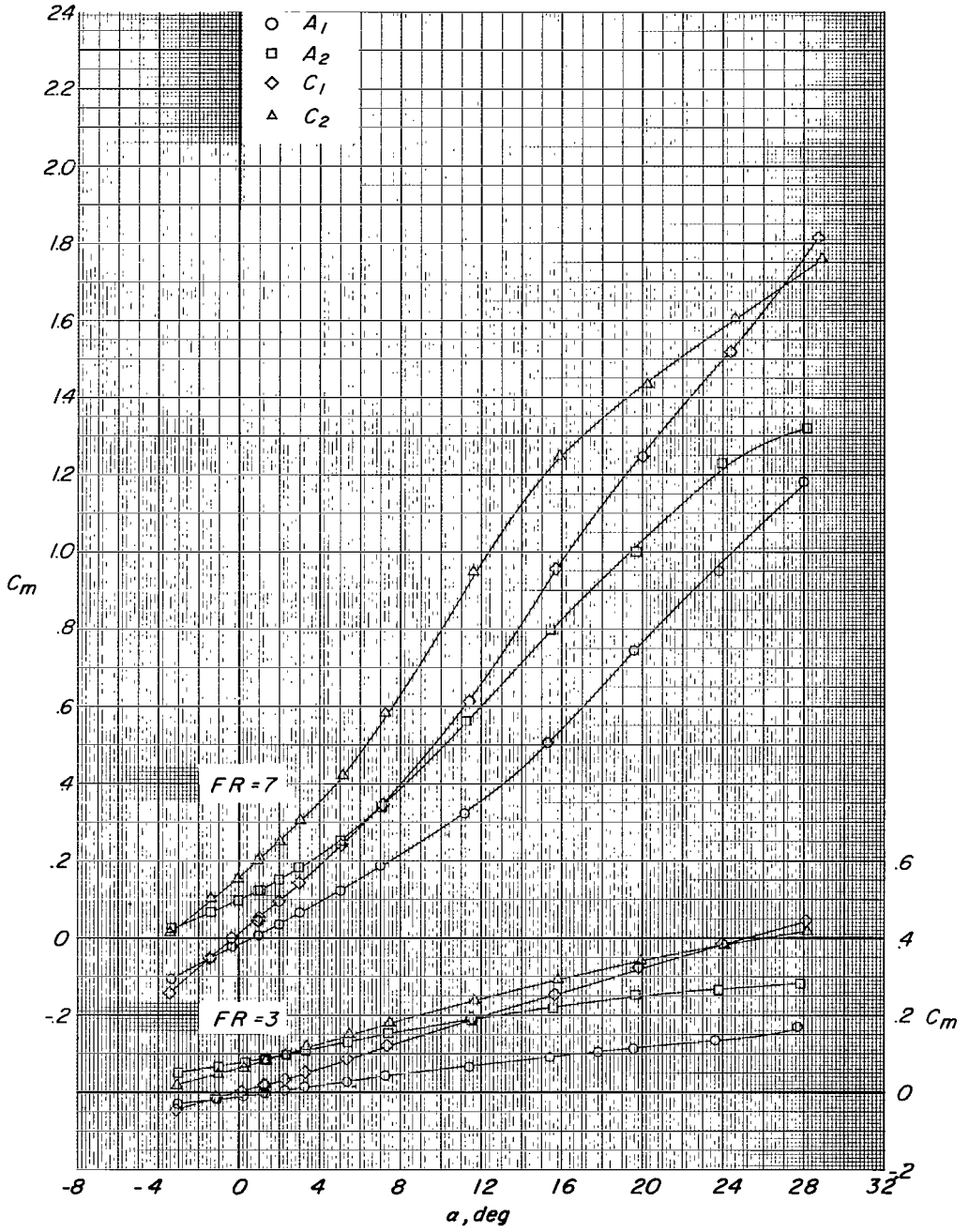

(c) Variation of C_m with α.

Figure 10.- Continued.

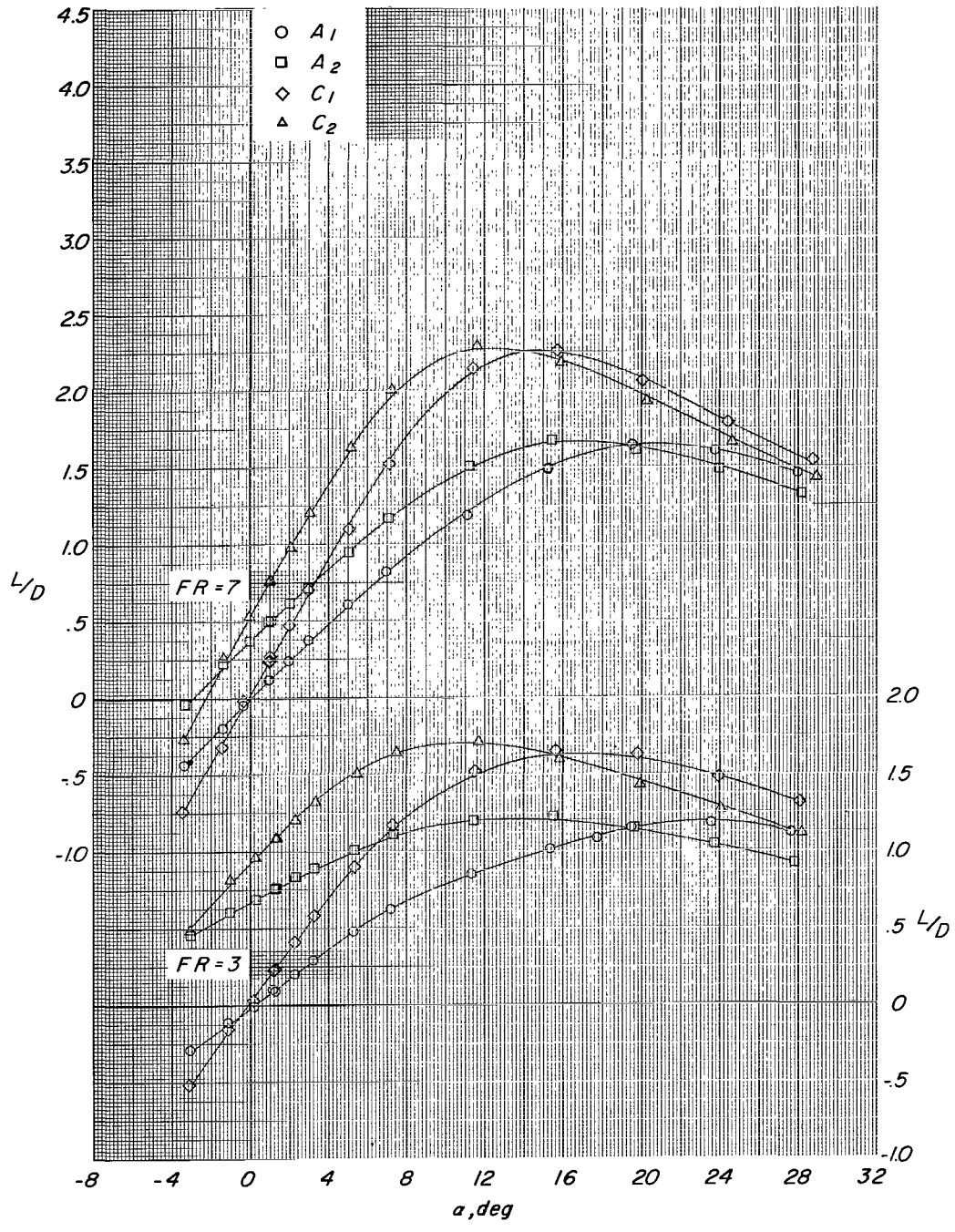

(d) Variation of L/D with α.

Figure 10.- Concluded.

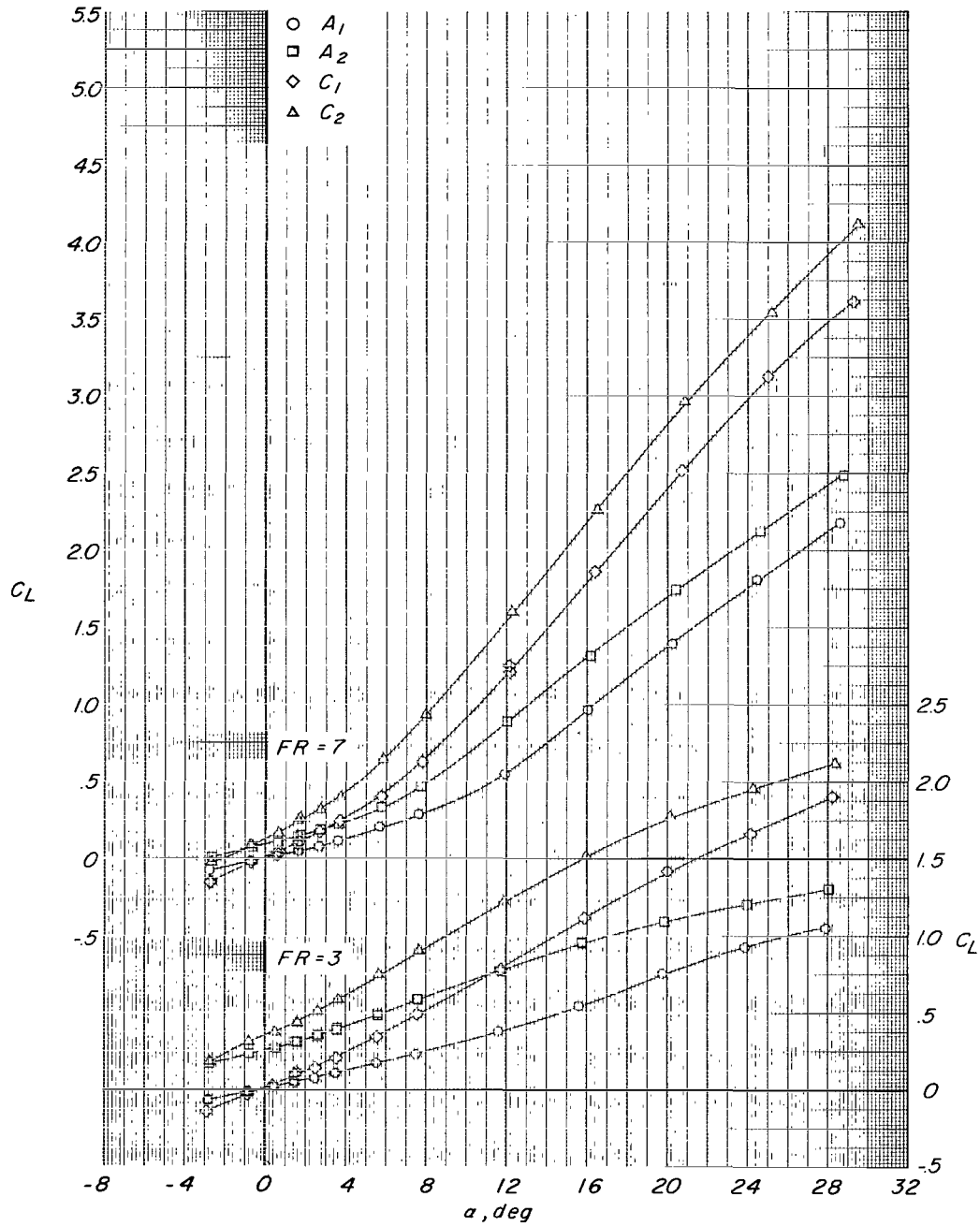

(a) Variation of C_L with α.

Figure 11.- Effect of body section displacement on longitudinal aerodynamic characteristics for bodies with fineness ratios 3 and 7, and a/b ratios 1.00 and 2.00 at $\phi = 0^\circ$ and Mach number 2.36.

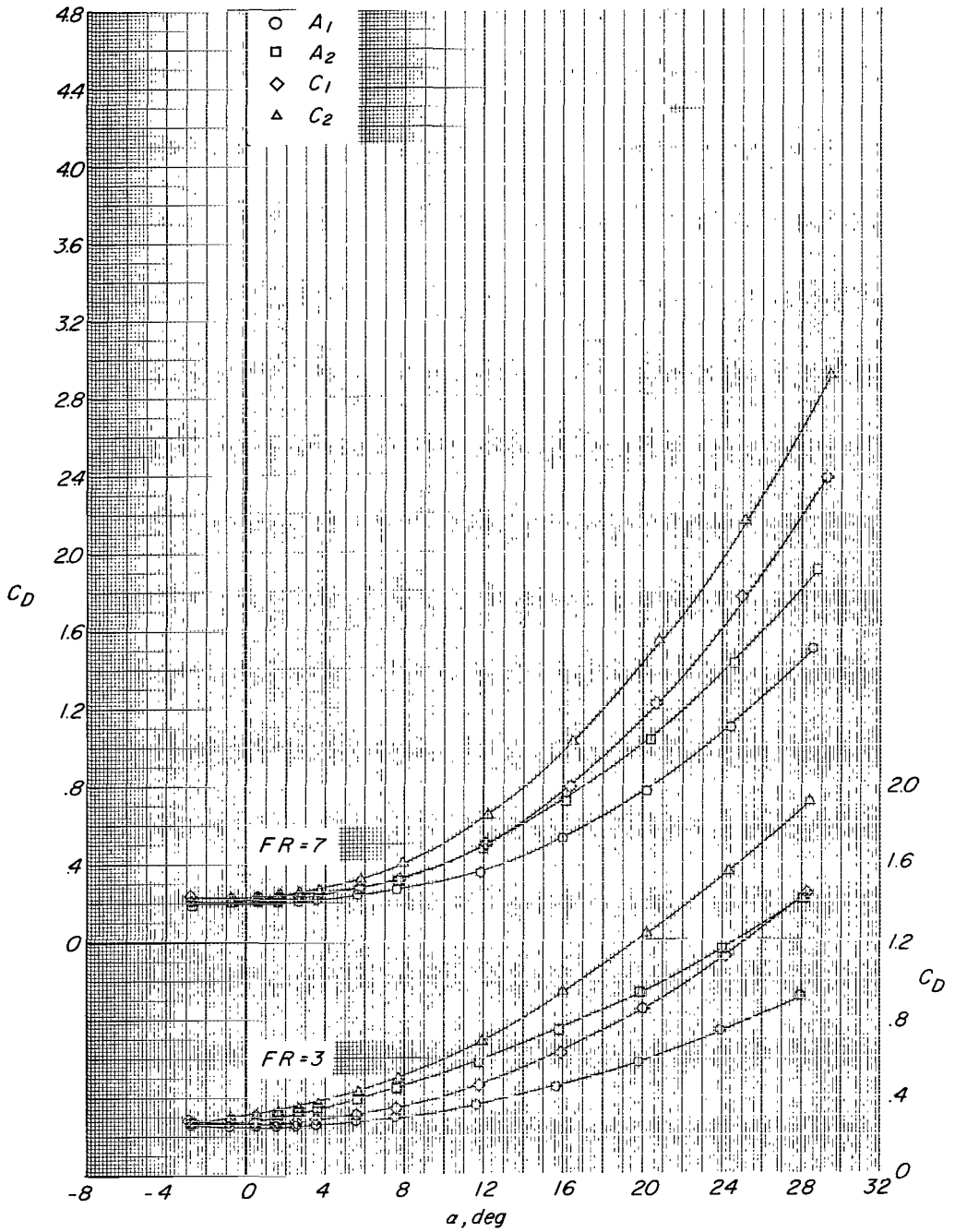

(b) Variation of C_D with α.

Figure 11.- Continued.

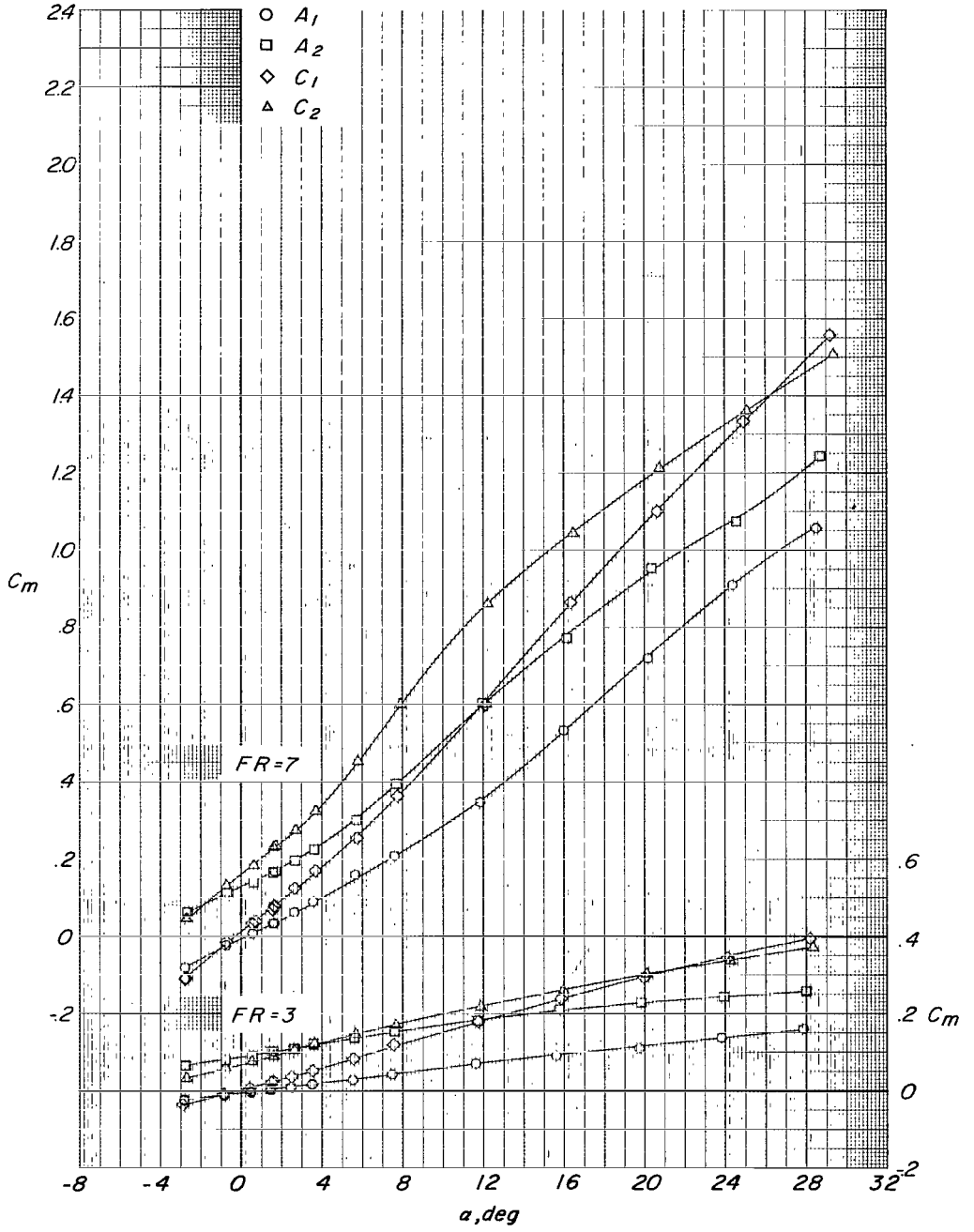

(c) Variation of C_m with α.

Figure 11.- Continued.

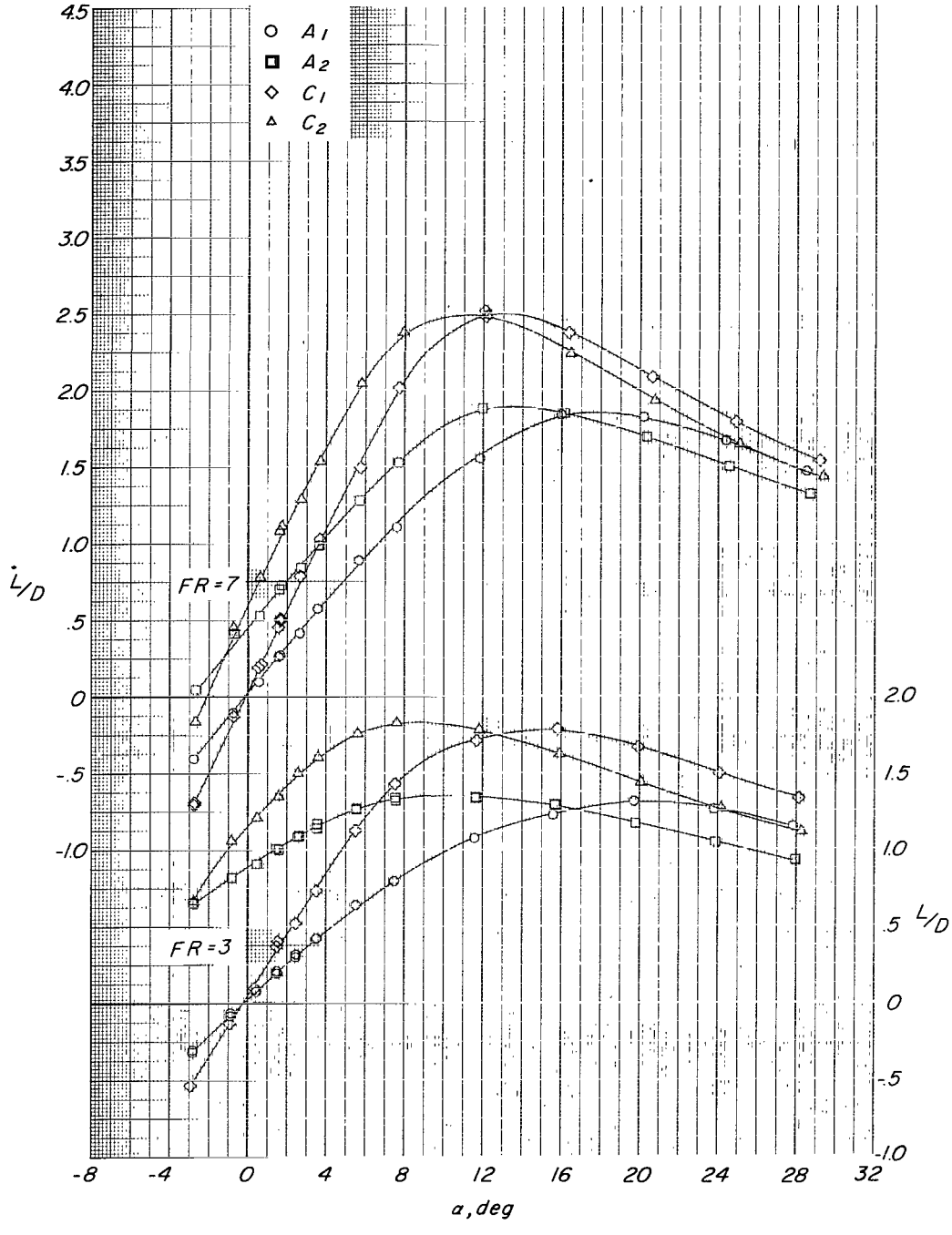

(d) Variation of L/D with α.

Figure 11.- Concluded.

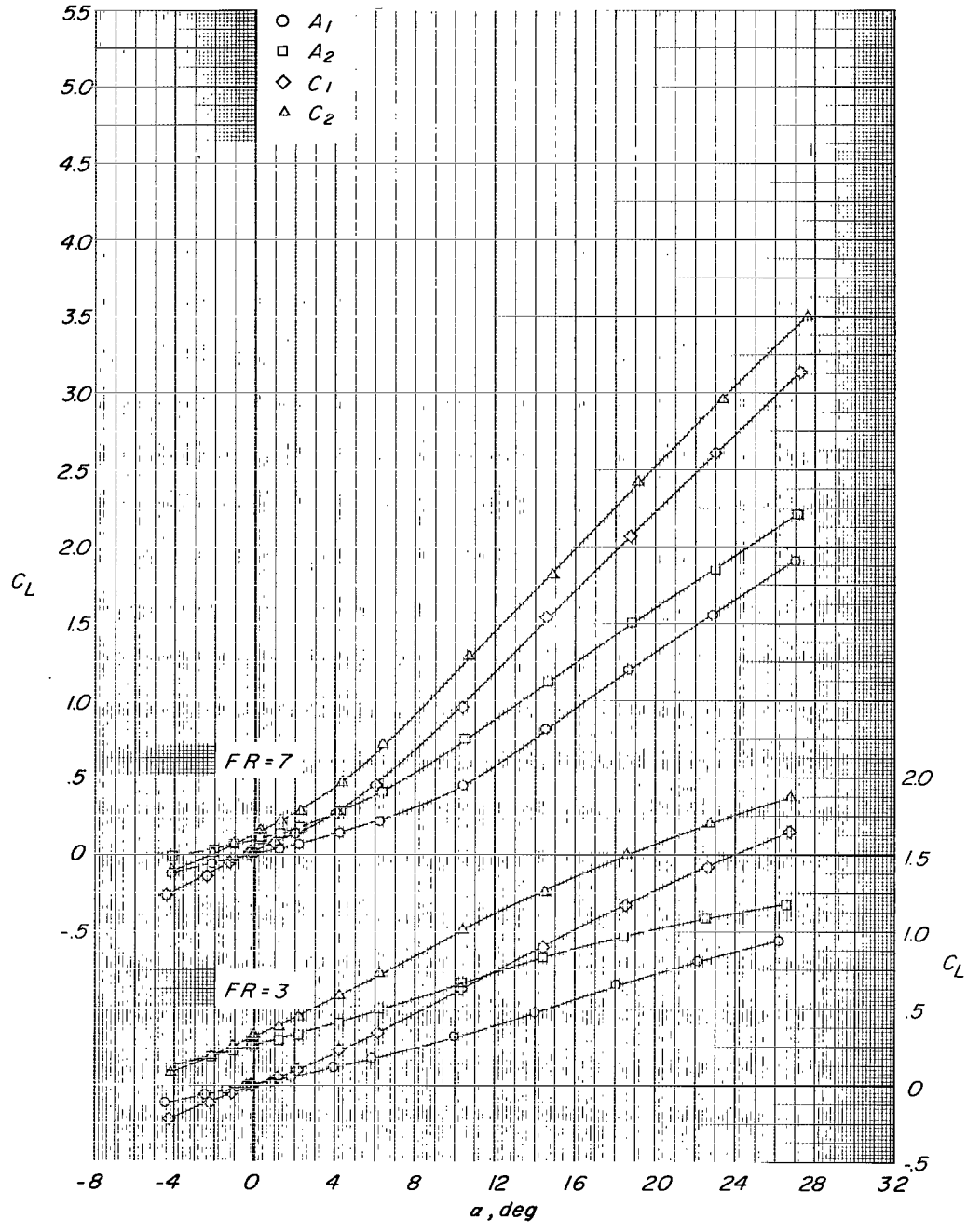

(a) Variation of C_L with α.

Figure 12.- Effect of body section displacement on longitudinal aerodynamic characteristics for bodies with fineness ratios 3 and 7, and a/b ratios 1.00 and 2.00 at $\phi = 0^\circ$ and Mach number 2.86.

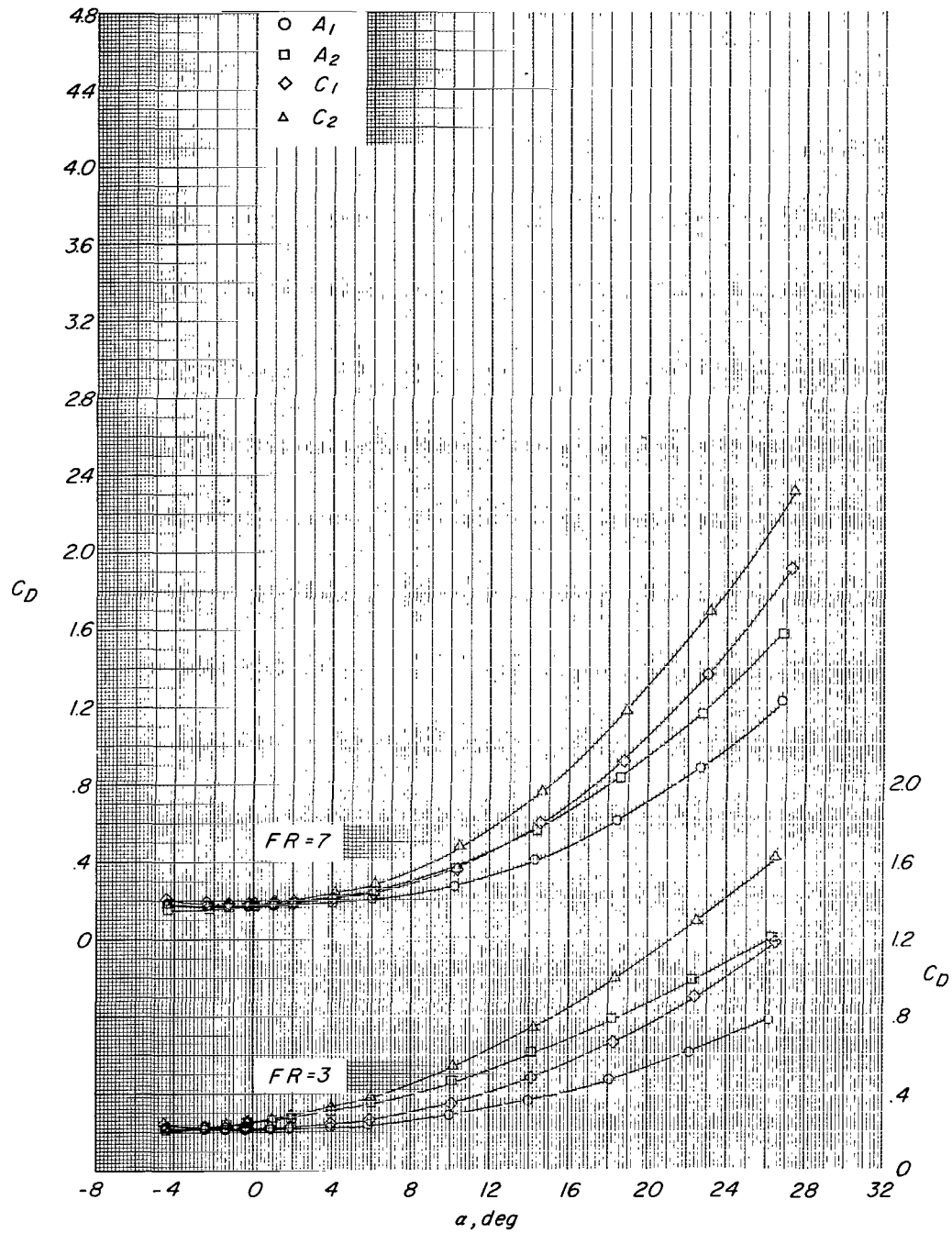

(b) Variation of C_D with α.

Figure 12.- Continued.

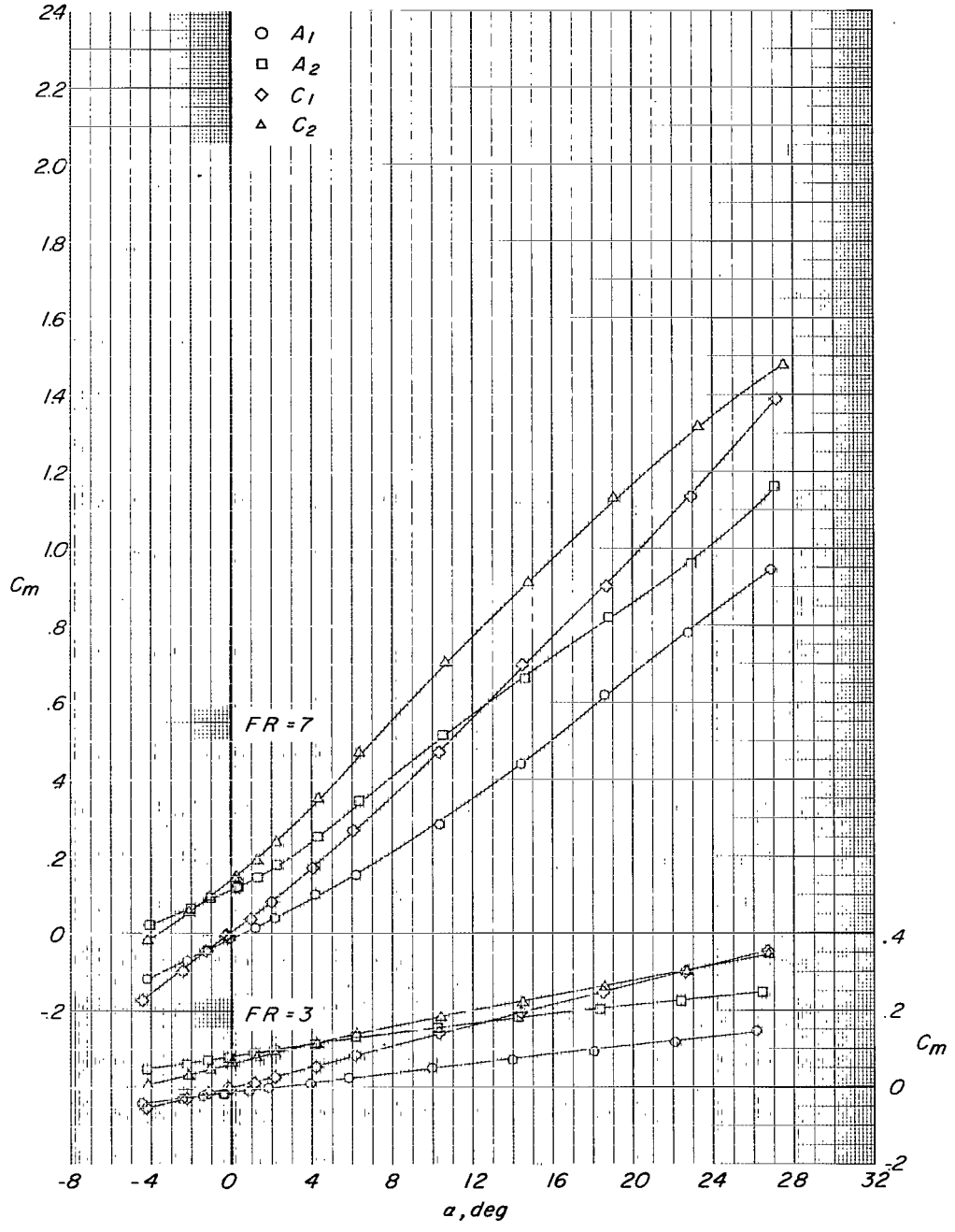

(c) Variation of C_m with α.

Figure 12.- Continued.

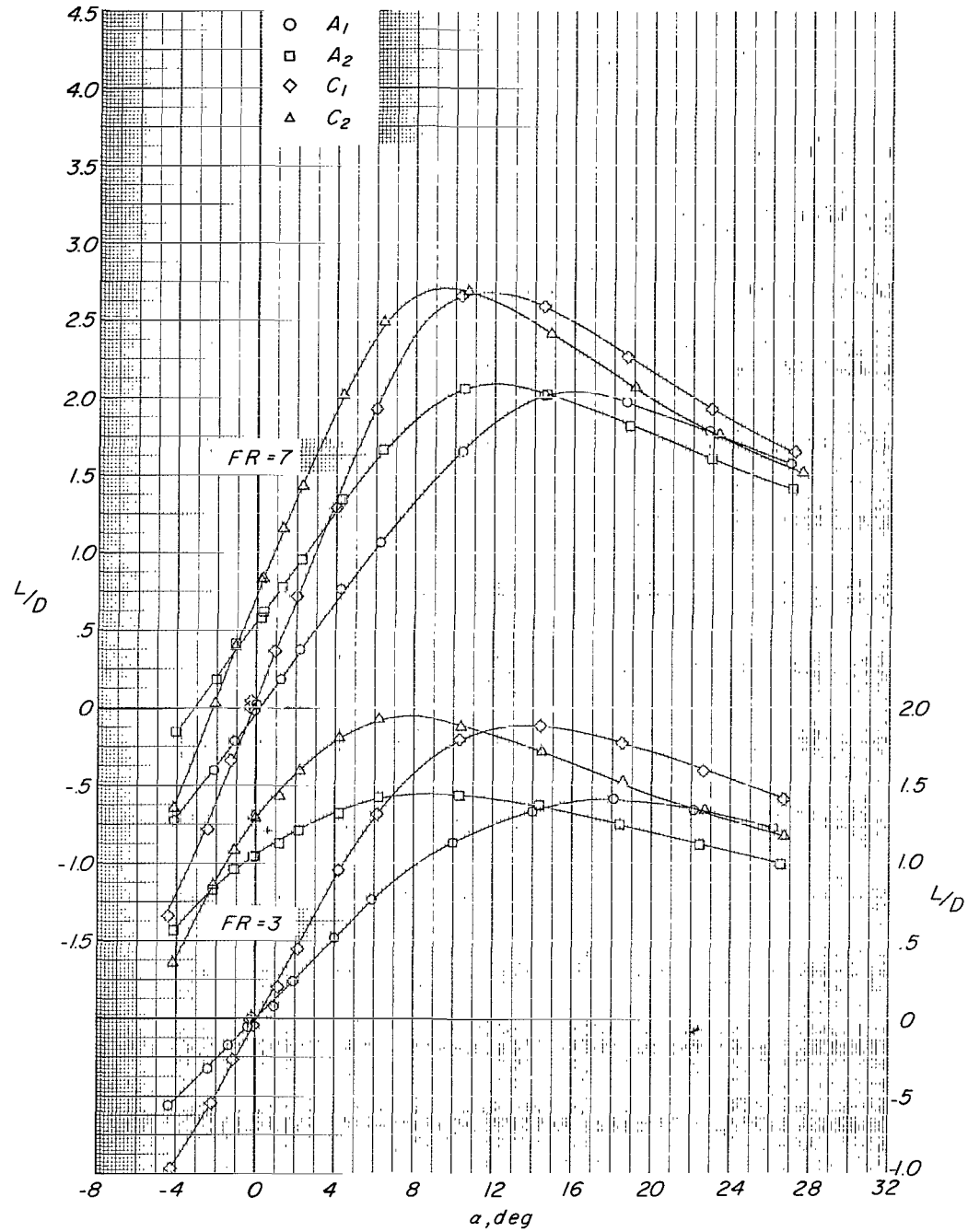

(d) Variation of L/D with α.

Figure 12.- Concluded.

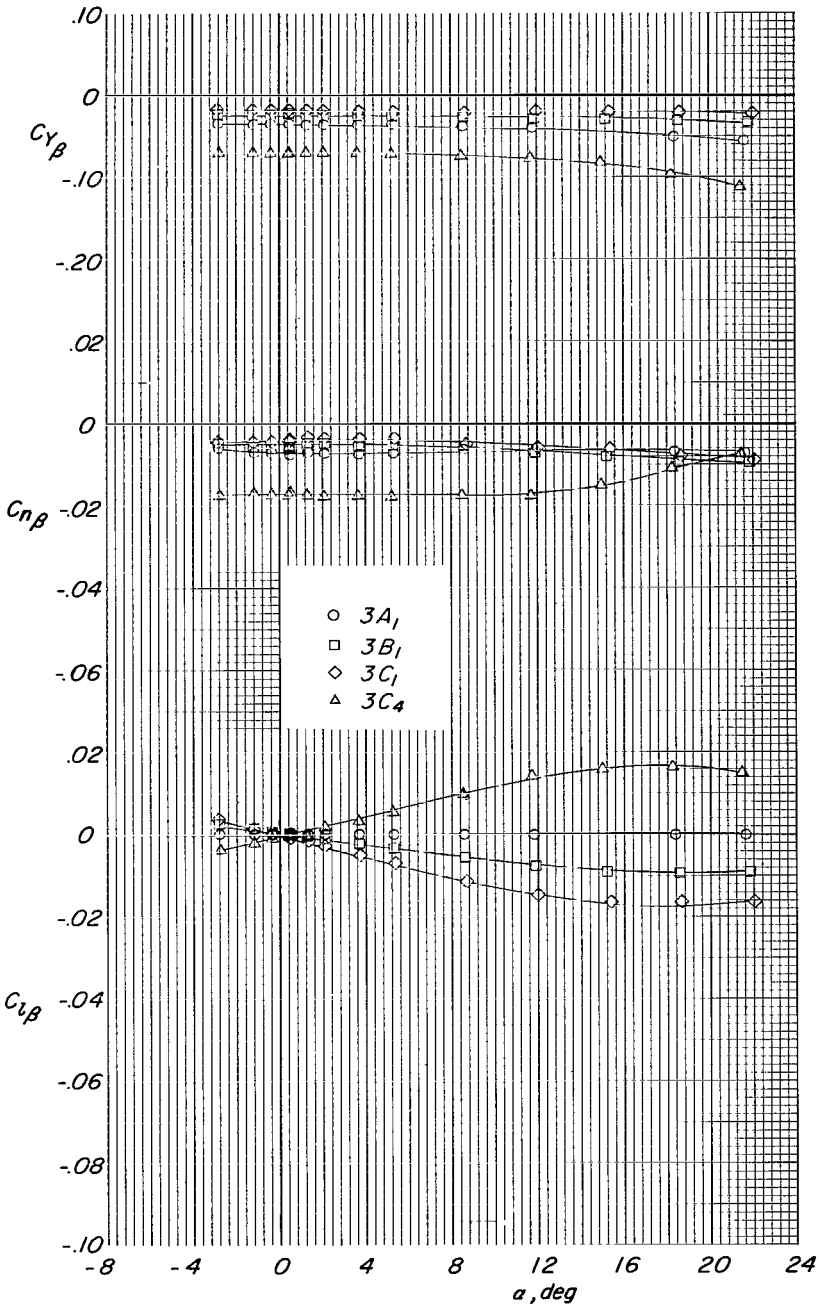

(a) M = 1.50.

Figure 13.- Effect of increasing a/b ratio from 1.00 to 2.00 on variation of lateral directional derivatives with angle of attack for symmetrical body with fineness ratio 3 at roll angles 0° and 90°.

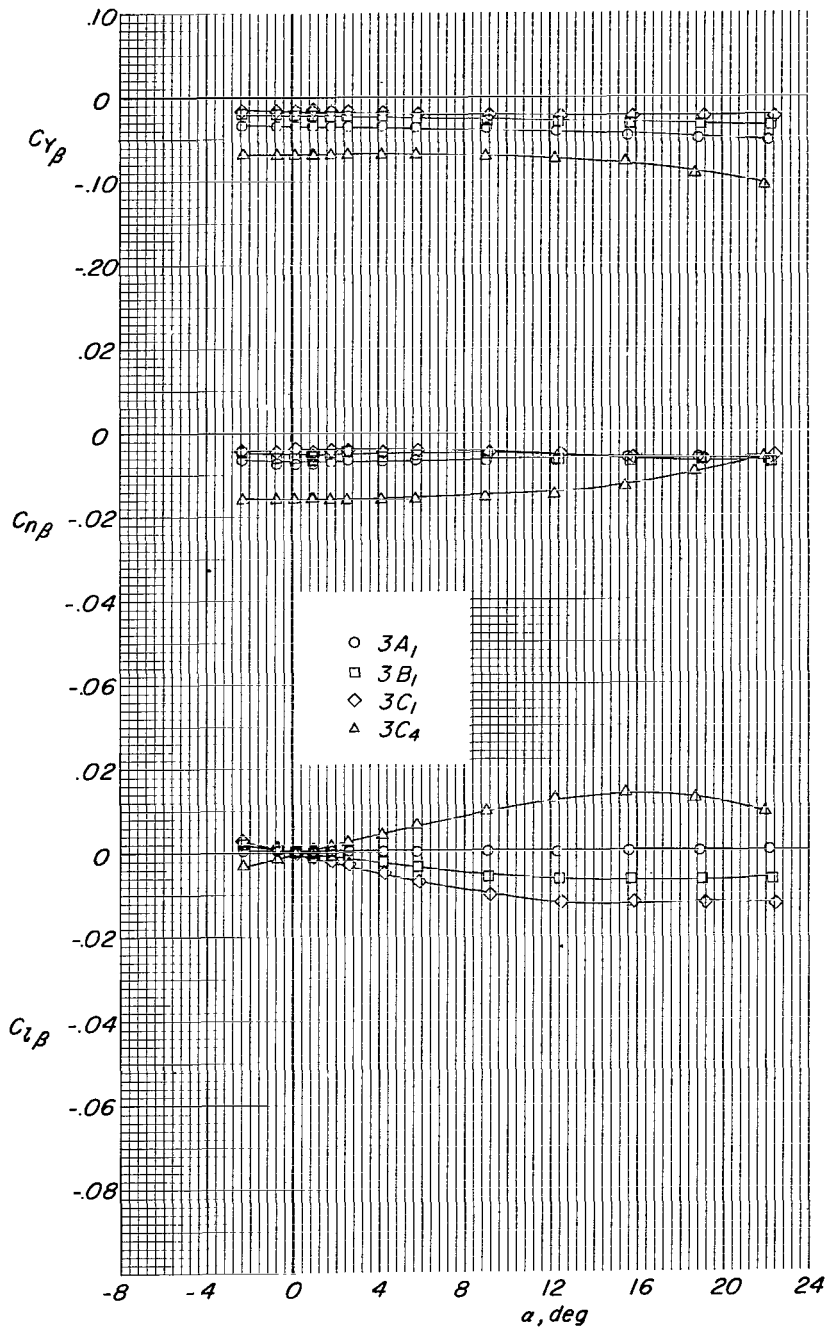

(b) M = 1.90.

Figure 13.- Continued.

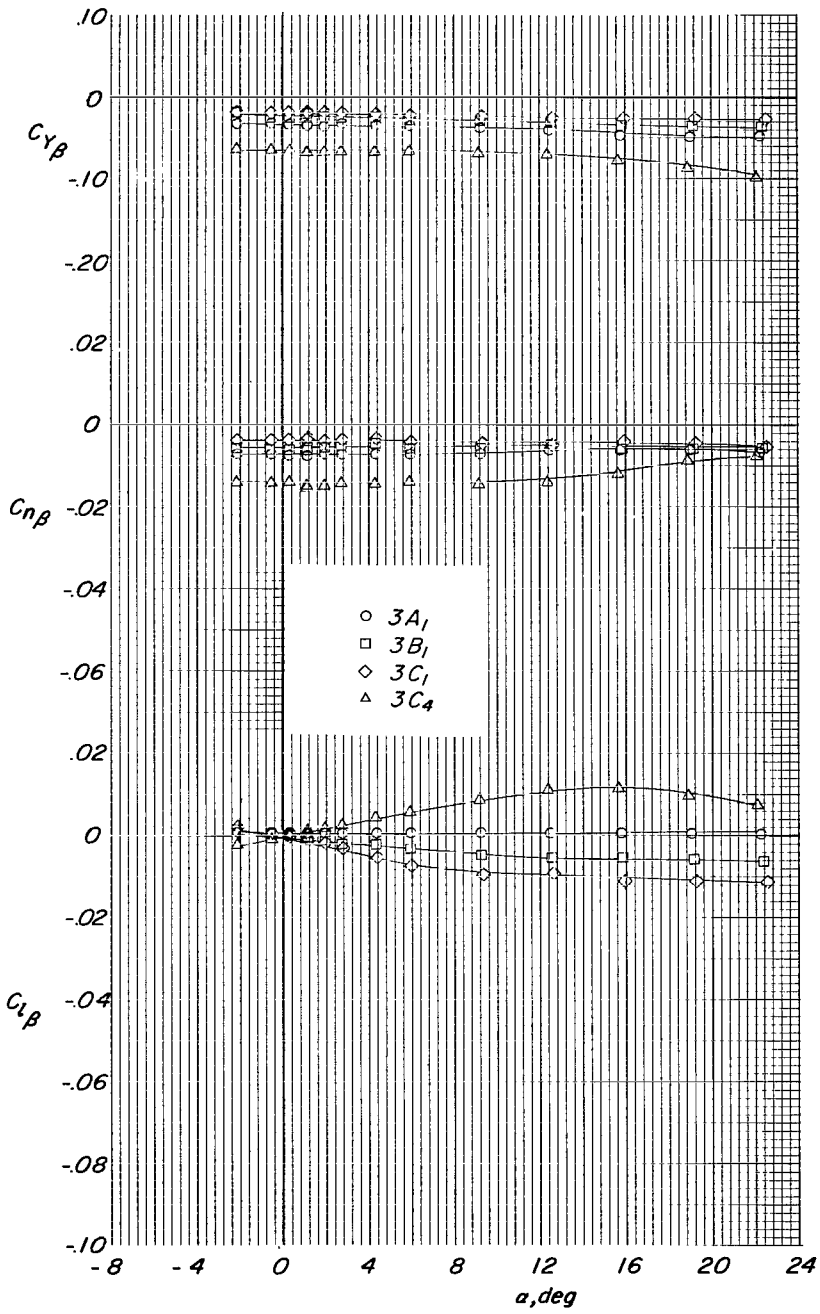

(c) M = 2.36.

Figure 13.- Continued.

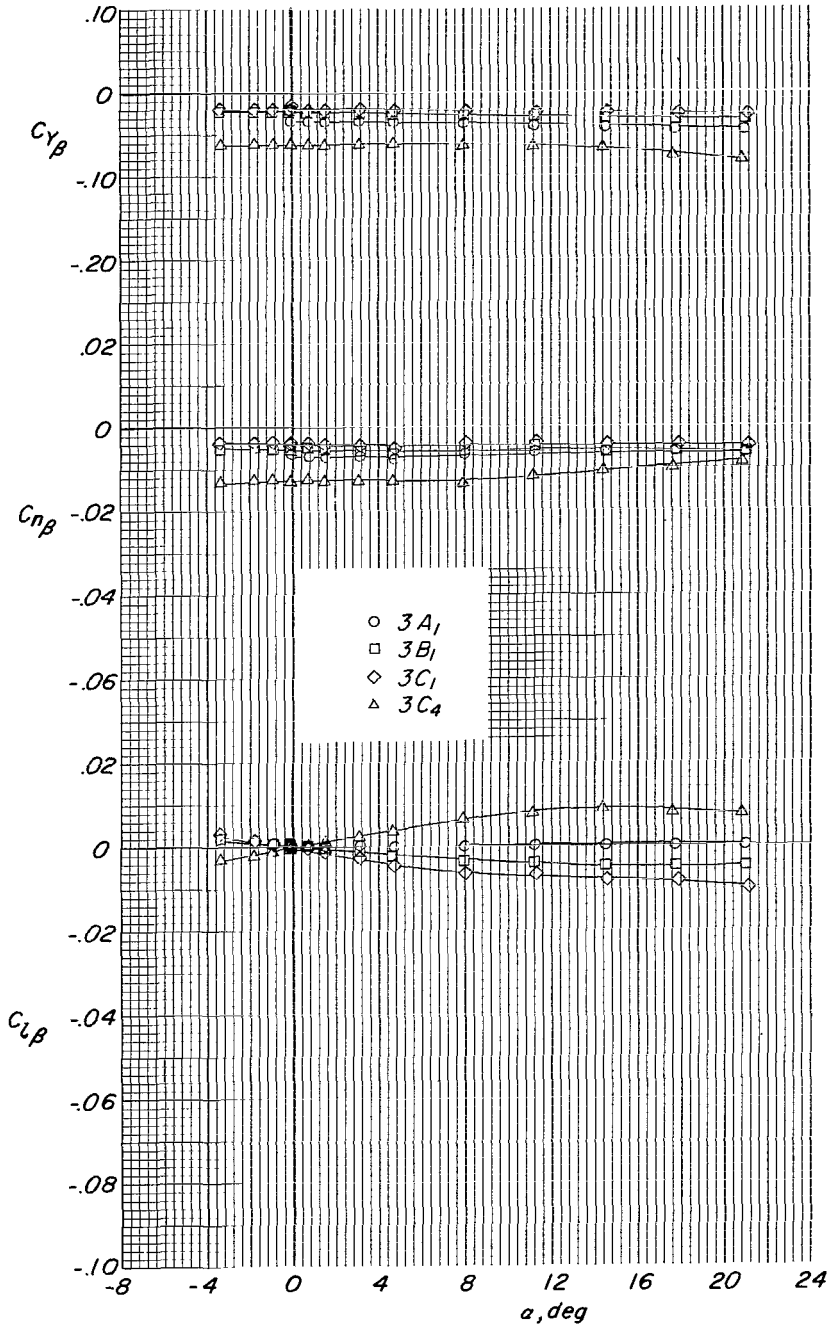

(d) M = 2.86.

Figure 13.- Concluded.

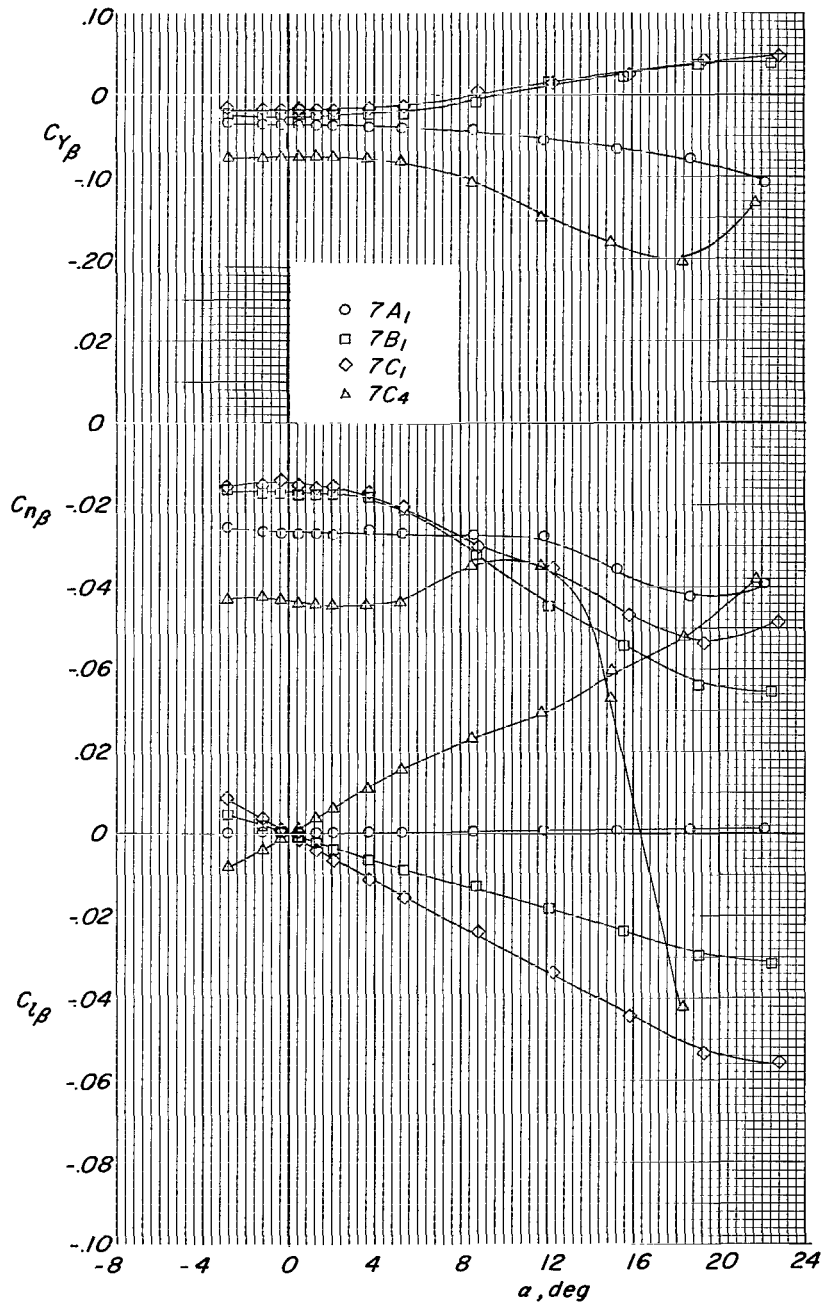

(a) M = 1.50.

Figure 14.- Effect of increasing a/b ratio from 1.00 to 2.00 on variation of lateral directional derivatives with angle of attack for symmetrical body with fineness ratio 7 at roll angles 0° and 90°.

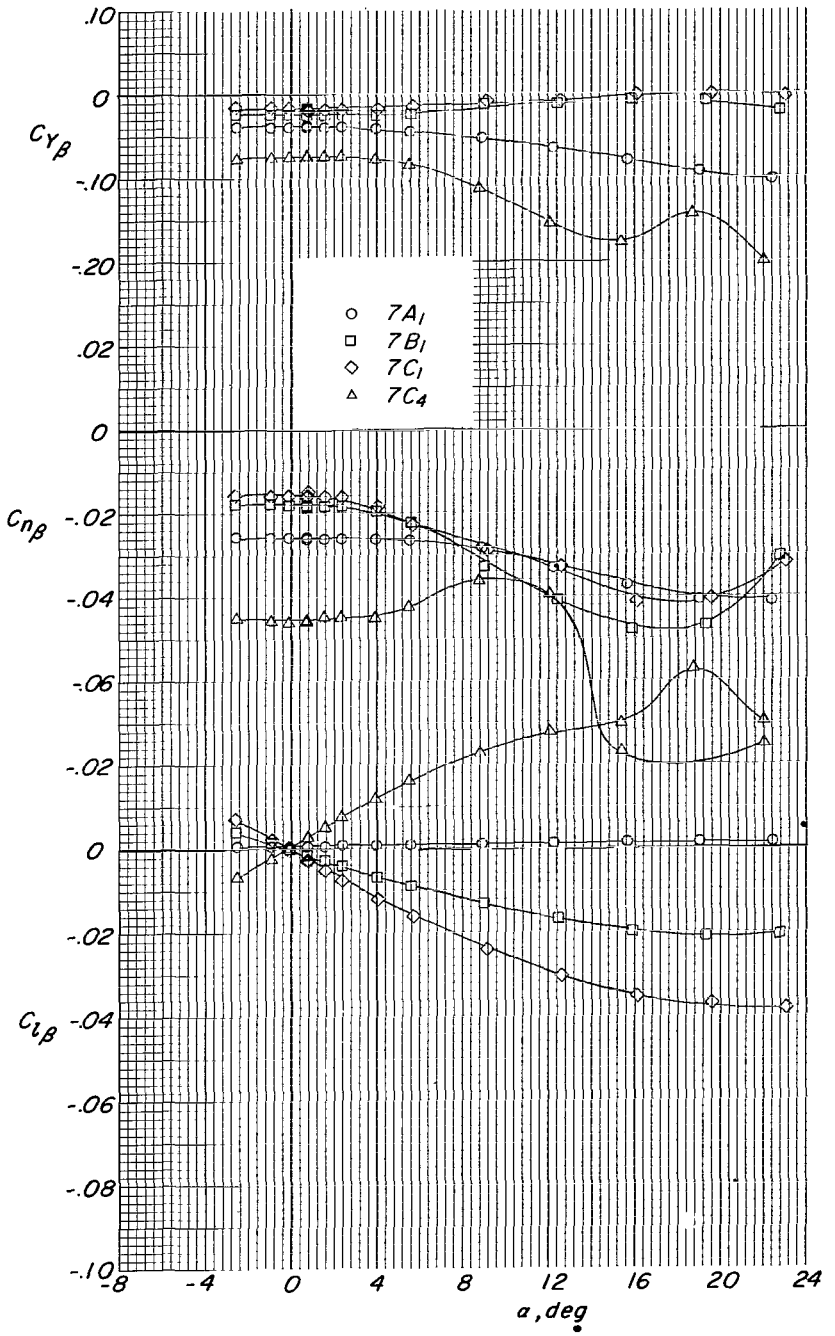

(b) M = 1.90.

Figure 14.- Continued.

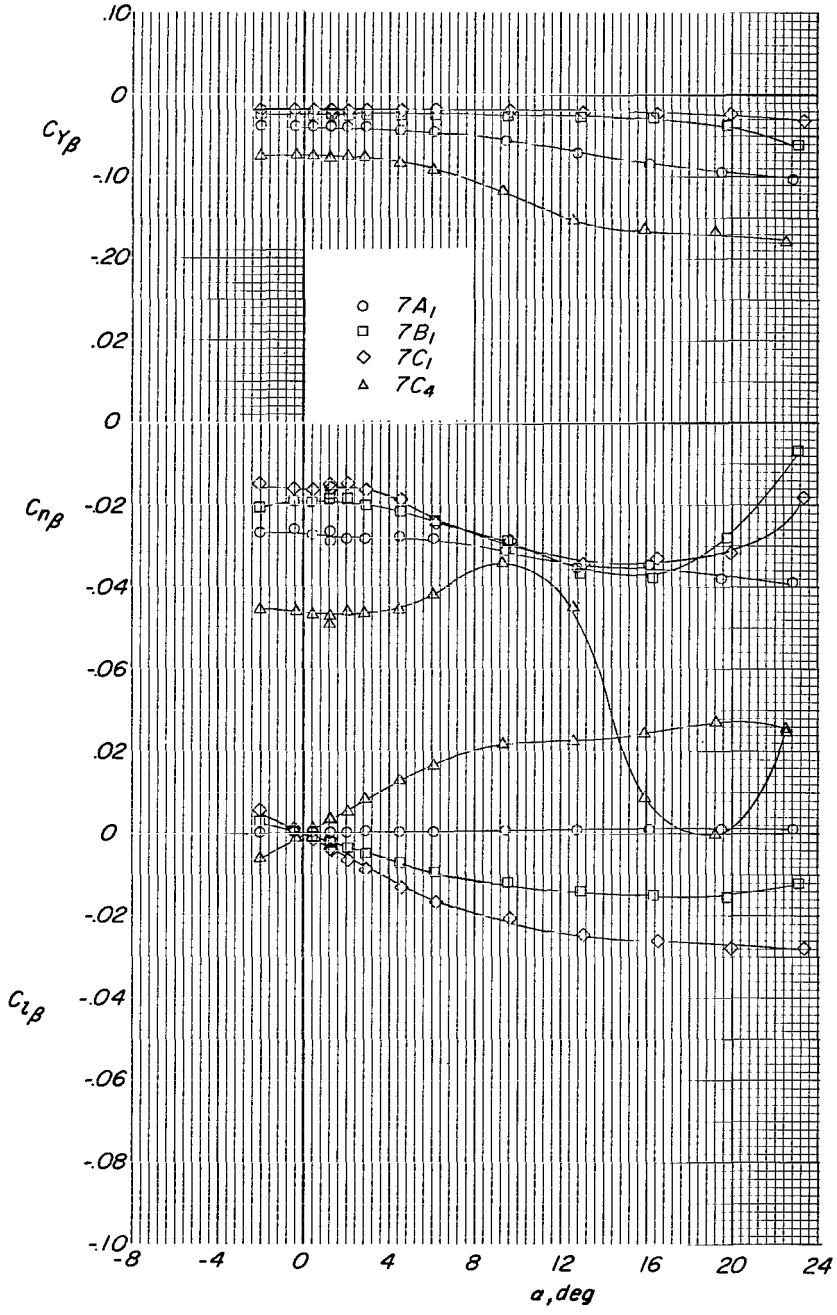

(c) M = 2.38.

Figure 14.- Continued.

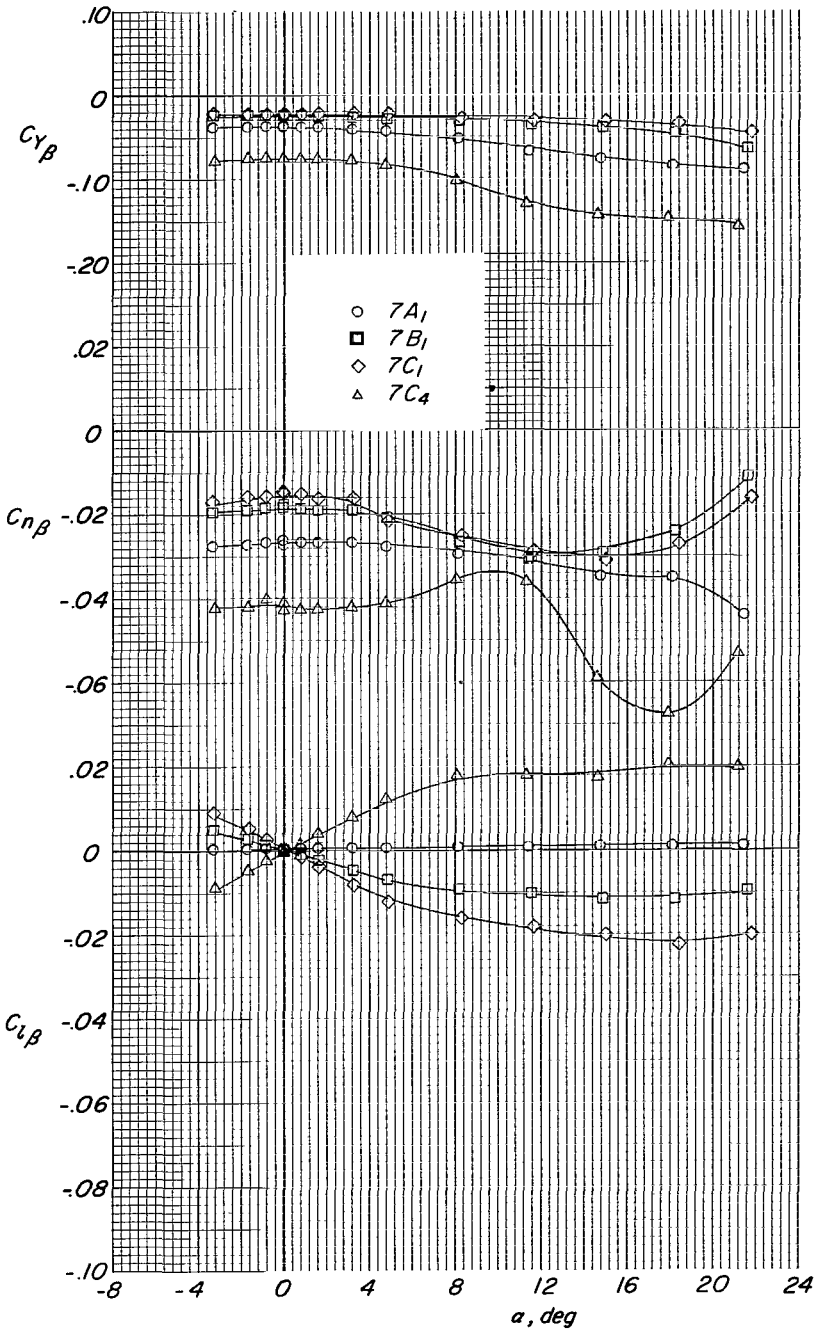

(d) M = 2.86.

Figure 14.- Concluded.

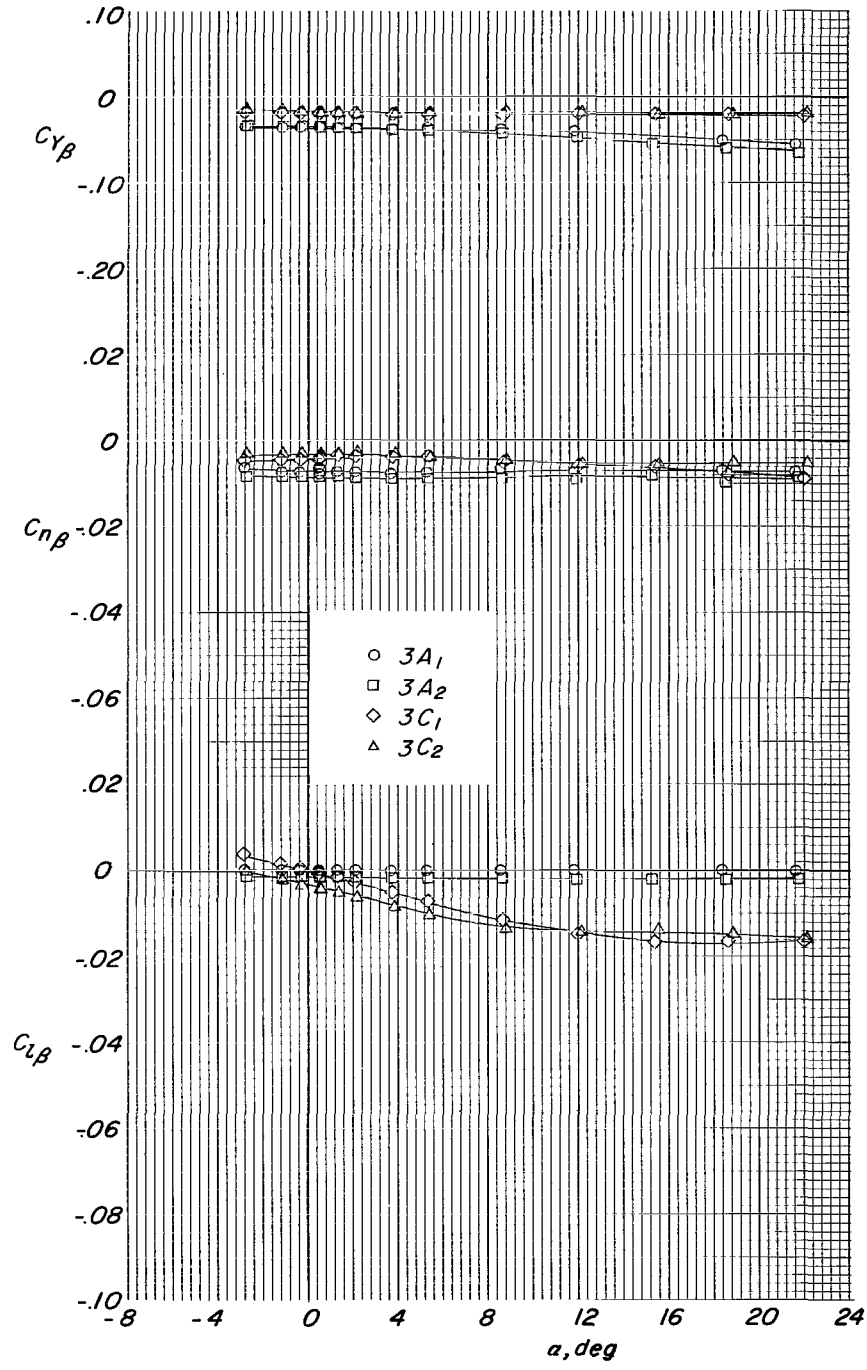

(a) M = 1.50.

Figure 15.- Effect of body section displacement on variation of lateral-directional derivatives with angle of attack for body with fineness ratio 3 at $\phi = 0^\circ$.

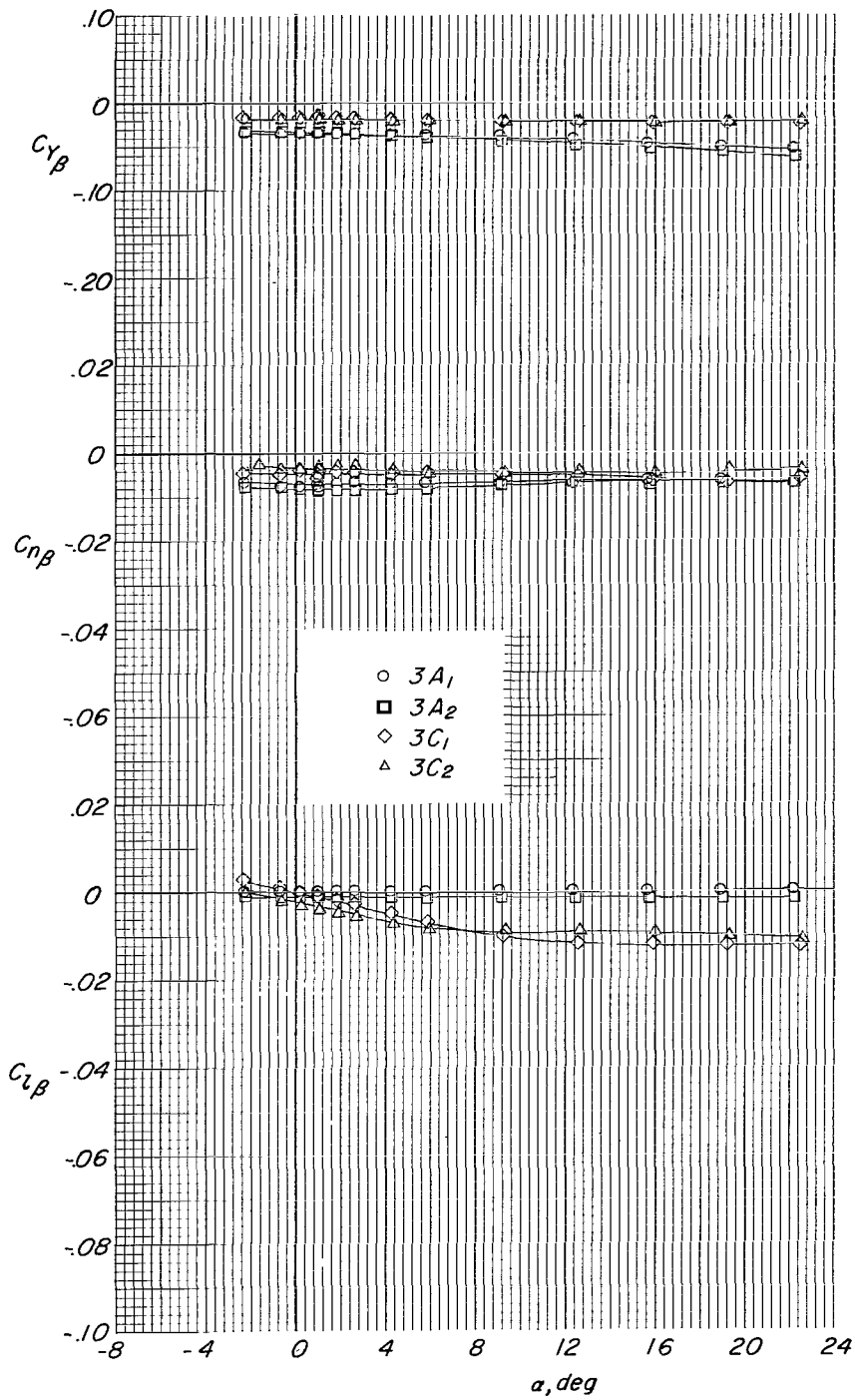

(b) M = 1.90.

Figure 15.- Continued.

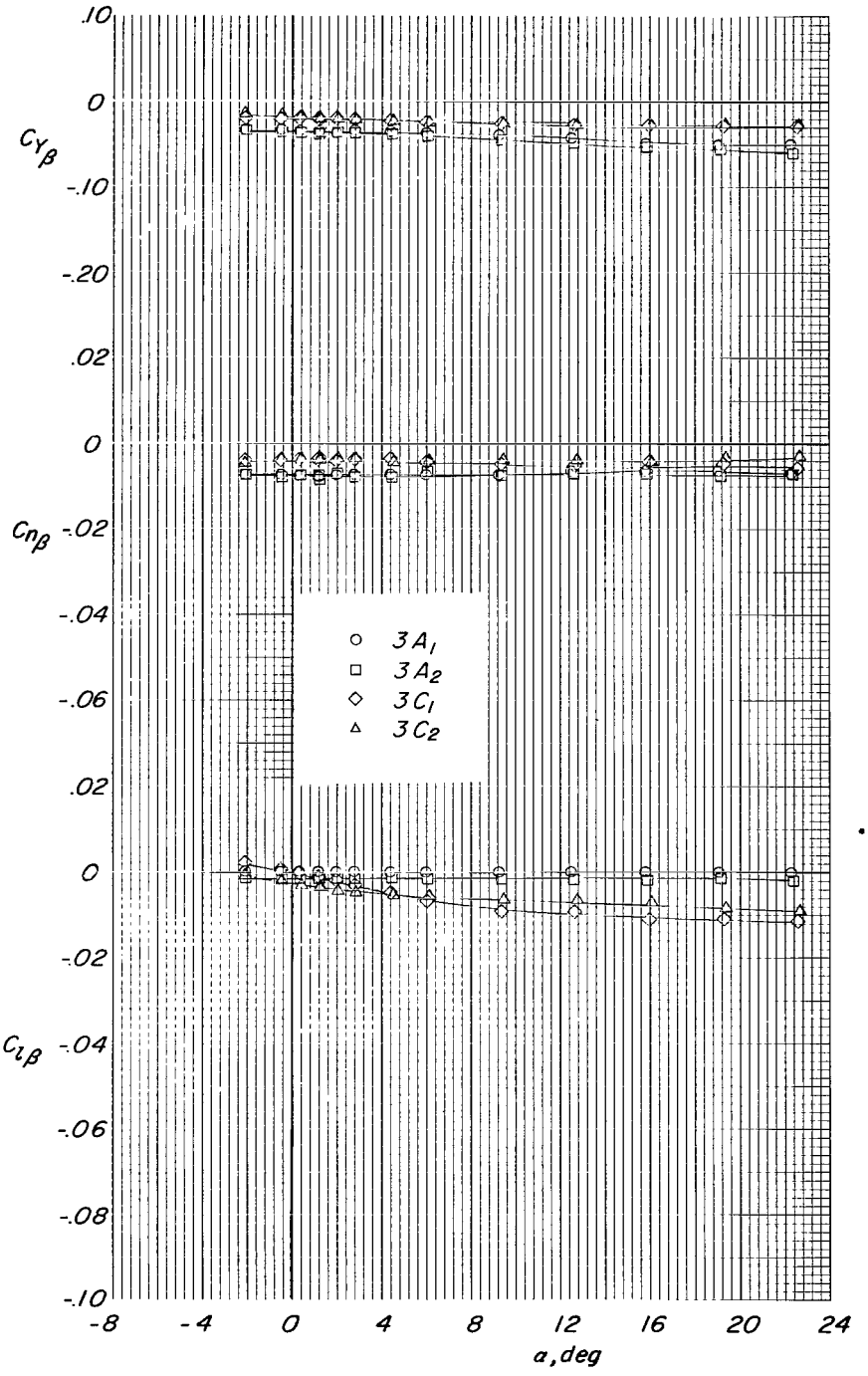

(c) M = 2.36.

Figure 15.- Continued.

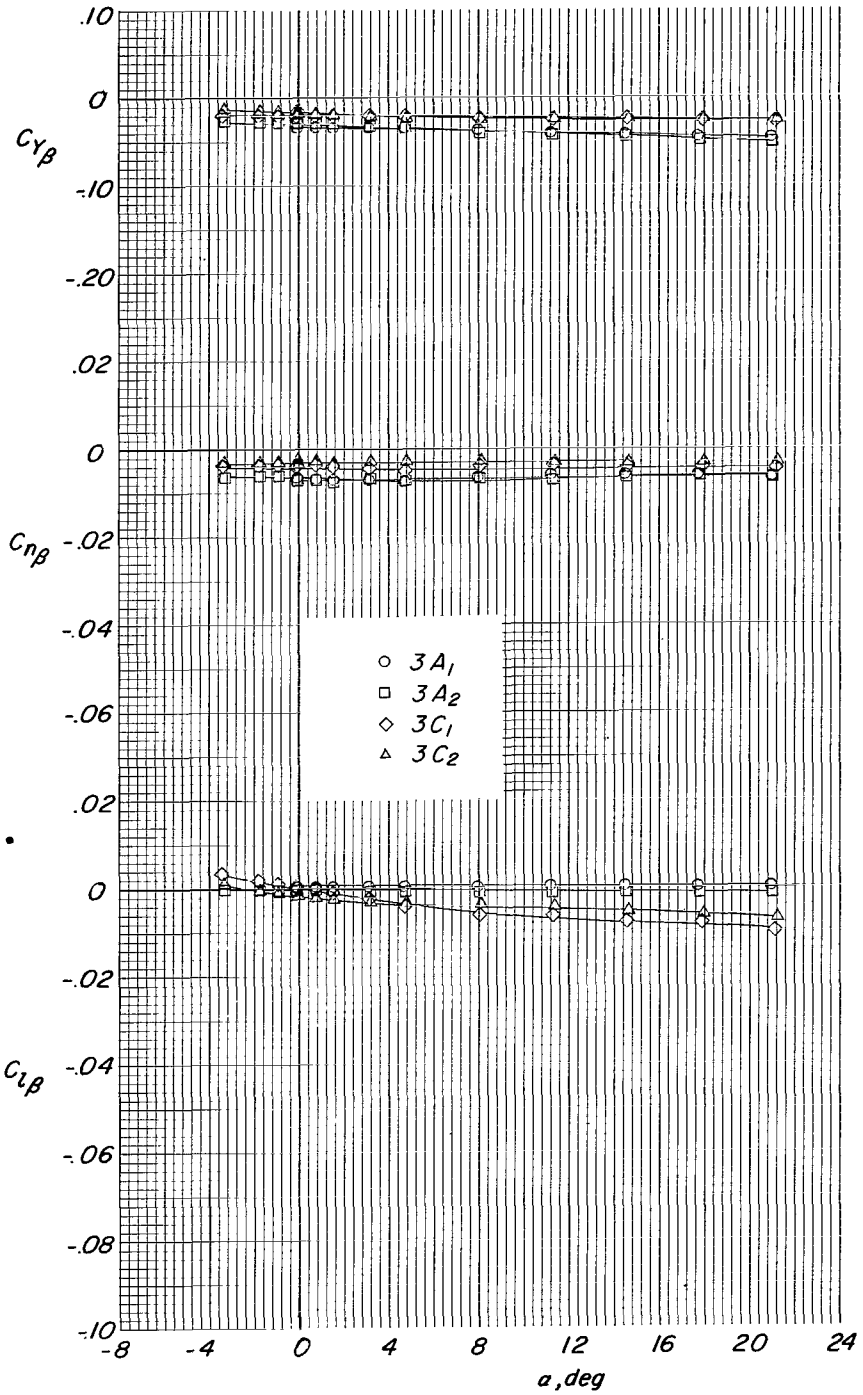

(d) M = 2.86.

Figure 15.- Concluded.

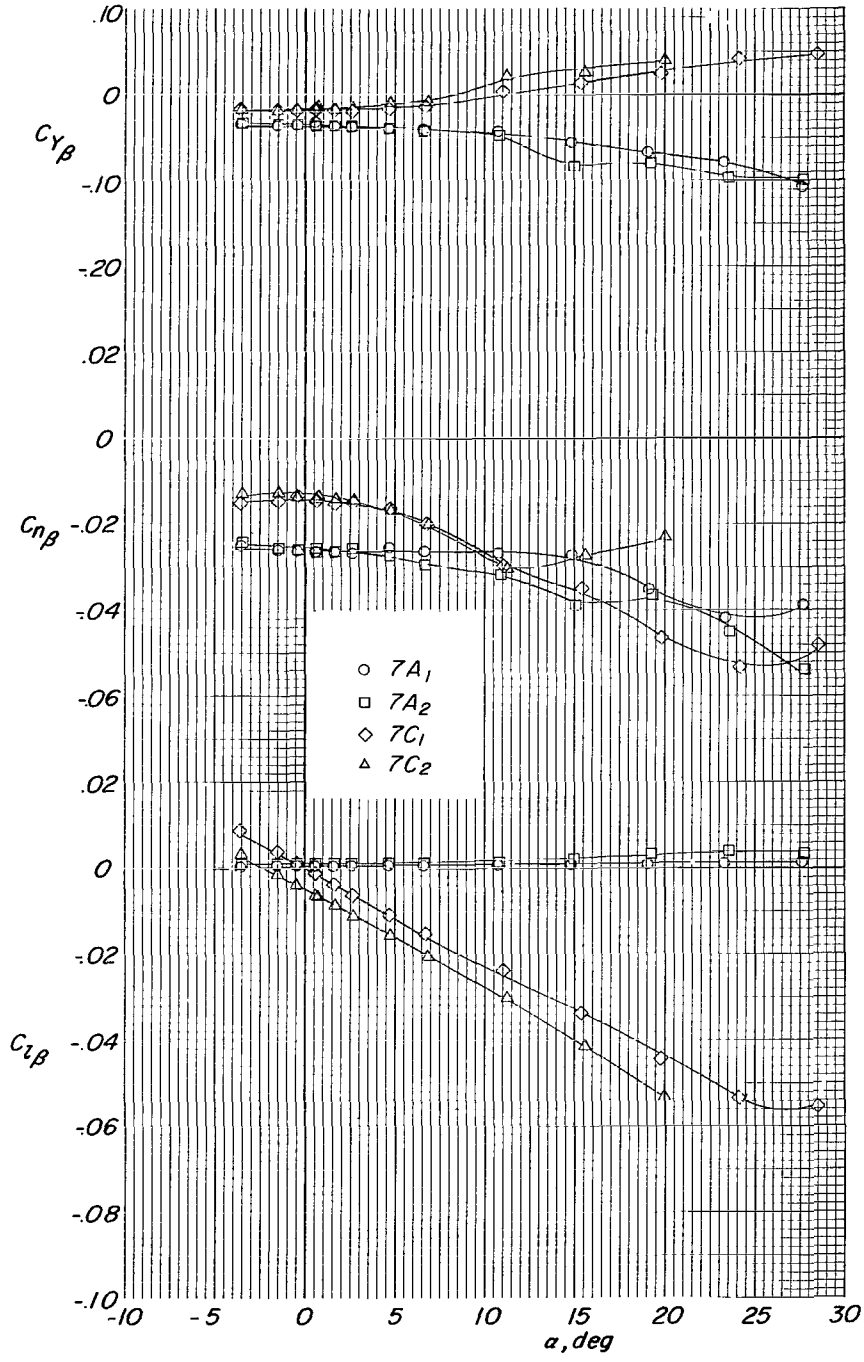

(a) M = 1.50.

Figure 16.- Effect of body section displacement on variation of lateral-directional derivatives with angle of attack for body with fineness ratio 7 at $\phi = 0^\circ$.

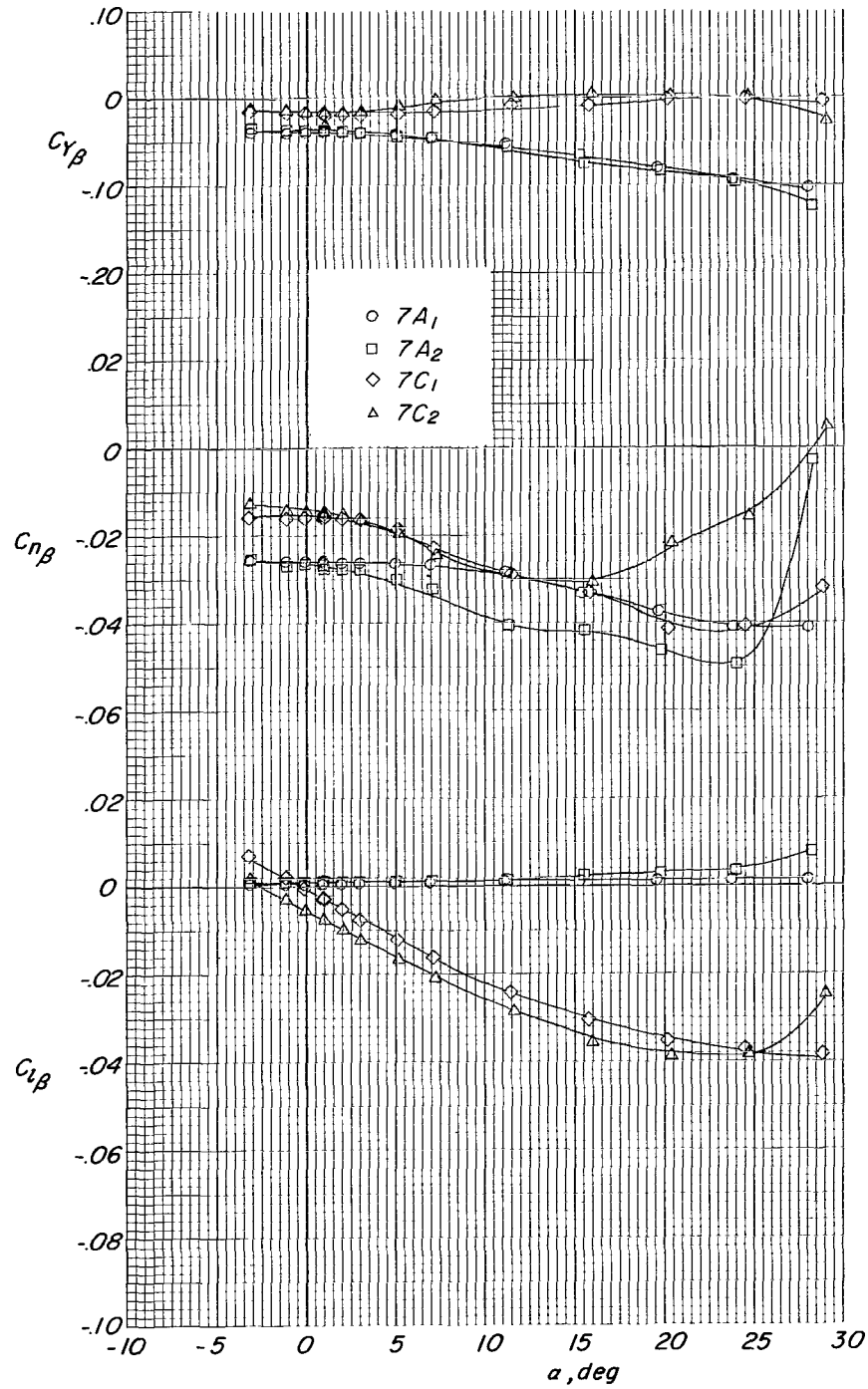

(b) M = 1.90.

Figure 16.- Continued.

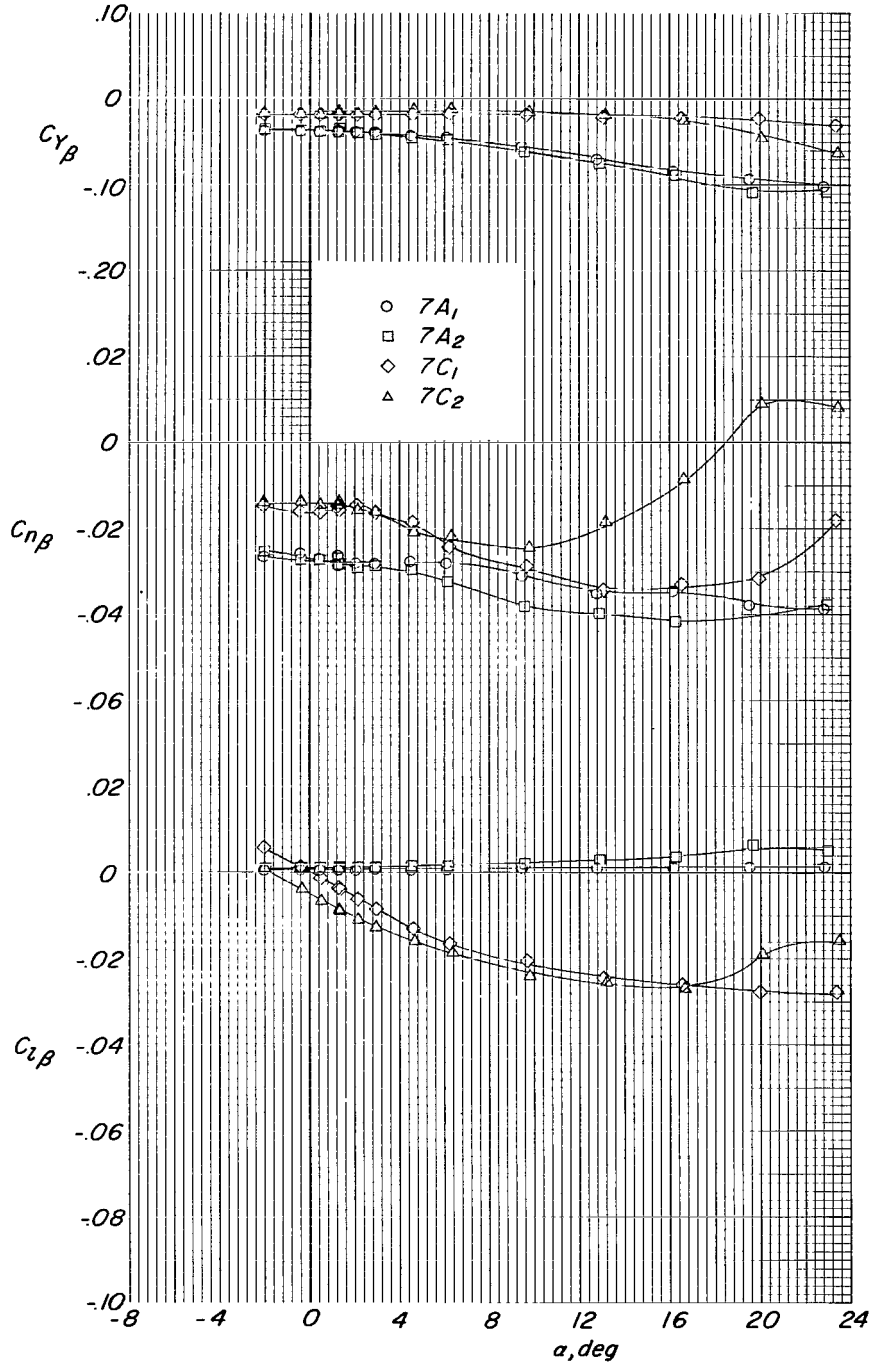

(c) M = 2.36.

Figure 16.- Continued.

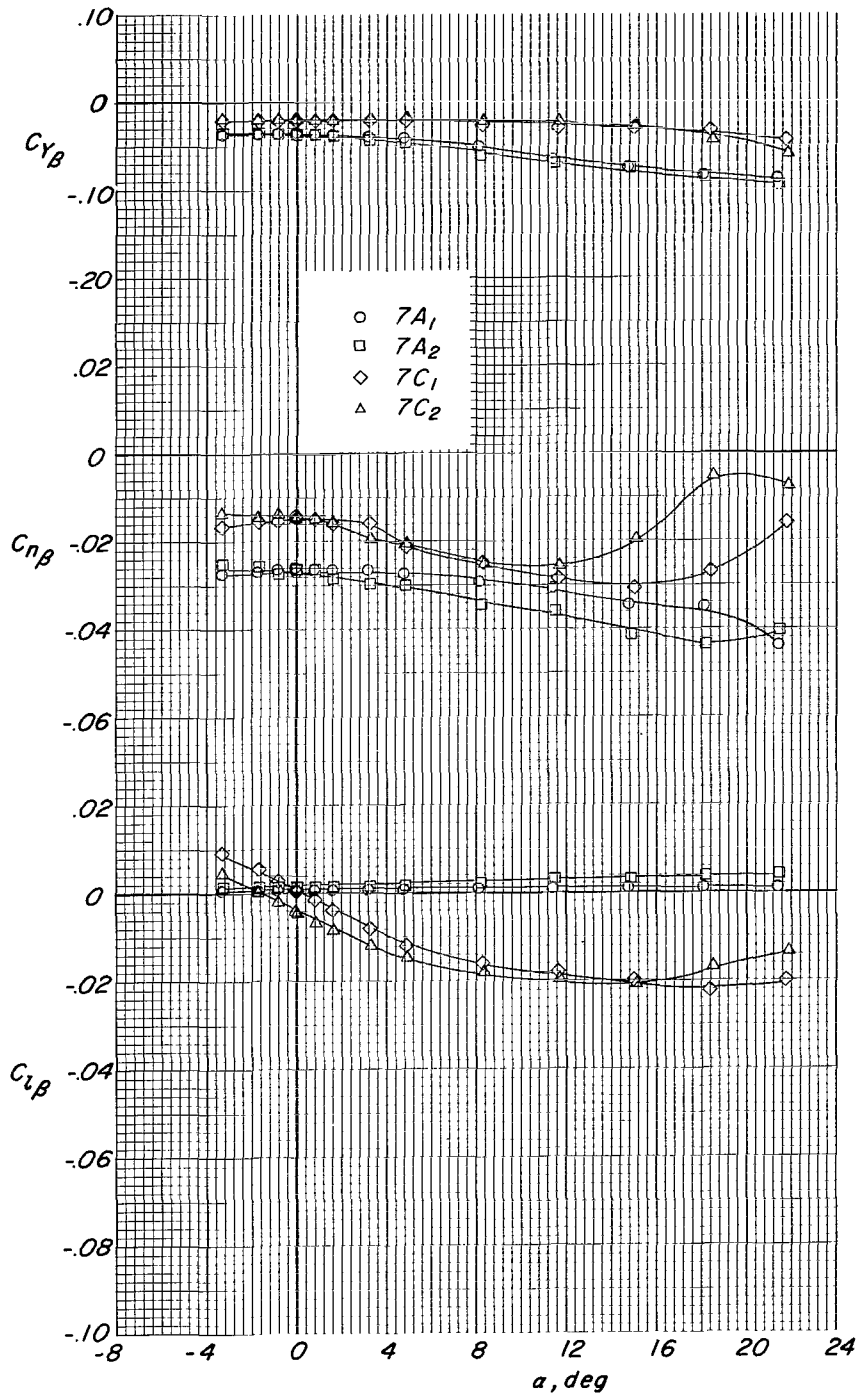

(d) M = 2.86.

Figure 16.- Concluded.

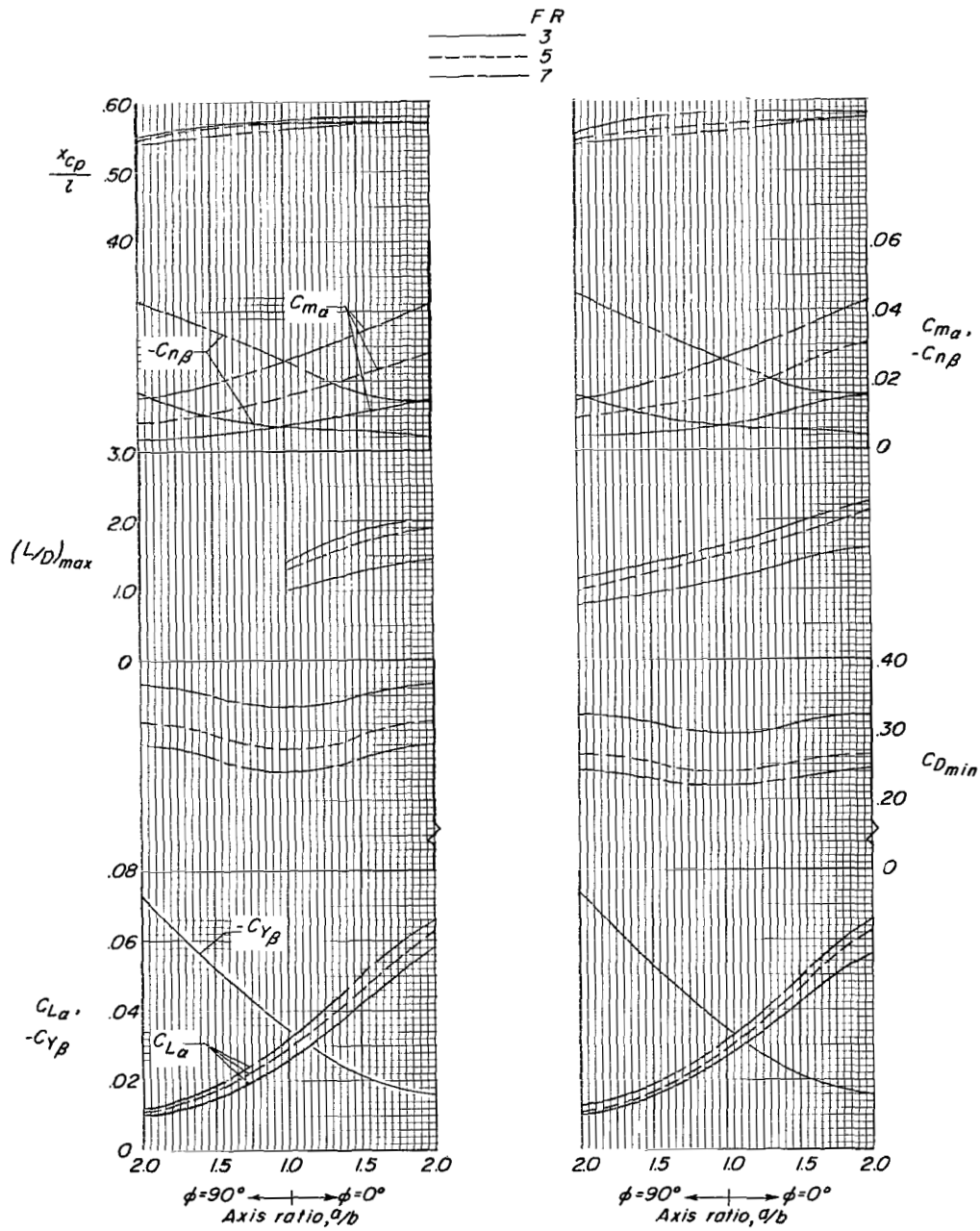

(a) M = 1.50. (b) M = 1.90.

Figure 17.- Summary of aerodynamic parameters C_{L_α}, C_{Y_β}, $C_{D_{min}}$, $(L/D)_{max}$, C_{m_α}, C_{n_β}, and $\frac{x_{cp}}{l}$ for various a/b ratios, fineness ratios, and Mach numbers.

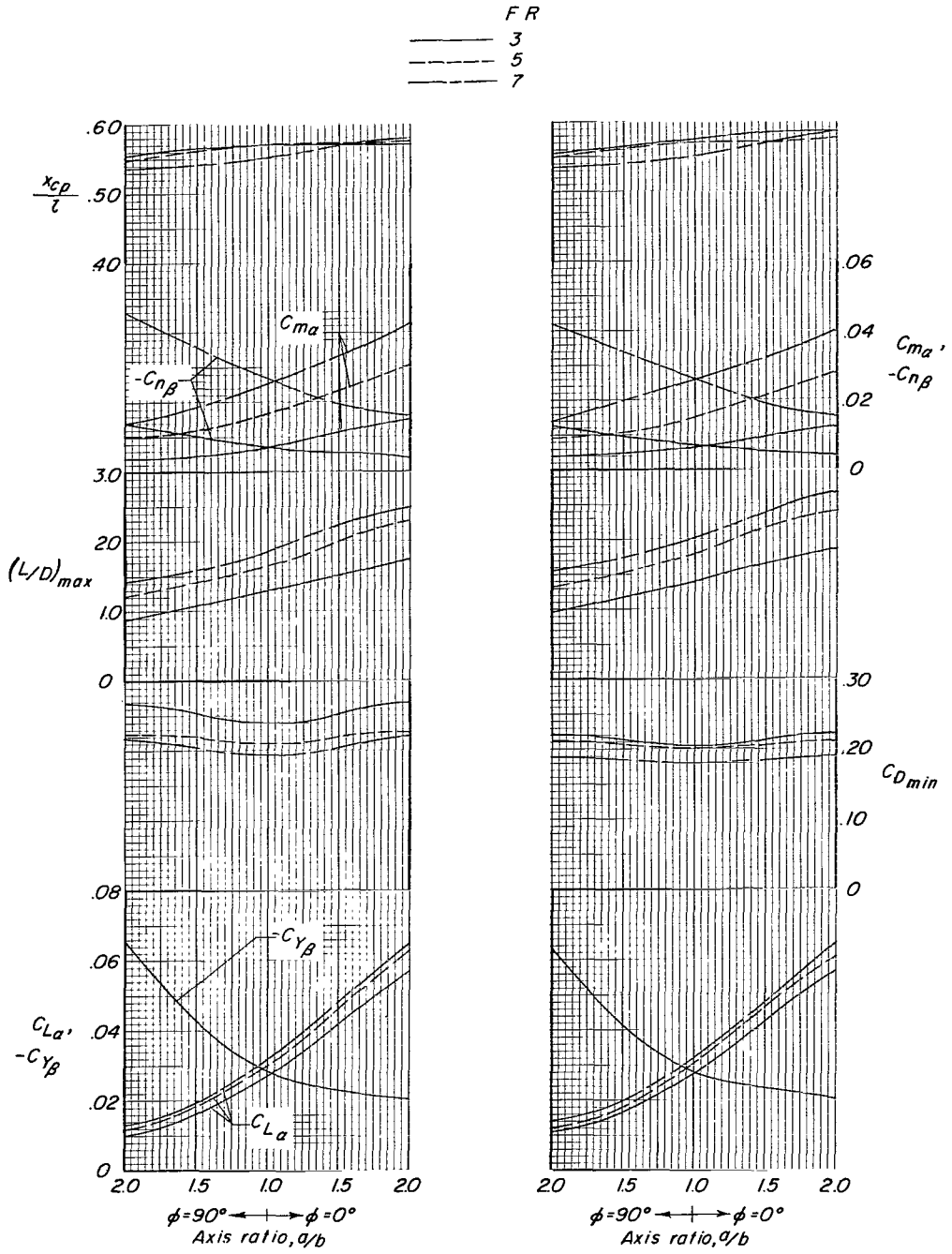

(c) M = 2.36.

(d) M = 2.86.

Figure 17.- Continued.

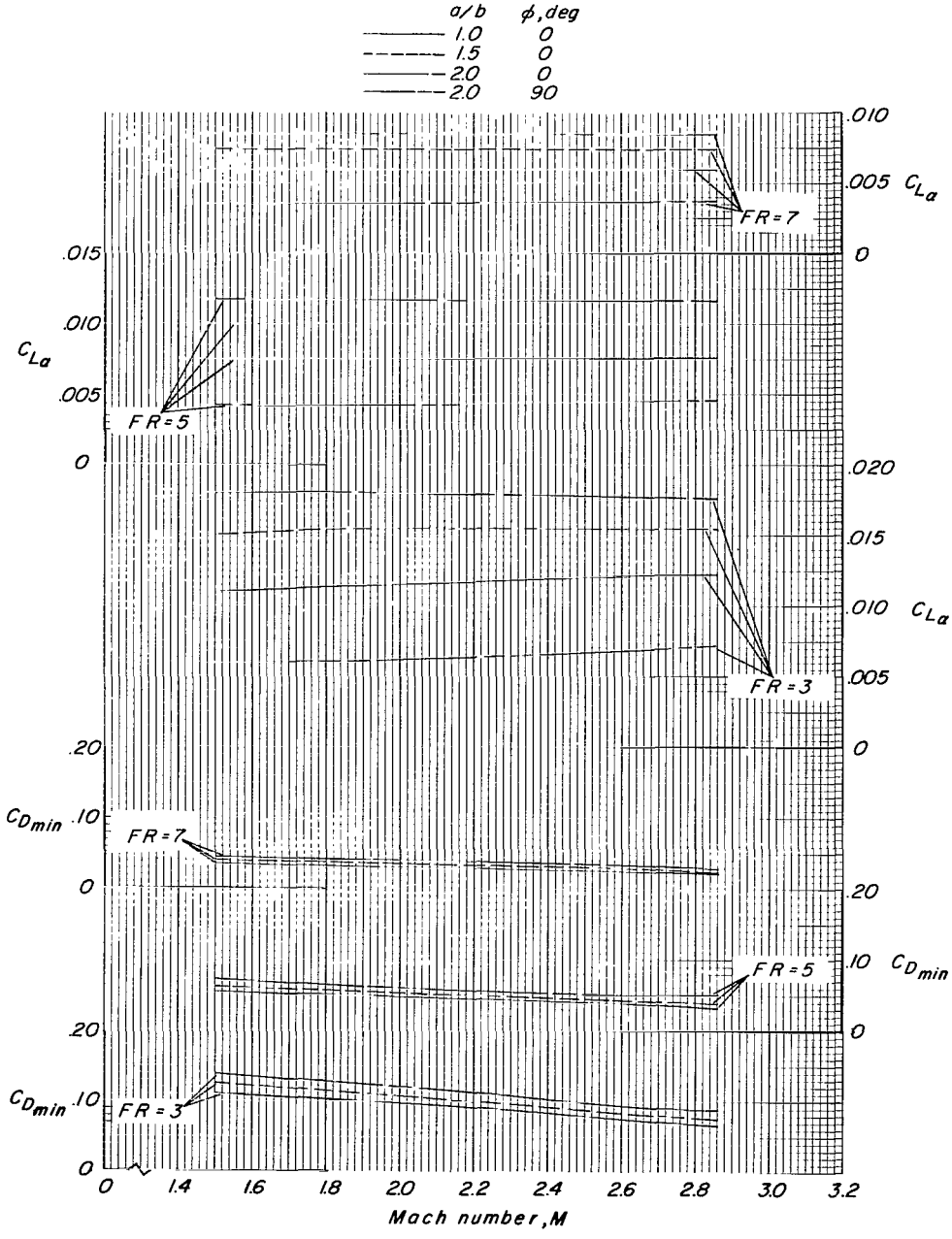

(e) C_{I_α} and $C_{D_{min}}$ based on each body projected planform.

Figure 17.- Concluded.

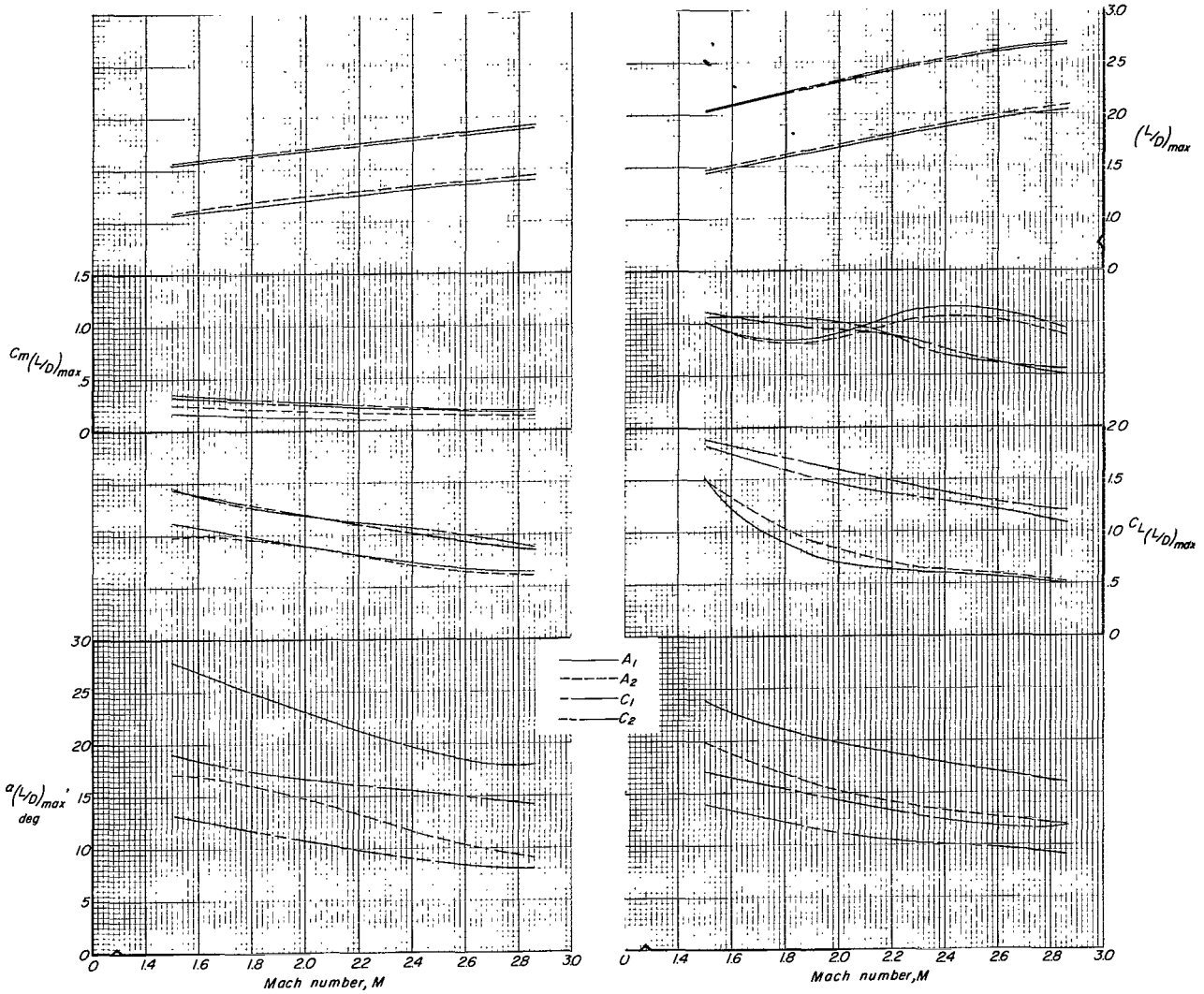

(a) FR = 3. (b) FR = 7.

Figure 18.- The effects of negative camber for the a/b = 1.00 and 2.00, $\phi = 0^{\circ}$ bodies, on the maximum lift-drag ratio and corresponding $C_{L_{(L/D)_{max}}}$, $C_{m_{(L/D)_{max}}}$, and $\alpha_{(L/D)_{max}}$ variations with Mach number.

"The aeronautical and space activities of the United States shall be conducted so as to contribute . . . to the expansion of human knowledge of phenomena in the atmosphere and space. The Administration shall provide for the widest practicable and appropriate dissemination of information concerning its activities and the results thereof."

—NATIONAL AERONAUTICS AND SPACE ACT OF 1958

NASA SCIENTIFIC AND TECHNICAL PUBLICATIONS

TECHNICAL REPORTS: Scientific and technical information considered important, complete, and a lasting contribution to existing knowledge.

TECHNICAL NOTES: Information less broad in scope but nevertheless of importance as a contribution to existing knowledge.

TECHNICAL MEMORANDUMS: Information receiving limited distribution because of preliminary data, security classification, or other reasons.

CONTRACTOR REPORTS: Technical information generated in connection with a NASA contract or grant and released under NASA auspices.

TECHNICAL TRANSLATIONS: Information published in a foreign language considered to merit NASA distribution in English.

TECHNICAL REPRINTS: Information derived from NASA activities and initially published in the form of journal articles.

SPECIAL PUBLICATIONS: Information derived from or of value to NASA activities but not necessarily reporting the results of individual NASA-programmed scientific efforts. Publications include conference proceedings, monographs, data compilations, handbooks, sourcebooks, and special bibliographies.

Details on the availability of these publications may be obtained from:

SCIENTIFIC AND TECHNICAL INFORMATION DIVISION

NATIONAL AERONAUTICS AND SPACE ADMINISTRATION

Washington, D.C. 20546